Technische Universität Ilmenau

Fakultät für Maschinenbau

Pontificia Universidad Católica del Perú

Escuela de Posgrado

Master Thesis

Integration of a visual tracking system into a four probe measuring system to evaluate the electrical sheet resistance of thin films

To achieve the Degree of:
Master of Science (M. Sc.)
in Mechatronik

Submitted by:	Osmar Giordano Adolfo Curi Grados
Supervisor (TU Ilmenau):	Dr. -Ing. Tom Ströhla
Supervisor (PUCP):	Dr. Francisco Rumiche
Practical Advisor (TU Ilmenau):	Dr. -Ing. Rolf Grieseler
Date and Place:	27/03/2017, Ilmenau, Germany

Tesis publicada con autorización del autor
No olvide citar esta tesis

Statement of Authorship

The present work has been made independently without use other than those specified sources. All points were taken literally or in accordance with their published sources are identified as such. The work has not been submitted in the same or similar form, or in part, under one or other tests.

Ilmenau, March 27, 2017

Osmar Giordano Adolfo Curi Grados

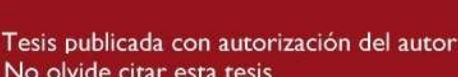

Abstract

In recent years, thin films have been extensively studied due to the wide range of technical applications, some of which are determined by the electrical properties such as the resistivity. Generally, some properties in macroscale are not necessarily longer valid when the material is reduced to the nanoscale. A number of studies demonstrate that resistivity in thin films depends on the sample thickness. Therefore, in the research and production of thin films for new applications, it is necessary an effective and accurate system to measure and characterize its electrical properties.

In order to overcome the constraints of measuring the resistivity in thin films, the aim of this thesis was to implement a measuring system, which consists of a LabVIEW software, Keithley electrical test instruments, and a digital microscope camera. This system presents two main characteristics:

1. A visual tracking system to determine the position of the four probes during the measurements. This system reduces the errors caused by the probes misalignment, provides a more user-friendly graphical interface and is the first step for the automation of the measuring system.
2. The system is able to measure the resistivity using four different methods (Van der Pauw, Linear Van der Pauw, Linear and Square Four-Point Probe). This feature provides the possibility to measure a wider range of both, material types and samples sizes.

The performance of the implemented system was proved by measuring standard samples of aluminum and tungsten having different thicknesses (100, 300 and 600 nm). The films were deposited on silicon substrate using magnetron sputtering. The films resistivity were measured using the four different methods obtaining a standard error less than 1%. In order to validate the effectiveness of the visual tracking system, the influence of probes misalignment and probes spacing on resistivity measurement was analyzed.

The results were validated by comparison with experimental data from literature and thin films theoretical models (Fuchs-Sondheimer, Mayadas-Shatzke and combination of both models). The results are in good agreement with both, experimental data and theoretical models. Besides, the resistivity dependence on the thickness was confirmed. Furthermore, it was shown that the increment of electrical resistivity could be explained by the contributions of both, grain-boundary and surface scattering mechanisms.

Tesis publicada con autorización del autor
No olvide citar esta tesis

Zusammenfassung

In den letzten Jahren wurden dünne Schichten aufgrund ihrer breiten Palette an technischen Anwendungen intensiv untersucht, von denen einige durch die elektrischen Eigenschaften wie den spezifischen Widerstand bestimmt werden. Im Allgemeinen sind einige Eigenschaften in Makroscale nicht unbedingt länger gültig, wenn das Material auf die Nanoskala reduziert wird. Eine Reihe von Studien zeigen, dass der spezifische Widerstand in dünnen Schichten von der Schichtdicke abhängt. Deshalb ist es bei der Erforschung und Herstellung von dünnen Schichten für neue Anwendungen notwendig, ein wirksames und genaues System zur Messung und Charakterisierung seiner elektrischen Eigenschaften zu verwenden.

Um die Einschränkungen der Messung des Widerstands in dünnen Schichten zu überwinden, war es das Ziel dieser Arbeit, ein flexibles Messsystem zu implementieren, das aus LabVIEW Software, Keithley Stromquelle und Multimeter sowie einer digitalen Mikroskopkamera besteht. Dieses System wird durch zwei Hauptmerkmale charakterisiert:

1. Ein visuelles Tracking-System zur Bestimmung der Position der Messspitzen während der Messung. Dieses System reduziert die Fehler, die durch die Fehlausrichtung der Messspitzen verursacht werden, bietet eine benutzerfreundliche grafische Oberfläche und ist der erste Schritt zur Automatisierung des Widerstandsmesssystems.

2. Das System ist in der Lage, den Widerstand mit vier verschiedenen Methoden zu messen (Van der Pauw, Linear Van der Pauw und die Linear- und Square-Four-Point-Sondenmethoden). Diese Funktion bietet die Möglichkeit, eine breitere Palette von Materialarten und Probengrößen zu messen.

Die Leistung des implementierten Systems wurde durch die Messung von Standardproben aus Aluminium und Wolfram mit unterschiedlichen Dicken (100, 300 und 600 nm) bewiesen. Die Schichten wurden auf Siliziumsubstrat unter Verwendung des Magnetron-Sputterns abgeschieden. Der Schichtwiderstand wurde unter Verwendung der vier verschiedenen Verfahren gemessen, die einen Standardfehler von weniger als 1% erhalten. Um die Wirksamkeit des visuellen Trackingsystems zu validieren, wurde der Einfluss von Spitzenfehlausrichtung und Spitzenabstand auf die Widerstandsmessung analysiert.

Die Ergebnisse wurden im Vergleich zu experimentellen Daten aus Literatur und Dünnschicht-theoretischen Modellen (Fuchs-Sondheimer, Mayadas-Shatzke und eine Kombination beider Modelle) validiert. Die Ergebnisse stimmen gut mit den experimentellen Daten und den theoretischen Modellen überein. Außerdem wurde die Widerstandsabhängigkeit von der Dicke bestätigt. Weiterhin wurde gezeigt, dass das Inkrement des elektrischen Widerstands durch die Beiträge sowohl von Korngrenzen- als auch von Oberflächen Streuungsmechanismen erklärt werden könnte.

Tesis publicada con autorización del autor
No olvide citar esta tesis

Resumen

En los ultimos años, las películas delgadas han sido ampliamente estudiadas debido a la amplia gama de aplicaciones técnicas que presentan, algunas de las cuales están determinadas por sus propiedades eléctricas tales como la resistividad. Generalmente, algunas propiedades medidas en la macroescala no siguen siendo válidas cuando el material es reducido a la nanoescala. Varios estudios demuestran que la resistividad en películas delgadas depende del espesor de la muestra. Por lo tanto, en la investigación y producción de películas delgadas para nuevas aplicaciones, es necesario un sistema eficaz y preciso para medir y caracterizar sus propiedades eléctricas.

Con el fin de superar las limitaciones en la medición de la resistividad en películas delgadas, el objetivo de esta tesis es la de implementar un sistema de medición de la resistividad flexible implementado utilizando el software LabVIEW y conformado por instrumentos de medición Keithley y una cámara digital tipo microscopio. Este sistema presenta dos características principales:

1. Un sistema de seguimiento automático de posición (visual tracking) para determinar la ubicación de las puntas de medición sobre la muestra. Este sistema reduce los errores ocasionados por el desalineamiento de las puntas, proporciona una apropiada interfaz gráfica y es el primer paso para la automatización del sistema de medición.
2. El sistema es capaz de medir la resistividad utilizando cuatro métodos distintos (Van der Pauw, Linear Van der Pauw, y el método de las cuatro puntas lineal y cuadrado). Esta característica proporciona la posibilidad de medir una gama más amplia tanto de materiales como de dimensiones de las muestras.

El desempeño del sistema desarrollado se validó midiendo muestras estándar de aluminio y tungsteno de diferentes espesores (100, 300 and 600 nm). Las películas se depositaron sobre sustrato de silicio mediante sputtering. La resistividad de las películas se midió aplicando los diferentes cuatro métodos y se obtuvo un error estándar menor a 1%. Con el fin de validar la eficacia del sistema de seguimiento visual (visual tracking), se analizó la influencia, tanto del desalineamiento como de la distribución de las puntas en la medición de la resistividad.

Los resultados fueron validados por comparación con datos experimentales de la literatura y modelos teóricos de películas delgadas (Fuchs-Sondheimer, Mayadas-Shatzke y combinación de ambos modelos). Los resultados están en correlación con los datos experimentales y los modelos teóricos. Además, se confirmó la dependencia de la resistividad con el espesor. Asimismo, se demostró que el incremento de la resistividad eléctrica podría explicarse por las contribuciones de los mecanismos de dispersión en los limites de grano y en la superficie de la película delgada.

Tesis publicada con autorización del autor
No olvide citar esta tesis

Acknowledgements

I would like to express my sincere gratitude to my advisor Dr. Grieseler for the continuous support of my master study and related research, for his patience, motivation, and friendship. His guidance helped me in all the time of research and writing of this thesis.

Besides, I would like to thank my advisor in Perú, Dr. Rumiche, for their insightful comments and encouragement; and Dr. Ströhla for his helpful advice during the master studies.

My deepest gratitude to CONCYTEC for the financial support that has made this experience in my life possible.

I also thank the professors of the Master Programm in PUCP, Dr. Tafur and Prof. Barriga for their coordination and cooperation in the double degree of the master studies.

Nobody has been more important to me in the pursuit of this project than the members of my family. I would like to thank my mother, Eva, and my brother, Piero, whose love and guidance are with me in whatever I pursue. I likewise wish to thank my partner, Martha, who supported me through this venture.

My greatest gratitude goes to my friends, thank you for listening, offering me advice, supporting me and sharing together great moments during this time.

Tesis publicada con autorización del autor
No olvide citar esta tesis

Contents

1 Introduction **1**
1.1 Motivation 1
1.2 Objectives of the thesis 2

2 State of the art **3**
2.1 Resistivity measurement in thin films 3
2.1.1 Linear Four Probes Method 4
2.1.2 Square Four Probes Method 5
2.1.3 Correction factors 5
2.1.4 Van der Pauw Method 8
2.1.5 Linear Van der Pauw Method 10
2.1.6 Summary of resistivity measurement methods 11
2.2 Image processing fundamentals 12
2.2.1 Digital image 12
2.2.2 Grayscale image 12
2.2.3 Binary image 12
2.2.4 Color image 13
2.2.5 Image resolution 13
2.2.6 Region of interest (ROI) 14
2.3 Visual tracking applications in characterization and manipulation of micro and nano materials 14
2.3.1 Vision tracking for resistivity measurement in nanomaterials 14
2.3.2 Vision tracking for nanorobotic manipulation 16
2.4 Matching patterns algorithms 18
2.4.1 Cross-correlation 18
2.4.2 Normalized cross-correlation 19
2.4.3 Pyramidal matching 20

3 Implementation and operation of the measuring system **21**
3.1 Setup of the measuring system 21
3.1.1 Hardware 21
3.1.2 Software 24
3.2 Graphical User Interface and Statechart 26
3.3 Camera system characteristics 33
3.4 Real-time Probes Visual Tracking 34
3.5 Implementation of the resistivity measuring methods 37
3.5.1 Van der Pauw Method 37
3.5.2 Linear Van der Pauw Method 41
3.5.3 Linear Four Probes Method 41
3.5.4 Square Four Probes Method 44
3.6 Calibration of the visual system 46

Tesis publicada con autorización del autor
No olvide citar esta tesis

3.7 Circular samples shape recognition . . . 49
3.8 Set distance for probes spacing . . . 51
3.9 Probes Alignment in the Symmetry Line . . . 53
3.10 Automatic calculation of area and distances . . . 54
3.11 Correction factors application . . . 56
3.12 Preparation of thin films samples . . . 57

4 Results and discussion **59**
4.1 Experimental results . . . 59
4.2 Results validation with experimental data . . . 60
4.3 Theoretical models . . . 63
4.3.1 Fuchs-Sondheimer (F-S) model . . . 63
4.3.2 Mayadas-Shatzke (M-S) model . . . 63
4.3.3 Combined model . . . 64
4.3.4 Mola-Heras model . . . 64
4.4 Results validation with the theoretical models . . . 64
4.5 Effect of probes misalignment . . . 69
4.6 Influence of the probes spacing . . . 71

5 Conclusions **73**

Appendices **78**

A Resistivity and standard errors for Al, Al-400 and W using the four methods **79**

Tesis publicada con autorización del autor
No olvide citar esta tesis

List of Figures

2.1 Commercial four-probes manipulators used to measure and manipulate thin films. . . . 3
2.2 Electrical resistivity measurement using Linear four probe method 4
2.3 Electrical resistivity measurement using the square four probes method . . 5
2.4 Correction factor F_1 6
2.5 Correction factor F_2 7
2.6 Correction factor F_3 for linear and square four probes method 8
2.7 Electrical configuration for Van der Pauw Method 9
2.8 Configuration for Van der Pauw method applied in a symmetric sample . . 10
2.9 Configuration of the probes using Linear Van der Pauw method 10
2.10 Grayscale image 12
2.11 Color image 13
2.12 Region of interest (ROI) 14
2.13 Four nanomanipulators used four resistivity measurement 15
2.14 Visual tracking in four probes method proposed by Ro 15
2.15 Visual tracking in linear four probes method proposed by Ro 16
2.16 Cross-correlation coefficient between an image and a pattern 17
2.17 Active Contour tracking in a SEM proposed by Fatikow 17
2.18 Cross-correlation procedure between two images 18
2.19 Cross-correlation application in the visual tracking system 19
2.20 Pyramidal Matching 20

3.1 Schematic diagram of system's hardware. 22
3.2 Connection boxes 24
3.3 Full view of the measurement system's hardware. 25
3.4 Probes distribution in Van der Pauw method 26
3.5 GUI of the system software developed with LabVIEW 27
3.6 State chart of the system's program 28
3.7 *Verify Probes* function. 29
3.8 *Select Method* section 29
3.9 Schematic representation of the four different methods 30
3.10 Configuration of the parameters for the measurement 31
3.11 Display of the camera for visual tracking 31
3.12 Procedure box 32
3.13 Results table 32
3.14 Buttons for each of the four different methods 33
3.15 MicroCapturePro Camera 33
3.16 LabVIEW program for the Visual Tracking of the probes position 34
3.17 Visual tracking in the NI Vision Assistant for LabVIEW 35
3.18 Patterns for the three different sample colors 36
3.19 Configuration for the Matching Pattern in the LabVIEW Vision Assistant . 36
3.20 Selecting Van der Pauw Method in the GUI 37

Tesis publicada con autorización del autor
No olvide citar esta tesis

3.21 Configuration of the probes for Van der Pauw Method. 38
3.22 Parameters for Van der Pauw method measurements. 38
3.23 Program to solve the Van der Pauw equation by iterations 39
3.24 Van der Pauw Method - Lab VIEW program 40
3.25 Probes configuration for Square Four Probes Method 41
3.26 Probes configuration for Linear Four Probes 42
3.27 LabVIEW program to measure the resistivity using the Linear Four Probe Method 43
3.28 Configuration of the probes for Square Four Probes method 44
3.29 LabVIEW program to calculate the resistivity using the Square Four Probes Method 46
3.30 Procedure to calibrate the visual system 47
3.31 Lab VIEW Program for the CALIBRATE function 48
3.32 Procedure to detect the circular shape of the sample and draw the symmetry line on the sample 49
3.33 LabVIEW Program for Sample Recognition and Symmetry Line automatic drawing 50
3.34 Procedure to set the distance between the probes 51
3.35 Lab VIEW Program for SET PROBES DISTANCE function 52
3.36 Probes alignment along the symmetry line 53
3.37 Calculate area formed by the probes 54
3.38 LabVIEW Program to Calculate the area formed by the probes 55
3.39 Calculate distances between the probes 55
3.40 LabVIEW program to calculate the distances between the probes 56
3.41 Implementation of Correction Factor in LabVIEW 57
3.42 Sputtering Setup 58

4.1 Resistivity vs Thin film thickness 60
4.2 Standard errors obtained by using the four different methods 60
4.3 Experimental resistivity of Al samples prepared by different techniques . . 61
4.4 Experimental resistivity of W thin films prepared by different techniques . 62
4.5 Grain size of Al and Al-400 samples measured by XRD analysis 65
4.6 F-S, M-S and combined models compared to experimental results of aluminum 66
4.7 F-S, M-S and combined models compared to experimental results of Al-400 67
4.8 F-S, M-S and combined models compared to experimental results of tungsten 68
4.9 Contribution of both, F-S and M-S models to explain the experimental resistivity values of gold nanowires obtained by Durkan 69
4.10 Position of the probes for the analysis of the effect of the misalignment . . . 70
4.11 Resistivity vs Probes spacing without correction factor 71
4.12 Resistivity vs Probes spacing 72

Tesis publicada con autorización del autor
No olvide citar esta tesis

List of Tables

2.1 Comparison between the different methods to measure the resistivity in thin films . . . 11

3.1 Equipments of the measurement system . . . 23

4.1 Bulk resistivity and mean free path values for aluminum and tungsten . . . 64
4.2 Comparison of the errors caused by the probes misalignment using Linear Van der Pauw and Linear Four Probes methods . . . 70

A.1 Resistivity and standard errors for Al, Al-400 and W using the four methods 80

List of Abbreviations

CF	Correction Factors
CFL	Correction Factor for Linear Four Probes Method
CFS	Correction Factor for Square Four Probes Method
FOV	Field of View
GPIB	General Purpose Interface Bus
GUI	Graphical User Interface
L4P	Linear Four Probes Method
LVP	Linear Van der Pauw Method
ROI	Region of Interest
S4P	Square Four Probes Method
SEM	Scanning Electron Microscope
SSD	Sum of Squared Differences
VPM	Van der Pauw Method

Tesis publicada con autorización del autor
No olvide citar esta tesis

List of Symbols

a	Distance of the probes to the sample edge
Al	Aluminum
$Al - 400$	Aluminum prepared at 400°C via sputtering
d	Thickness of the thin film
D	Diameter of the sample
D_{grain}	Mean grain size
d_m	Distance of a probe's misalignment
F	Correction factor
I	Electrical current
k	Film thickness/mean free path
λ	Mean free path
p	Proportion of electrons that are specularly reflected at the film surfaces
$R_{electric}$	Electrical resistance
$R_{AB,CD}$	Sheet resistance when the current is applied between probes A and B; and the voltage is measured between C and D.
R	Grain-boundary reflection coefficient
ρ	Resistivity
$\rho_{\circ}$	Bulk resistivity
ρ_{F-S}	Resistivity according to Fuchs-Sondheimer model
ρ_{M-S}	Resistivity according to Mayadas-Shatzke model
R_{sht}	Sheet Resistance
s	Distance between the probes
Si	Silicon
t	Thin film thickness
V	Voltage
W	Tungsten

Tesis publicada con autorización del autor
No olvide citar esta tesis

Chapter 1

Introduction

1.1 Motivation

The Institute of Micro and Nanotechnologies at the TU Ilmenau develops materials for micro and nanosystems in a wide range of applications as conductors in electronics, optical elements, 3D biosystems, semiconductor devices, etc. The applications for a new material are determined by its properties. Among them, one of the most important is the electrical resistivity, which defines the electrical behavior of a material.

In the nanoscale, some electrical, mechanical and optical properties are altered due to material's size variations. The electrical properties of materials in the macroscale are not necessarily longer valid when the materials are in nanoscale size. Several studies have demonstrated that the electrical resistivity of a thin film will become higher as the thickness of the film decreases in size [1].

There are some methods to measure resistivity in thin films. Among them, Four Probes and Van der Pauw are the most effective and widely used methods. Furthermore, some researchers have implemented different variants of these methods, i.e. S. Lim *et al.* [2] developed a Modified Van der Pauw method for measuring resistivity placing the probes distant from the sample's boundary. Similarly, S. Thorsteinsson *et al.* [3] presented a variation of the Van der Pauw method in which the four probes are placed along a sample's symmetry line. Each method has its corresponding advantages depending on the application, the material, and the shape of the sample.

The correct alignment of objects and instruments is a basic task for handling and measurement operations in the micro and nanoscale. The objects positioning is acquired by processing images due to its higher accuracy in comparison to manual manipulation and some internal position sensors [4]. Visual tracking enables the development of more precise automated measurement systems. In this work, a visual tracking system is implemented to determine the position of the probes during the measurement. The system is implemented to reduce the error caused by the probes misalignment. Besides, the visual tracking system is the first step for the automation of the measuring system. In addition, visual tracking system provides a more user-friendly graphical user interface (GUI).

In the present work, a resistivity measurement system is developed with LabVIEW software applying image processing techniques. The system integrates GPIB Keithley instruments for sourcing and measurement of both, voltage and current, in the sample. A digital camera assists the visual tracking applications. The system allows the

Tesis publicada con autorización del autor
No olvide citar esta tesis

application of four different methods for resistivity measurement: Van der Pauw, Square Four Probes, Linear Van der Pauw and Linear Four Probes. Additionally, four wire measurement method was implemented to measure sheet resistances. The availability of four different methods produces a more flexible system and make it able to measure a wider range of sample's materials, shapes and sizes.

The resistivity of different samples was tested to validate the measurement system. The materials of the samples are Aluminum and Tungsten thin films deposited onto a silicon substrate using magnetron sputtering. Two different samples of Aluminum were tested. One of them deposited at room temperature and the other at 400°C. The prepared films have thicknesses of 100, 300 and 600 nm.

The samples were measured using the four different methods. The error of the measurements was less than 1%, specifically, Van der Pauw method presented the lowest error (0.3%) and Square Four Probes method, the highest (0.9%), the causes of these errors are discussed. In order to quantify the effectiveness of the visual tracking, the influence of the probes misalignment and the probes spacing on the results are analyzed. The results demonstrates that the visual tracking reduces the error caused by misalignment and the application of correction factors eliminates the influence of the variation of the probes spacing in the measurements.

The results were validated by comparison with experimental data from literature and thin films theoretical models (Fuchs-Sondheimer, Mayadas-Shatzke and combination of both models). The results are in good agreement with both, experimental data and theoretical models. In addition, the resistivity vs films thickness curves were presented for the three materials verifying the dependence of the resistivity on the film thickness, as expected. Furthermore, it was shown that the increment of electrical resistivity could be explained by the contributions of both, grain-boundary and surface scattering mechanisms.

1.2 Objectives of the thesis

The principal aim of this thesis is to implement a system to measure resistivity in thin films with a visual tracking system that improves the accuracy, this system provides an adequate graphical user interface and give the user the possibility to apply different measuring methods. In order to achieve this objective the following topics will be accomplished and examined in the presented work:

- Implement functions to improve the usability of the four different methods to measure the resistivity in thin films based on the visual tracking system.
- Test the performance of the implemented system by measuring films of different materials using the four different methods and calculate the corresponding errors.
- Validate the results by comparison with experimental data from literature and thin films theoretical models.
- Show the dependence of the resistivity on the film thickness for the three different materials.
- Quantify the errors caused by the misalignment and analyze the effect of the probes spacing in the measurements.

Tesis publicada con autorización del autor
No olvide citar esta tesis

Chapter 2

State of the art

This chapter presents a summary of the most widely used methods for the measurement of resistivity in thin films, the characteristics and equations of each method are described. Besides, the state of the art for visual tracking applications in nano- and micro measurements is reviewed. Finally, the principal algorithms for pattern matching used in the visual tracking system will be detailed.

2.1 Resistivity measurement in thin films

Thin films have increasing relevance in several industrial and scientific applications. Thin films are used in semiconductor devices, solar cells, sensors, actuators, photoconductors, micro electromechanical systems (MEMS), anticorrosive and multifunctional coating and other emerging technologies. Mechanical and electrical properties of thin films generally differ from the bulk materials. Electrical properties of thin films depend on the film thickness, lattice dimensions, purity, surface roughness, grain boundaries and imperfect level of the layer [5]. Figure 2.1 shows some commercial four-probes manipulators used to measure and manipulate thin films.

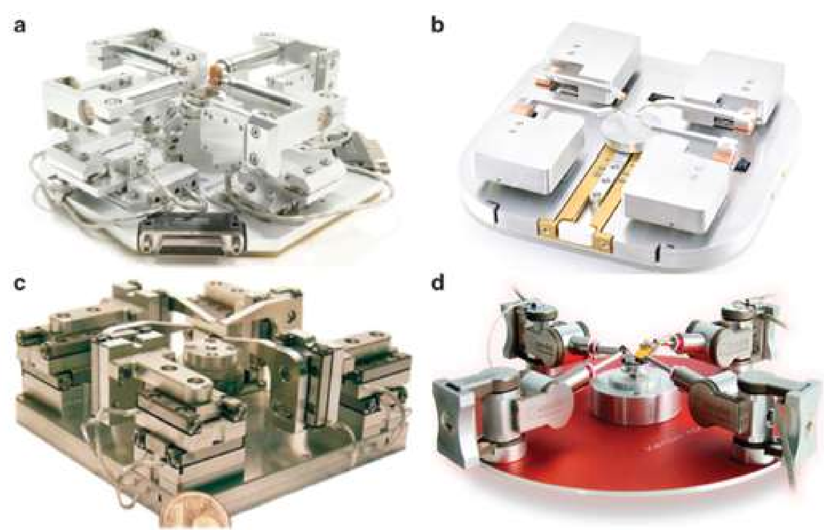

Figure 2.1: Commercial four-probes manipulators used to measure and manipulate thin films. a.Zyvex. b.Lifeforce. c.SmartAct system. d.Kleindiek [6].

In the next section, the most important and widely used methods to measure the resistivity

Tesis publicada con autorización del autor
No olvide citar esta tesis

in thin films are detailed. The respective equations, configuration of the probes and particular considerations are presented for each method.

2.1.1 Linear Four Probes Method

Linear Four Probes Method (L4P) is considered a classical method for resistivity measurements in infinite 2D thin films. This method uses 4 measuring probes arranged linearly on the surface of the sample . The two outer probes are used to source current and the two inner are used to measure voltage [7], as shown in Figure 2.2. This method is valid when the distances between the probes are small compared to the dimension of the sample and the probes must not be placed proximate to the perimeter of the film. [8].

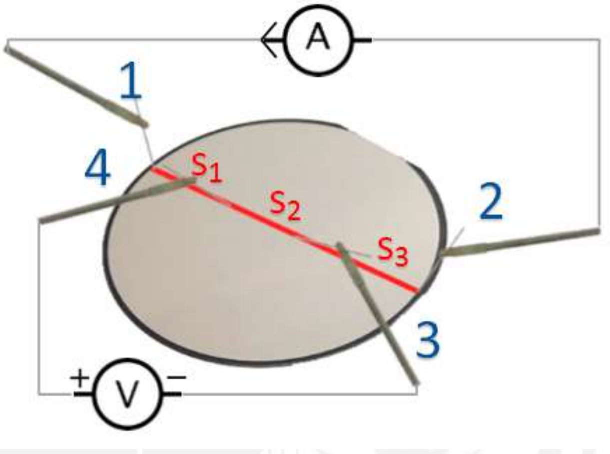

Figure 2.2: Electrical resistivity measurement using four probe arranged in a straight line [9].

According to I. Miccoli *et al.* [10] the resistivity of a thin film can be expressed in terms of the voltage and the current applying the Equation 2.1:

$$\rho = (\frac{V}{I})(\frac{2\pi}{ln(\frac{(s_2+s_3)(s_1+s_2)}{s_1 s_3})})d \tag{2.1}$$

where V is the voltage measured between the inner probes, I, the current applied to the sample, d, the thickness of the sample and s_1, s_2, s_3, the distances between each pair of probes. When the probes are equally spaced (with $s_1 = s_2 = s_3 = s$), the Equation 2.1 could be simplified to Equation 2.2. For this method is necessary only one 10/5000 simultaneous measurement of both voltage and current

.

$$\rho = (\frac{V}{I})(\frac{\pi}{ln2})d \tag{2.2}$$

Tesis publicada con autorización del autor
No olvide citar esta tesis

2.1.2 Square Four Probes Method

The Square Four Probes Method (S4P) is a variation of Linear Four Probes Method. In this method, the four probes are arranged in a square configuration, as can be seen in Figure 2.3. This setup has the advantage of requiring a smaller area for the measurement [10]. In the other side, it is difficult to place the probes forming a square arrangement. The misalignment could cause errors in the measurements.

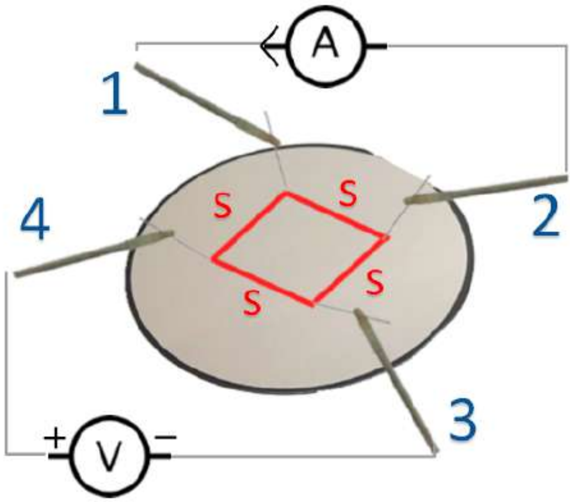

Figure 2.3: Electrical resistivity measurement using the square four probes method.

The corresponding formulation to calculate the resistivity using this method is presented in Equation 2.3, where $s_1 = s_4 = s$ and $s_2 = s_3 = \sqrt{2}s$

$$\rho = 2(\frac{V}{I})(\frac{2\pi}{ln2})d \tag{2.3}$$

2.1.3 Correction factors

Correction factors are required when using the L4P and S4P in order to eliminate the influence of geometrical factors such as the sample's shape, the configuration of the probes or the thickness of the sample in the measurements. Applying the correction factors, the resistivity will be expressed according to Equation 2.4.

$$\rho = CF\ R_{sht}\ d \tag{2.4}$$

Where $CF = F_1\ F_2\ F_3$ is the correction factor to eliminate the geometric influences in the measurements, d, the sample thickness and R_{sht}, the sheet resistance. F_1 considers the effect of the thickness of the sample, F_2, the alignment of the probes when they are close to the boundaries of the sample, and F_3, the shape of the sample [10].

Tesis publicada con autorización del autor
No olvide citar esta tesis

2.1.3.1 Correction factor 1 (F_1): Thickness of the sample

Albers and Berkowitz [11] established an expression for the correction factor, F_1, that consider the influence in the thickness, utilizing an approximated solution of the equation of Laplace and can be written as shown in Equation 2.5

$$F_1 = \frac{ln2}{ln\{\frac{sinh(\frac{d}{s})}{sinh(\frac{d}{2s})}\}} \tag{2.5}$$

In addition, the resistivity of a thin films of thickness, d, measured using the L4P, can be calculated using Equation 2.6.

$$\rho = (\frac{\pi d}{ln2})(\frac{V}{I})(\frac{d}{s})F_1 \tag{2.6}$$

The correction factor F_1 curve depending on thickness and probes spacing is shown in Figure 2.4.

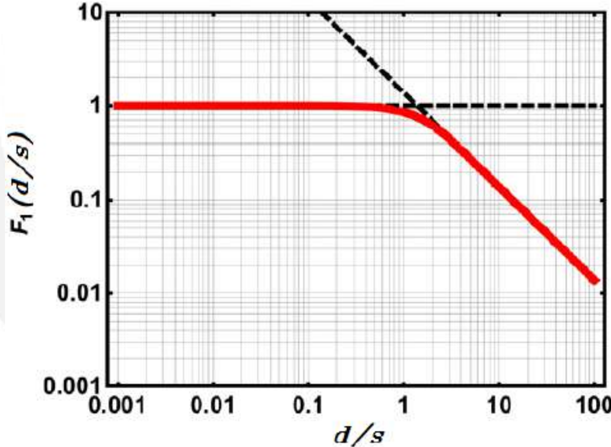

Figure 2.4: Correction factor F_1, where d is the thickness of the sample and s, the distance between the probes [10].

2.1.3.2 Correction factor 2 (F_2) : Probes placed close to the sample boundaries

The correction factor F_2 considers the position of the probes with respect to the boundaries of the sample. Figure 2.5 shows a curve for the factor F_2 depending on the relation between a (the distance of the probes to the sample boundaries) and s (the distance between the probes).
The resistivity of a film having the thickness d, measured with the L4P, can be calculated applying Equation 2.7.

$$\rho = (2\pi s\frac{V}{I})F_2(\frac{a}{s}) \tag{2.7}$$

Tesis publicada con autorización del autor
No olvide citar esta tesis

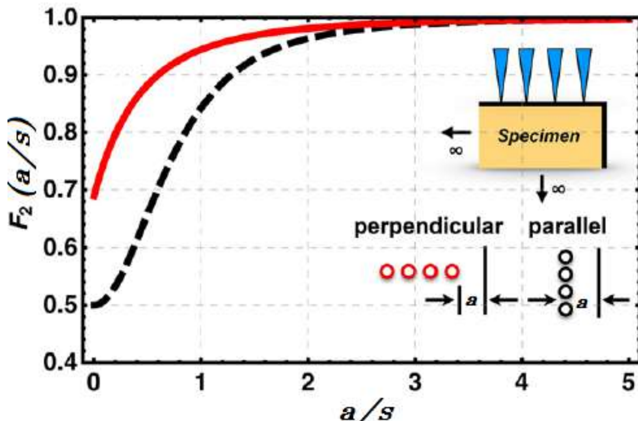

Figure 2.5: Correction factor F_2, where a is the distance of the probes to the sample boundaries and s, the distance between the probes [10]. Two cases are considered: when the probes are placed perpendicular (red curve) and parallel (black curve) to the sample perimeter.

Where F_2 can be expressed according to Equation 2.8.

$$F_2 = 1 + \frac{s}{2a+s} - \frac{s}{2a+2s} - \frac{s}{2a+4s} + \frac{s}{2a+5s} \tag{2.8}$$

It can be noted that F_2 obtain its minimum value $F_{2_{min}} = \frac{1}{2}$ when the four probes are aligned parallel to the sample perimeter.

2.1.3.3 Correction Factor 3 (F_3): Influence of samples shape

The correction factor F_3 reduce the influence of the samples shape on the obtained value of the resistivity. In this section, factor F_3 will be presented for circular shapes. For the L4P, the probes array is placed in the diameter of the circular sample and the resistivity can be calculated with Equation 2.9.

$$\rho = (\frac{\pi d}{ln2})(\frac{V}{I})F_3(\frac{D}{s}) \tag{2.9}$$

Where D is the diameter of the sample. In addition, the correction factor F_3 can be calculated according to Equation 2.10.

$$F_3 = \frac{ln2}{ln2 + ln(\frac{(\frac{D}{s})^2 + 3}{(\frac{D}{s})^2 - 3})} \tag{2.10}$$

Figure 2.6 shows the curve for the correction factor F_3 depending on the sample diameter, D, and s, the probes spacing for both, linear (A) and square (B) four probes methods.

For the S4P, the resistivity can be calculated applying Equation 2.11.

$$\rho = (\frac{2\pi d}{ln2})(\frac{V}{I})F_3(\frac{D}{s}) \tag{2.11}$$

Tesis publicada con autorización del autor
No olvide citar esta tesis

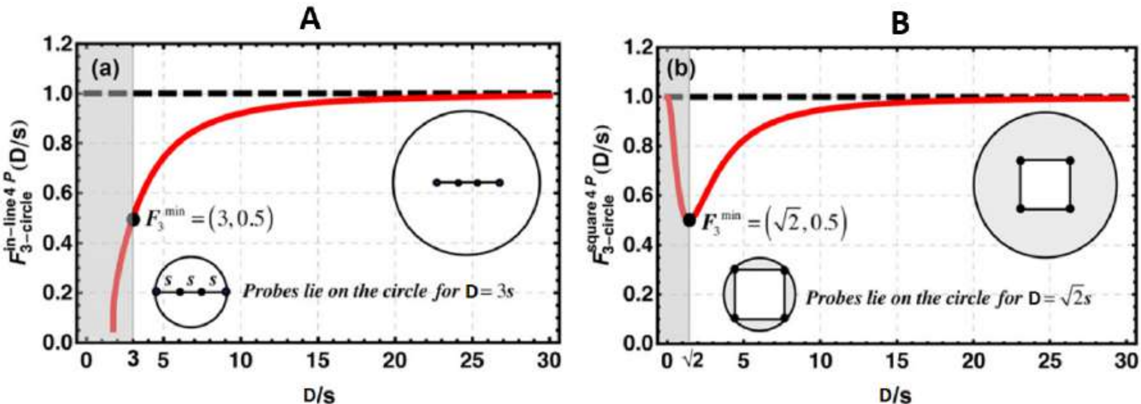

Figure 2.6: Correction factor for linear (A) and square (B) four probes method, where D is the diameter of the sample and s, the probes spacing [10].

Where D is the diameter of the sample. Moreover, the correction factor F_3 is obtained from Equation 2.12.

$$F_3 = \frac{ln2}{ln2 + ln(\frac{(\frac{D}{s})^2 + 2}{(\frac{D}{s})^4 - 4})} \tag{2.12}$$

The total correction factor is the product of the three correction factors described in this section according to Equation 2.13.

$$CF = F_1 * F_2 * F_3 \tag{2.13}$$

2.1.4 Van der Pauw Method

The Van der Pauw Method (VPM) is a technique used for measuring the resistivity of thin films with substrates having an arbitrary shape [12]. This method uses four thin contacts that are placed at the boundary of the sample; two of them are used to source current and the others two to measure voltage. The probes configuration are switched, as shown in Figure 2.7, in order to calculate 2 different values of resistance, which are required for the VPM formulation presented in Equation 2.14, where the resistance $R_{12,34}$ is the potential difference $V_4 - V_3$ between the contacts 4 and 3 per unit of current through the contacts 1 and 2, ρ is the resistivity and d is the thickness of the sample.

$$e^{-\frac{\pi d}{\rho}R_{12,34}} + e^{-\frac{\pi d}{\rho}R_{23,41}} = 1 \tag{2.14}$$

According to Van der Pauw [13], this method is applicable when the following conditions are fulfilled:

Tesis publicada con autorización del autor
No olvide citar esta tesis

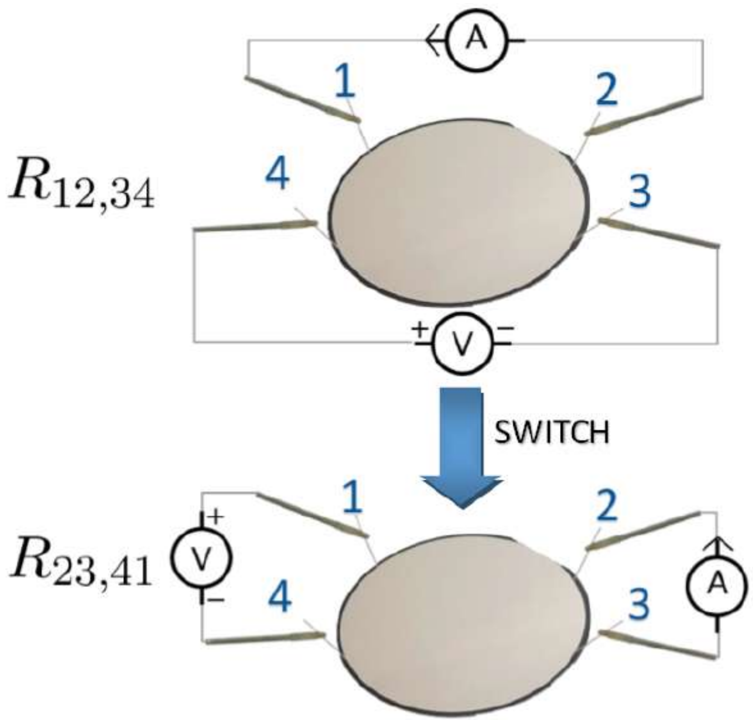

Figure 2.7: Electrical configuration for Van der Pauw Method. Two different measurements of resistance is required for this method.

a) The contacts are placed at the boundaries of the sample.

b) The contacts are sufficiently small.

c) The sample has a homogeneous thickness.

d) The surface of the sample is singly connected. Hence, the sample does not have isolated holes.

In order to simplify the solution of the resistivity ρ, Van der Pauw [13] rewrites Equation 2.14 as a function of $R_{12,34}$ and $R_{23,41}$ and the thickness d.

$$\rho = \frac{\pi d}{ln2}(\frac{R_{12,34} + R_{23,41}}{2})f(\frac{R_{12,34}}{R_{23,41}}) \tag{2.15}$$

Where $f\frac{R_{12,34}}{R_{23,41}}$ is a Van der Pauw's function of the ratio $\frac{R_{12,34}}{R_{23,41}}$ and satisfies the relation 2.16

$$\frac{R_{12,34} - R_{23,41}}{R_{12,34} + R_{23,41}} = \frac{f}{ln2} arccosh(\frac{e^{\frac{ln2}{f}}}{2}) \tag{2.16}$$

Equation 2.14 can be simplified for samples that present a plane of symmetry, where two probes are placed on the symmetry line while the other two are placed symmetrically with respect to this line, as shown in Figure 2.8.
This configuration allows to obtain $R_{12,34} = R_{23,41} = R$ and the resistivity can be calculated according to Equation 2.17.

$$\rho = \frac{\pi d}{ln2}(\frac{V}{I}) \tag{2.17}$$

Tesis publicada con autorización del autor
No olvide citar esta tesis

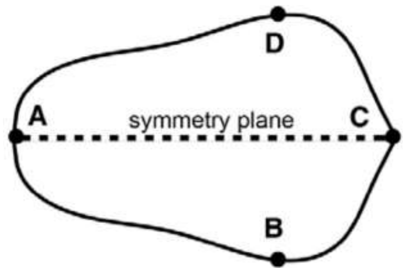

Figure 2.8: Configuration for Van der Pauw method applied in a symmetric sample [10].

2.1.5 Linear Van der Pauw Method

An alternative Van der Pauw method, proposed by Thorsteinsson [3] can be applied by placing the four probes along a symmetry line of the sample, as shown in Figure 2.9.

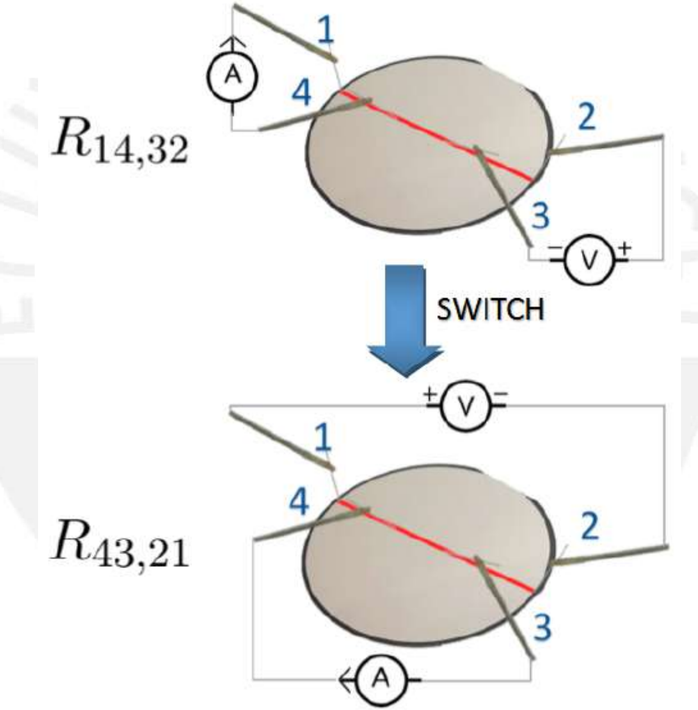

Figure 2.9: Configuration of the probes using Linear Van der Pauw method. The probes are placed along a symmetry line.

For this configuration, the resistivity is calculated applying a variation of the Van der Pauw formulation, where the exponential factors are multiplied by a factor of two, as can be seen in Equation 2.18.

$$e^{-2\frac{\pi d}{\rho}R_{14,32}} + e^{-2\frac{\pi d}{\rho}R_{43,21}} = 1 \tag{2.18}$$

Tesis publicada con autorización del autor
No olvide citar esta tesis

2.1.6 Summary of resistivity measurement methods

Table 2.1 presents a summary of the methods to measure the resistivity with four probes. This table includes the respective probes configuration, equation, advantages, and disadvantages of each method.

Table 2.1: Comparison between the different methods to measure the resistivity in thin films

Method	Equation	Description
Linear Four Probes	$\rho = (\frac{V}{I})(\frac{\pi}{ln2})d$	**Advantage:** Allows to measure very low resistance values. **Disadvantages:** Error due to probes misalignment. Correction factor for geometry is required.
Square Four Probes	$\rho = 2(\frac{V}{I})(\frac{\pi}{ln2})d$	**Advantage:** Smaller area required than linear method. **Disadvantages:** Difficult to place probes forming a square. Correction factor for geometry.
Van der Pauw 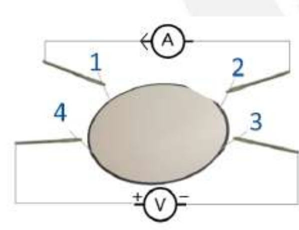	$e^{-\frac{\pi d}{\rho}R_{12,34}} + e^{-\frac{\pi d}{\rho}R_{23,41}} = 1$	**Advantage:** Measure samples with arbitrary shapes. **Disadvantages:** Difficult to place probes at the boundaries.
Linear Van der Pauw 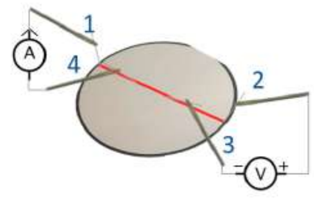	$e^{-2\frac{\pi d}{\rho}R_{14,32}} + e^{-2\frac{\pi d}{\rho}R_{43,21}} = 1$	**Advantage:** Equidistant probes is not mandatory. **Disadvantages:** Error for probes misalignment. Symmetry shape required.

Tesis publicada con autorización del autor
No olvide citar esta tesis

2.2 Image processing fundamentals

This section presents fundamental concepts and definitions of image processing technique and its relevance in the application of this thesis.

2.2.1 Digital image

An image I is generally defined as a rectangular matrix, with image rows (row index x) and image columns (column index y). An element of the matrix determines a small image area called pixel. A value is assigned to the pixel representing its corresponding brightness [14]. Equation 2.19 defines the image matrix.

$$I = [f(x, y)] \tag{2.19}$$

2.2.2 Grayscale image

For a grayscale image, the value of a pixel indicates the corresponding brightness in a range from black to white. In a 8-bit image, the pixel can have 256 values (2^8) from 0 to 255. The value of 0 for a pixel represents the darkest image pixel (black) and 255, the brightest image pixel (white). Figure 2.10 shows a gray scale image with a size of 300 x 250 pixels. The magnification shows a portion of the image with pixels values representing its brightness.

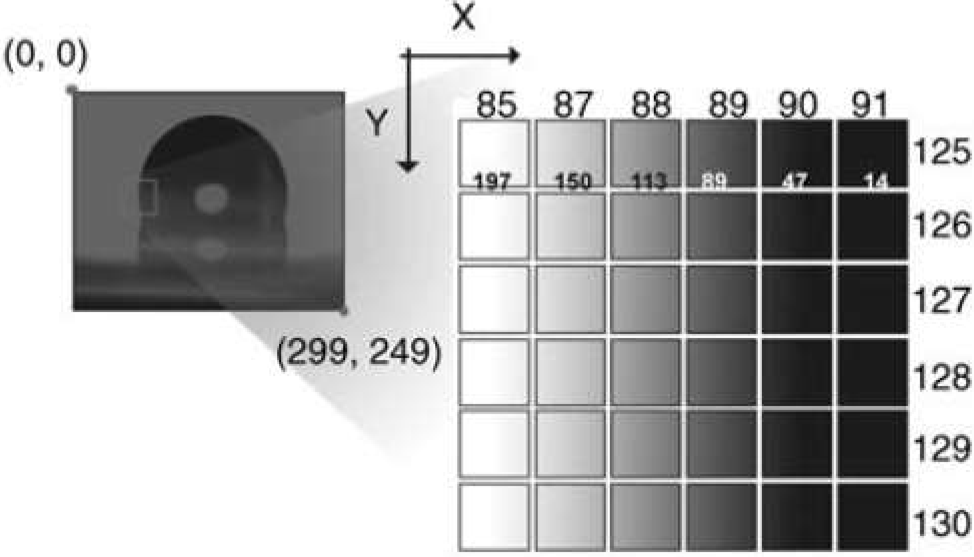

Figure 2.10: Grayscale image. A 300 x 250 pixels image is shown. Magnification shows a part of the image. The values in the pixels indicates its corresponding brightness with a value 0 being black and 255 representing white. [15].

2.2.3 Binary image

A pixel of a binary image can have only two different values, 0 and 1. It is often called a 1-bit image that means the image has a bit depth of 1 (2^1). The binary image is usually

Tesis publicada con autorización del autor
No olvide citar esta tesis

used to find the existence, size information or location of an object, where, usually, the object has the value of 1 and the background the value of 0.

2.2.4 Color image

In a digital color image, the image pixel is usually represented by a combination of three colors: R (red), G (green) and B (blue). The 24 or 32-bit images are usually used for the digital color images. In a 32-bit image, 8 bits (values from 0 to 255) are used for the R, G and B components and the other 8 bits are commonly unused [15] . The Figure 2.11 shows a color image.

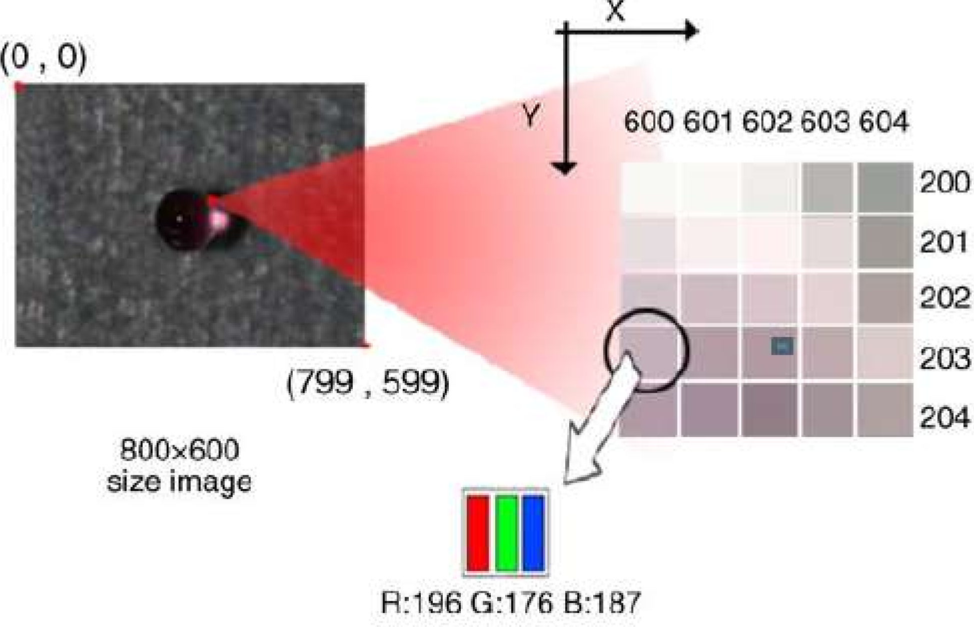

Figure 2.11: Color image. The values for R,G and B varies from 0 to 255. The selected pixel has different values for each color, Red:196, Green:176, and Blue:187. This combination generates the color of the selected pixel [15].

2.2.5 Image resolution

The resolution of a camera system can be defined as the smallest detail of the object which can be recognized by the camera. This characteristic is important because it is related to the accuracy for the measurements performed using the camera system.

According to Kwon [15], the image resolution can be determined by the Equation 2.20.

$$Resolution = \frac{2(FOV)}{number\, of\, camera\, pixels\, in\, one\, direction} \tag{2.20}$$

Where FOV (Field of View) is the physical dimension that the image represents.

Tesis publicada con autorización del autor
No olvide citar esta tesis

2.2.6 Region of interest (ROI)

The region of interest (ROI) is a part of the image that has a particular interest for the processing tasks. A ROI saves a specific location in an image [16]. An example for the ROI is shown in Figure 2.12. It shows a license plate with a defined ROI around the characters. It is used in order to facilitate the optical recognition of the characters.

Figure 2.12: Region of interest (ROI). Car license plate with a defined ROI [16].

2.3 Visual tracking applications in characterization and manipulation of micro and nano materials

Visual tracking enhances the development of precise automated systems for measurements and manipulation of micro and nanomaterials. The precise alignment of objects and instruments is an fundamental task for handling and measurement of objects or samples in the micro and nanoscale. The positioning of objects is acquired by processing images due to its higher accuracy in comparison to manual manipulation [4]. In the present section, the most recent works in visual tracking applications in nano- and microscale are presented.

2.3.1 Vision tracking for resistivity measurement in nanomaterials

Ru et al. [17] developed an automated four-point probe measurement system inside a Scanning Electron Microscope (SEM). In this work, the four-points probe method to measure the resistivity, described in Chapter 2, is implemented in the nanoscale. For that purpose, four nanomanipulators are installed inside a SEM as can be seen in Figure 2.13.

The probes are recognized and identified through a sequence of image processing operations. The areas surrounded by the contours are compared to distinguish the probes. The centroids of the probe's contour positions are used to distinguish each probe from another. The highest or lowest point of the probe's contour determines the position of each tip. Figure 2.14 shows the visual recognition of probes developed by Ru et al.

In that work, the tracking of each probe's position is achieved using an algorithm called sum of squared differences (SSDs). The system recognizes the coordinates of each tip

Tesis publicada con autorización del autor
No olvide citar esta tesis

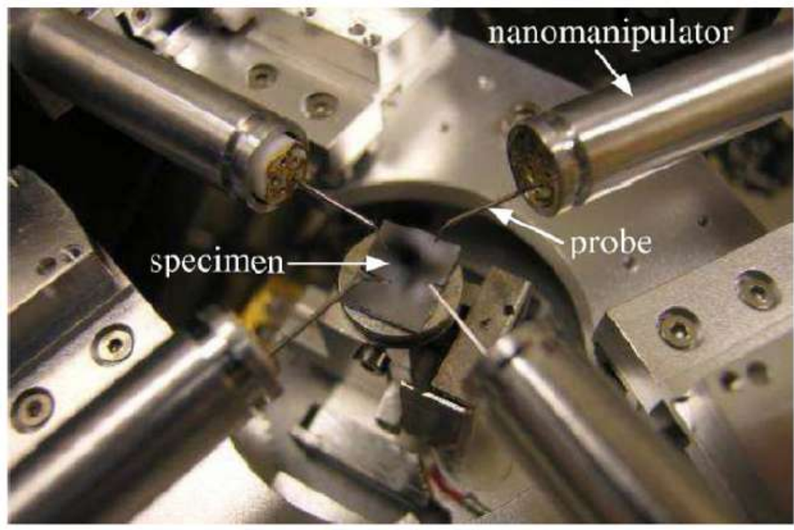

Figure 2.13: Four manipulators with probes used four resistivity measurement [17].

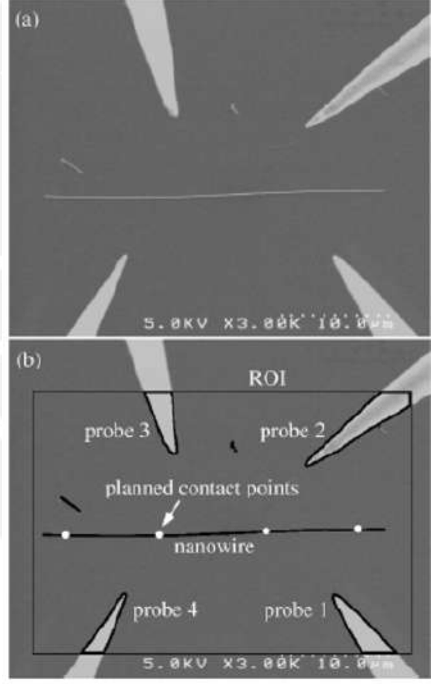

Figure 2.14: Visual tracking in four probes method proposed by Ro. a. Four probes b. Probes and nanowires are recognized using image processing techniques [17].

(x,y) and saves a rectangular image of the tip (ROI). The SSD value is calculated for each displacement of the probes. The displacement that produces the minimum value of SSD is considered to be the probe's displacement [17].

The L4P is applied for the measurement of the resistivity. The system determines the position of each probe along a line. Afterward, they are placed in their target position as can be seen in Figure 2.15.

Tesis publicada con autorización del autor
No olvide citar esta tesis

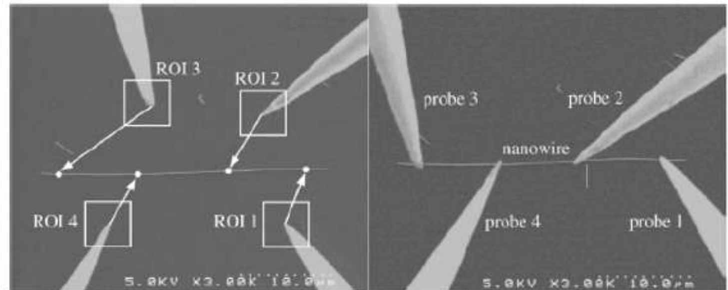

Figure 2.15: Visual tracking in linear four probes method proposed by Ro. a. Four probes being placed in their target position b. Probes situated on target position [17].

2.3.2 Vision tracking for nanorobotic manipulation

A variety of algorithms for visual tracking and recognition of objects have been developed for nanorobotic manipulation. In this scale, generally, the images are obtained with a SEM [6]. The algorithms can be divided into feature-based and model-based approaches [4]. The selection of an algorithm for a certain application depends on many factors such as the characteristics of the camera, noise levels, non-linearities and computational complexity.

2.3.2.1 Feature-based tracking approaches

The feature-based algorithms track specific visible features or details in the images. The most used algorithms are cross-correlation and active contours, that are explained more in detail in the following section.

Cross-correlation is an algorithm implemented to track an image using a pattern matching technique [18]. The goal of this technique is to find specific features in an image that match a predefined image template known as the pattern.

The cross-correlation coefficient is calculated considering the image and pattern matrices. The highest value of this coefficient, in a specific coordinate, indicates the position where the pattern match with the image as can be seen in Figure 2.16. The formulation of cross-correlation for 2-D images is presented in the next section in Equation 2.21. This algorithm can track a vast range of different objects when they have sufficient details to be recognized. Additionally, it can be applied to noisy images acquired at a high scan speed. The disadvantages of this method are the high computational cost required and the difficulty to track a variance, rotation or magnification of the object's shape [19].

Gharav [20] proposed a matching algorithm to find the best match by reducing the number of matching candidates using the results of an initial coarse search. Sievers [19] applied this technique for vision tracking in a SEM with a high level of noise.

Active contours is a method that consists of fitting a contour around the tracked object. The contour is formed by several splines. The principal advantage of this method is the capacity to track the rotation, deformation, and magnification of an object. Fatikow [21] implemented vision tracking inside a SEM proposing an active contour

Tesis publicada con autorización del autor
No olvide citar esta tesis

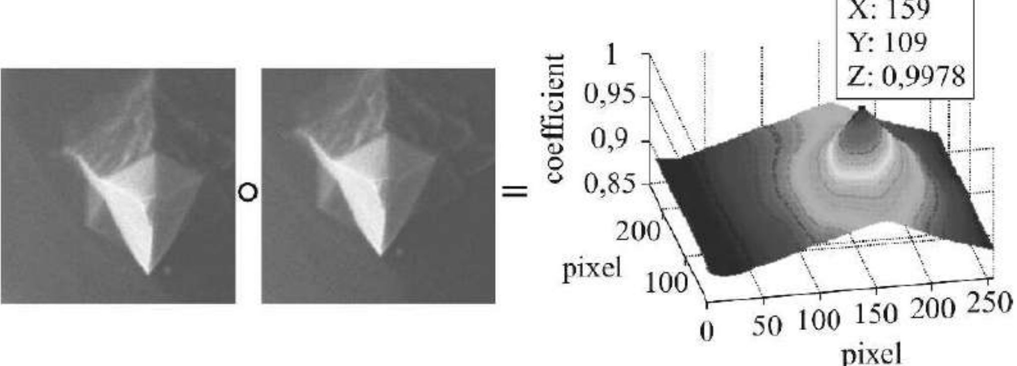

Figure 2.16: Cross-correlation coefficient between an image and a pattern. Displacement between the input image (left) and pattern (middle) is estimated by the cross-correlation matrix [19].

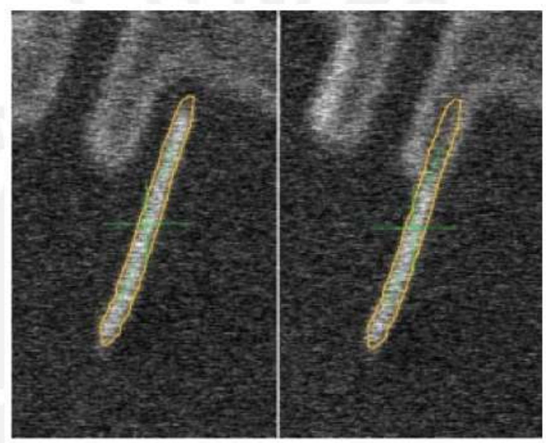

Figure 2.17: Active Contour tracking in a SEM proposed by Fatikow [21].

approach with region-based minimization. Figure 2.17 shows the sequence of two images corresponding to the tracking of carbon nanotubes having a diameter of 500 nm.

2.3.2.2 Model-based tracking approaches

The model-based tracking algorithms determines the object position in an image using the pre-existing knowledge of its geometry and possible displacements. Yesin and Nelson [22] presented an alternative method for visual tracking of micro components using a CAD model with a multi-camera vision approach. Kratochvil [23] defined a rigid-body model of the objects for manipulation tasks. The rigid-body models provide more precise motion feedback to apply a model-based algorithm.

Tesis publicada con autorización del autor
No olvide citar esta tesis

2.4 Matching patterns algorithms

The LabVIEW Vision tools are based on cross-correlation algorithms, for this reason, and considering the advantages of using this technique demonstrated by other works; the visual tracking system in this work will be implemented using cross-correlation algorithms. The theory and formulations for most used cross-correlations algorithms will be presented in this section: Basic, normalized and pyramidal matching.

2.4.1 Cross-correlation

The correlation process consist of moving the template or pattern image, p, over the input image area I (provided by the camera), then a correlation value, C, is calculated. Each pixel in the template or pattern is multiplied by the image pixel that it overlaps, then, the results over all the image pixels are summed. The maximum value of C indicates the position where p best matches I [24].

The Equation 2.21 represents the correlation between the pattern $p(x, y)$ and the input image $I(x, y)$ at the point (i, j). The pattern have a size of axb and the image, AxB. The summation is performed in the area of the image where p and I are intersected [24]. Figure 2.18 represents the correlation procedure between the image I and the pattern image p.

$$C(i,j) = \sum_{x=0}^{a-1} \sum_{y=0}^{b-1} p(x,y)\; I(x+i, y+j) \tag{2.21}$$

where i=0,1,2...A-1, j=0,1,2...B-1.

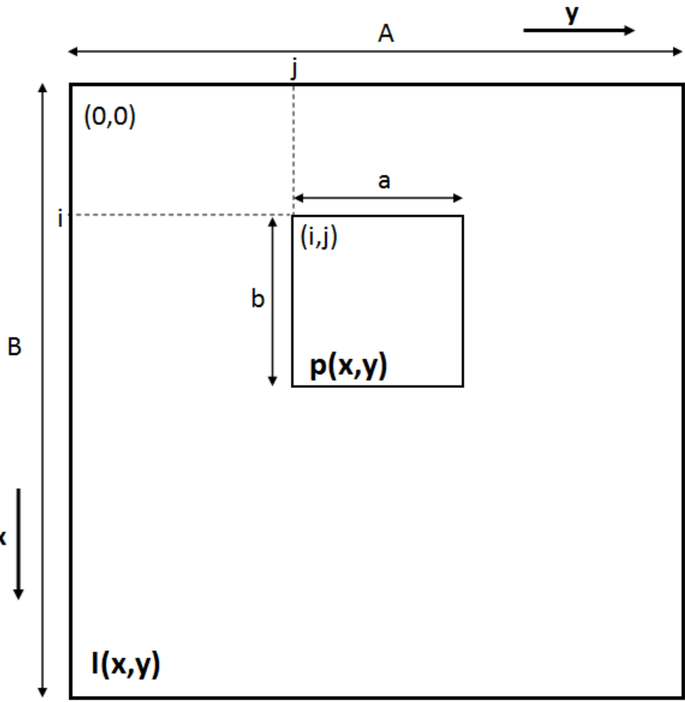

Figure 2.18: Cross-correlation procedure between the pattern p and the input image I. [24].

Tesis publicada con autorización del autor
No olvide citar esta tesis

Figure 2.19 shows the application of the cross-correlation algorithm to determine the position and track a probe to measure the resistivity.

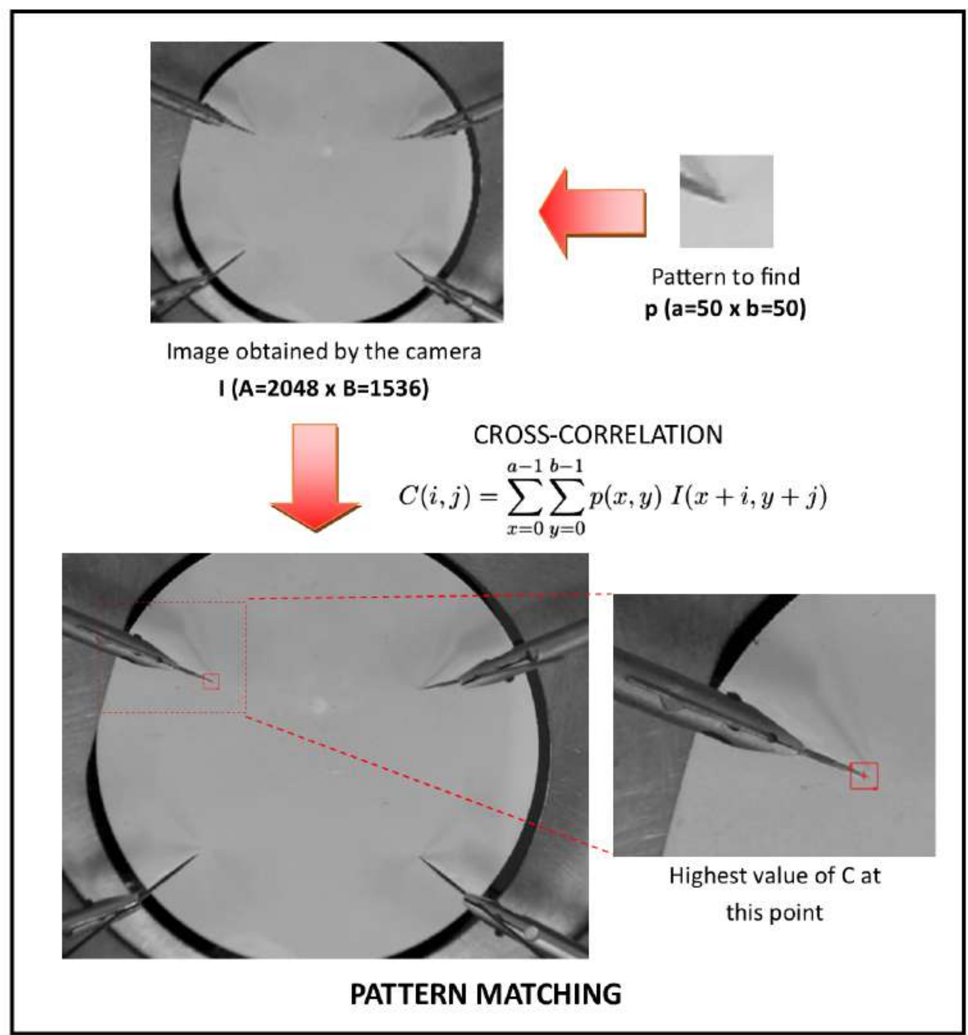

Figure 2.19: Cross-correlation application in the visual tracking system. Cross-correlation between the pattern p (probe 1) and the input image acquired by the digital camera I.

2.4.2 Normalized cross-correlation

Normalized Cross-Correlation is the most common method for pattern matching [24]. This method overcomes some constraints of the basic cross correlation, e.g. the high sensitivity to changes in the input image. The disadvantage of the normalized method is the higher computational time required. In order to reduce the computational time, the image size and the region of interest can be reduced. The normalized cross-correlation is defined by Equation 2.22.

$$R(i,j) = \frac{\sum_{x=0}^{a-1}\sum_{y=0}^{b-1}(p(x,y)-\overline{p})(I(x+i,y+j)-\overline{I}(i,j)}{\sqrt{\sum_{x=0}^{a-1}\sum_{y=0}^{b-1}(p(x,y)-\overline{p})^2}\sqrt{\sum_{x=0}^{a-1}\sum_{y=0}^{b-1}(I(x+i,y+j)-\overline{I}(i,j))^2}}) \quad (2.22)$$

Where $\overline{p}$ is the average value of intensity of the pixels in the pattern image p and $\overline{I}$ is the

Tesis publicada con autorización del autor
No olvide citar esta tesis

average value of I in the region that coincides with the current position of p.

2.4.3 Pyramidal matching

Pyramidal matching reduces the time of computation compared to the traditional pattern matching algorithms. In this method, the size of the pattern and the input images are reduced applying Gaussian Pyramids, as can be observed in Figure 2.20. The cross-correlation algorithm is executed first in the reduced images requiring a shorter time; and then, only the areas with higher values of the correlation coefficient are considered for the cross-correlation calculation in the original image [24].

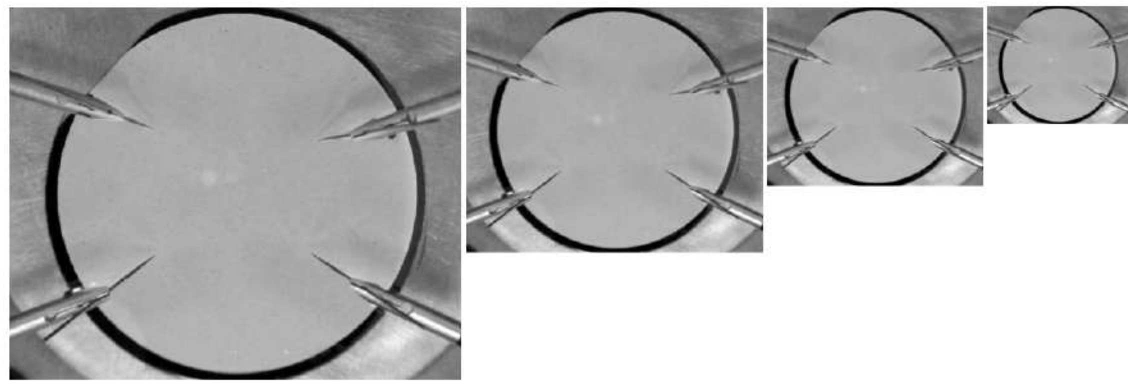

Figure 2.20: The size of the pattern and the input image are reduced applying Gaussian Pyramids for a preliminary faster computation of the cross-correlation algorithm.

Tesis publicada con autorización del autor
No olvide citar esta tesis

Chapter 3

Implementation and operation of the measuring system

In this chapter, the implementation and operation of the measuring system are explained in detail. First, the equipment and software that comprises the measuring system are presented. Then, the corresponding programs to apply the four different methods to measure the resistivity in thin films are described: Van der Pauw, Linear Van der Pauw, Linear Four Probes and Square Four Probes. The program presents particular steps and functions for each method.

A camera-based visual tracking system is implemented. The visual tracking system comprises several functions e. g., the program is able to indicate the correct positions (linear or square) to place the probes, check the correct probe's alignment, apply the corresponding geometrical correction factors and calculate the distances and areas formed by the probes positions. The design of implementation of these functions is detailed in the present chapter. Finally, the procedure followed to prepare the thin films samples of both, aluminum and tungsten is shown.

3.1 Setup of the measuring system

3.1.1 Hardware

The measurement system comprises a computer running a LabVIEW program that controls a Keithley 2400 Sourcemeter to output current, two multimeters Keithley 2000 and 2001 to measure current and voltage at the sample, respectively, and a switch equipment Keithley 7001 that changes automatically the pathway in the electrical circuits to use the probes either for sourcing current or voltage measurement. All this equipment works with an NI GPIB USB HS+ adapter developed by National Instruments that allows the communication between the Keithley instruments and the LabVIEW program. The system also has a digital microscope camera that assists with the measurement and determination of the probe's position for the visual tracking system. The Figure 3.1 shows a schematic diagram of system's hardware.

3.1.1.1 Equipment characteristics

Table 3.1 presents the characteristics of the equipments that integrates the measuring system.

Tesis publicada con autorización del autor
No olvide citar esta tesis

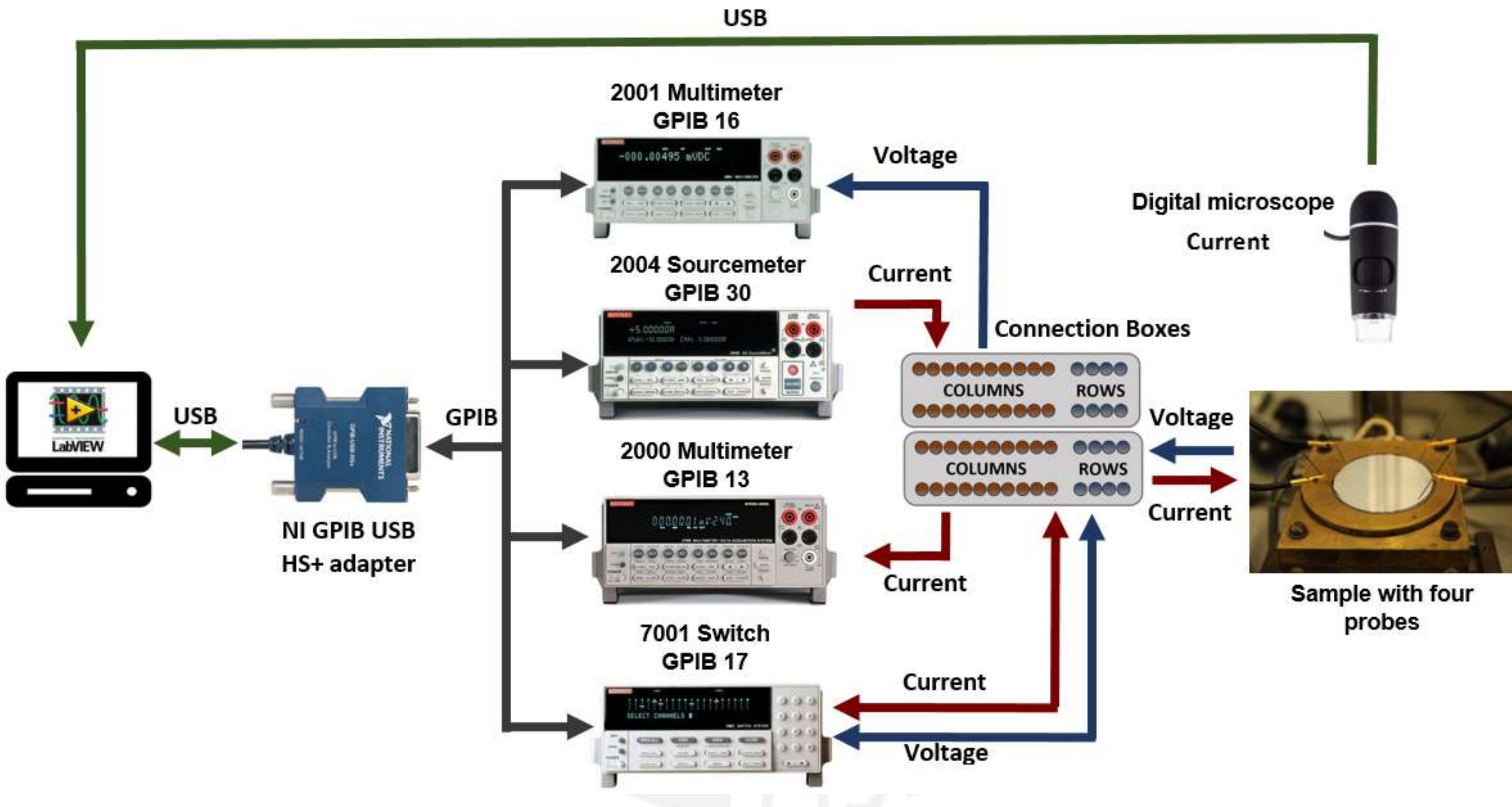

Figure 3.1: Schematic diagram of the system's hardware. A LabVIEW program controls the Keithley equipments. The Keithley instruments are connected to two connection boxes, which distributes the current and voltage signals between the probes via the switch equipment. The digital camera assists with the visual tracking system. [26–29]

Tesis publicada con autorización del autor
No olvide citar esta tesis

Table 3.1: Equipments of the measurement system

Instrument	Description
Keithley 2400 SourceMeter (GPIB 30)	This sourcemeter provides high precision voltage and current with a 6 1/2 resolution. It has an integrated multifunction of voltmeter and ampmeter that works with a GPIB interface [26].
Keithley 2000 Multimeter (GPIB 13)	Provides 6 1/2 digit resolution measurement. Works with GPIB and RS-232 interfaces. It measures DC voltage from 100nV to 1000V and DC current until 3A. [27].
Keithley 2001 Multimeter (GPIB 16)	Provides 7 1/2 digit resolution measurement with high speed and accuracy combined with a multiple measurement display and a GPIB interface. It measures DC voltage from 10nV to 1100V, and DC current from 10pA to 2.1 A [28].
Keithley 7001 Switch System (GPIB 17)	Two-slot mainframe that switches signals from nanoVolts to 1100V and femtoAmps to 5A. Each slot supports 40 channels [29].
Digital microscope camera	MicroCapturePro Camera provided by DNT with 5 MP of resolution including a led to illuminate the sample. It works with a 2.0 USB interface and provides a high magnification rate.
Manual Micropositioner	Manual Micropositioner Karl Suss PH100 (x4). Resolution: 5 μm. Travel Range: X:8mm, Y:6mm, Z:25mm.
NI GPIB USB HS+	NI GPIB USB HS+ National Instruments adapter that convert the USB port into a IEEE 488.2 controller able to connect until 14 programmable GPIB instruments.

Tesis publicada con autorización del autor
No olvide citar esta tesis

The switch equipment Keithley 7001 includes two cards 4x10 Matrix model 7012-S with screw terminals. The Keithley equipment and the probes are connected to these switching cards through two connection boxes as can be seen in Figure 3.2. The fourth and first rows join the input and output current, respectively. The second and third rows are connected to the high and low pole of the voltmeter, respectively. The first 4 columns are connected to the 4 probes.

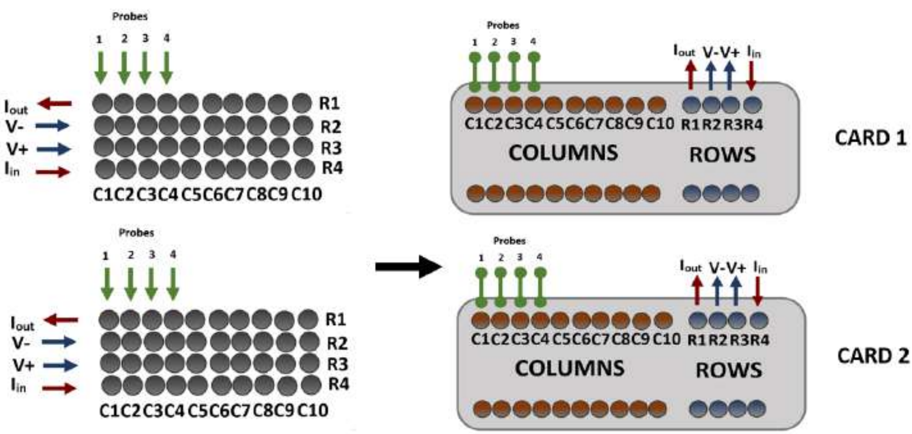

Figure 3.2: Connection boxes join the Keithley equipments and probes with the switch equipment.

Figure 3.3 shows a full view of the measurement system hardware. Figure 3.4 shows the distribution of the four probes placed at the boundary of the sample when Van der Pauw method is applied. The sample has a thickness of 600 nm and a diameter of 2 inches.

3.1.2 Software

The software of the system was developed with the graphical programming software LabVIEW that provides characteristics for controlling the measurement system's hardware. Furthermore, a state-based program was developed with the LabVIEW Statechart Module. This LabVIEW module provides features that facilitate the design of applications taking advantages of states, events and transition, like a flowchart design.

Tesis publicada con autorización del autor
No olvide citar esta tesis

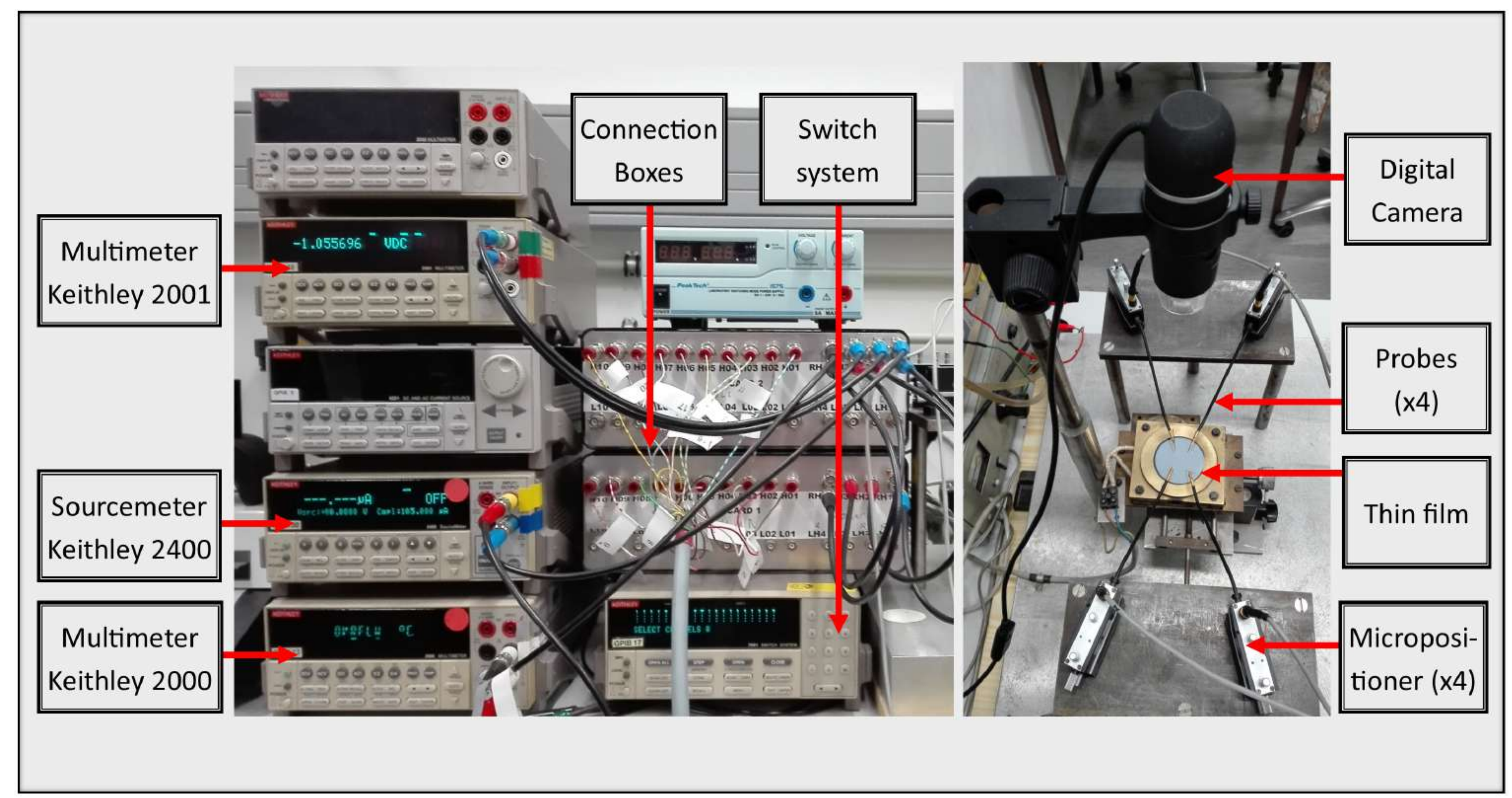

Figure 3.3: Full view of the measurement system's hardware.

Tesis publicada con autorización del autor
No olvide citar esta tesis

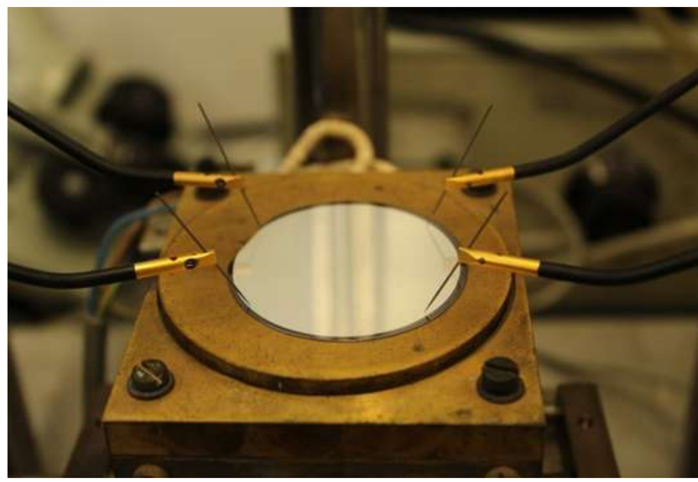

Figure 3.4: Probes distribution in Van der Pauw method. Circular sample of aluminum of 2 inches having a thickness of 600 nm

3.2 Graphical User Interface and Statechart

The Graphical User Interface (GUI) can be seen in Figure 3.5. In this section, each part of the GUI will be described. Figure 3.6 shows the StateChart design of the program.

The first step in the program consists of verifying the electrical continuity between the probes and the sample using the function **VERIFY PROBES**, which is shown in Figure 3.7. This step is important in order to avoid errors in the measurements caused by the electrical discontinuity between the probes and the sample. The system applies a current between each pair of probes and measure it to calculate the error. If the error is lower than the tolerance value, the electrical continuity is confirmed and a LED is lightened indicating the correct continuity for each probe. This method is good for conductor materials, but in a future work there should be considered other methods, in special for non-conductive materials, since they could be damaged by the application of the current. The user can select the value of the verification current value in mA, and the tolerance (%). When the electrical continuity is checked, the four LED's are lightened and the user can continue with the measurement.

Tesis publicada con autorización del autor
No olvide citar esta tesis

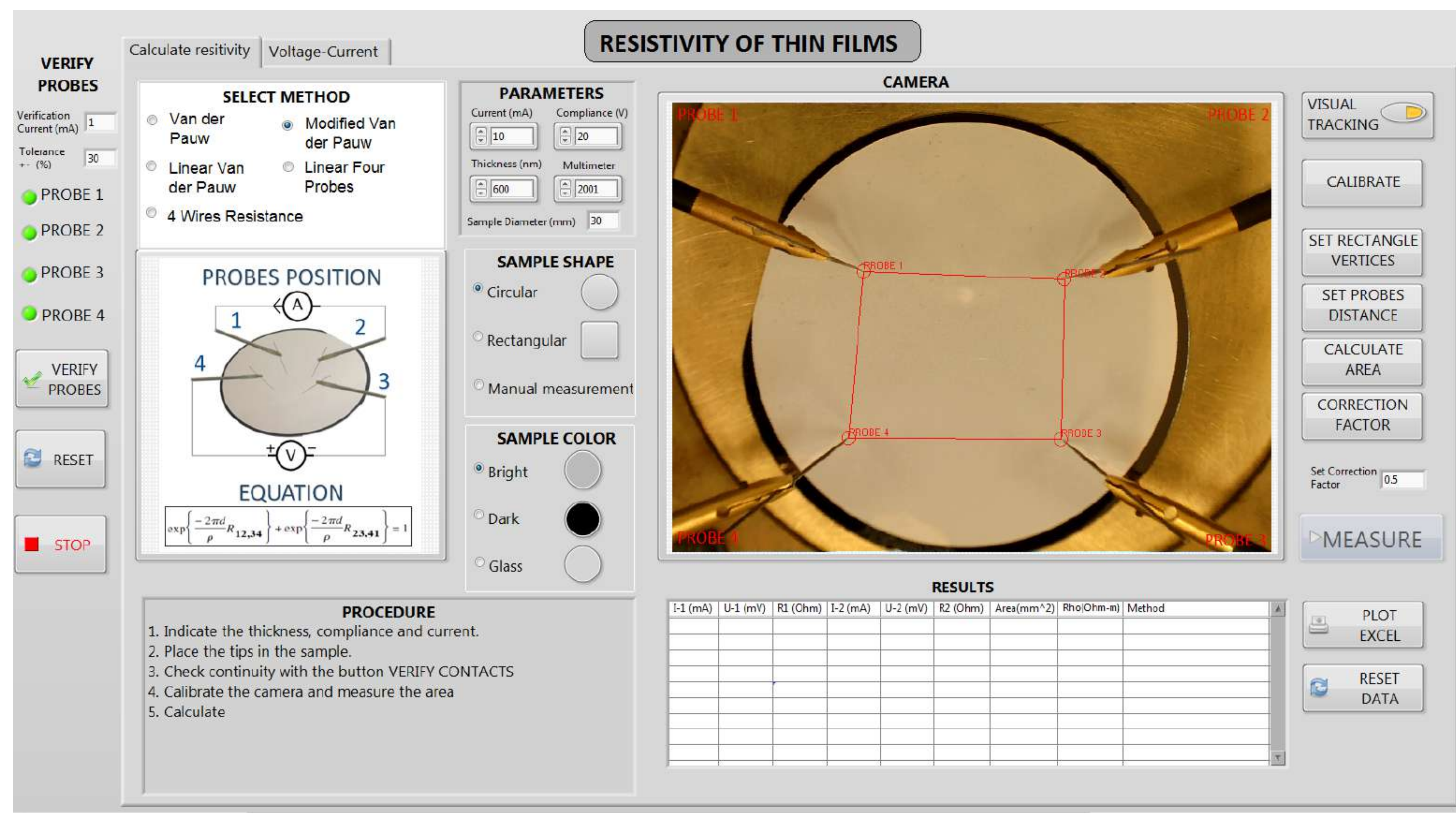

Figure 3.5: GUI of the system software developed with LabVIEW.

Tesis publicada con autorización del autor
No olvide citar esta tesis

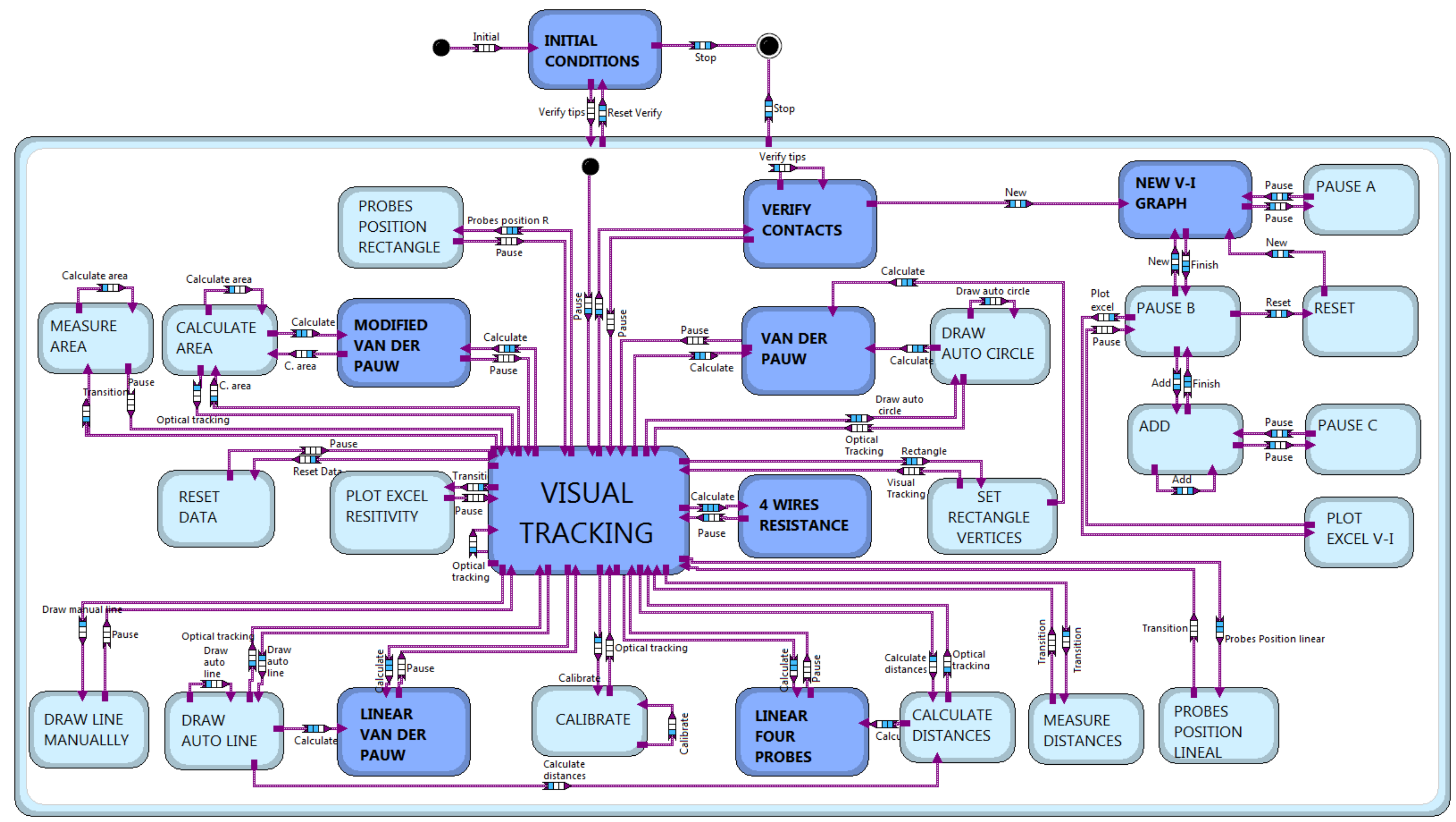

Figure 3.6: State chart of the system's program.

Tesis publicada con autorización del autor
No olvide citar esta tesis

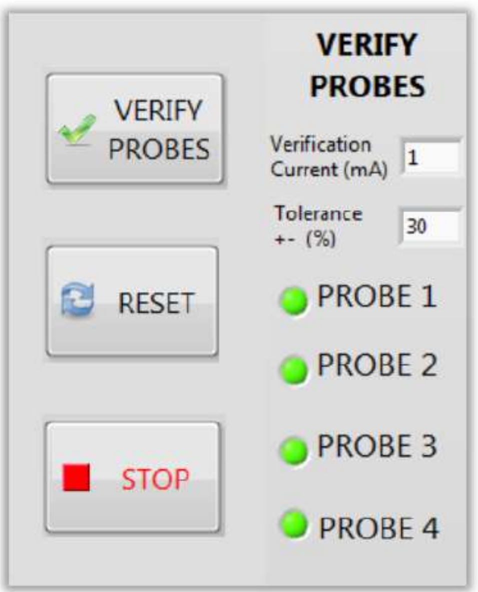

Figure 3.7: *Verify Probes* function. Verifies the electrical continuity between the four probes and the sample.

The next step consist of selecting one of the four different methods to measure the resistivity in the section shown in Figure 3.8. Additionally, a function to measure the resistance using four wires was implemented. Each method is represented by a schematic probes configuration and its corresponding equation. Figure 3.9 shows a schematic representation of the particular probes configuration for each method.

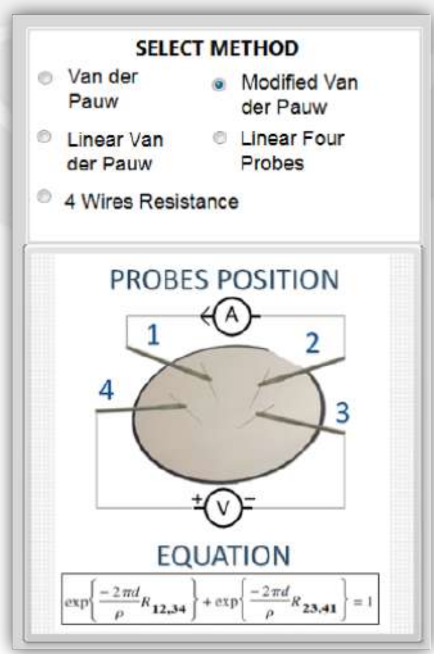

Figure 3.8: *Select Method* section. The user can select one of the four different methods to measure the resistivity as well as a simple four wire measurement to measure the resistance.

Tesis publicada con autorización del autor
No olvide citar esta tesis

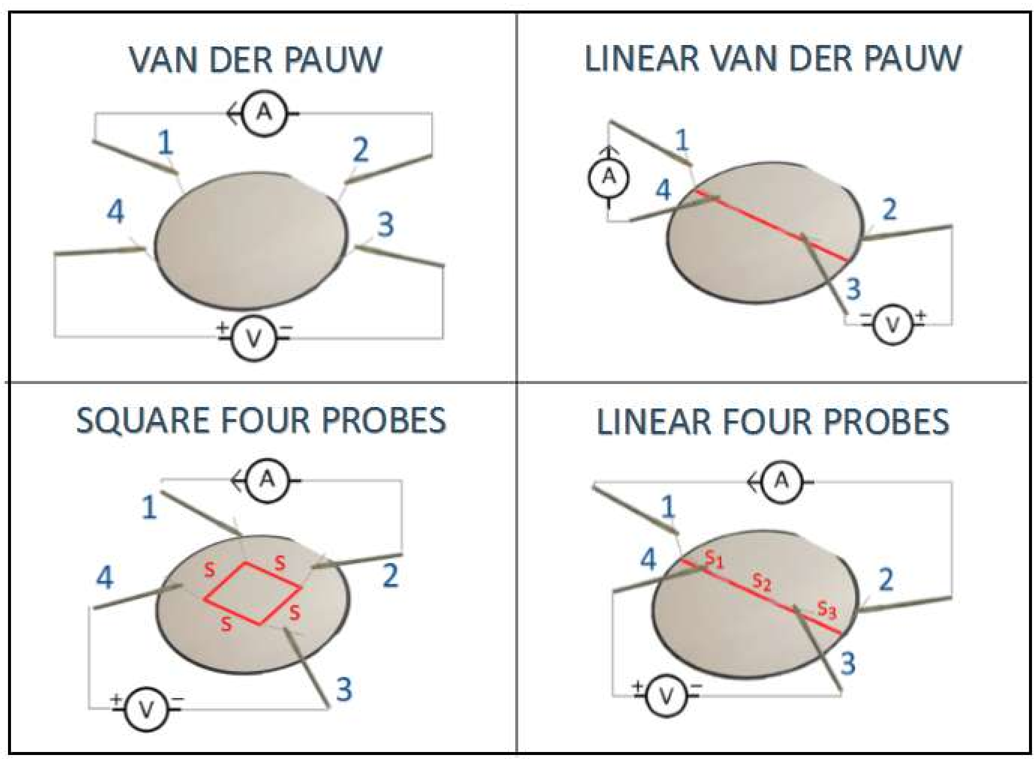

Figure 3.9: Schematic representation of the four different methods to measure the resistivity.

The next section corresponds to the configuration of the measurement parameters. It contains three subsections: **PARAMETERS**, **SAMPLE SHAPE** and **SAMPLE COLOR** as can be seen in Figure 3.10.

In PARAMETERS section, the user sets the Current (mA), the multimeter compliance (V), which is the maximum voltage the current source will reach sourcing the desired current; the sample's thickness(nm), the multimeter model and the diameter of the sample (mm).

In SAMPLE SHAPE section, the user sets the shape of the sample: Circular, Rectangular or Manual Measurement. Some functions depends on the sample shape e.g., the correction factors. The Manual measurement can be used when the sample is neither circular nor rectangular; in this case, some data (e.g., correction factors) will be enter manually.

In SAMPLE COLOR section, the user indicates the brightness of the sample. It is important because the recognition of the probes in the visual tracking system is based on the contrast of the probes with respect to the sample, which changes when the sample brightness varies. The system present three cases: Bright as in the case of an aluminum samples, Dark, as in the case of a tungsten samples or glass.

Tesis publicada con autorización del autor
No olvide citar esta tesis

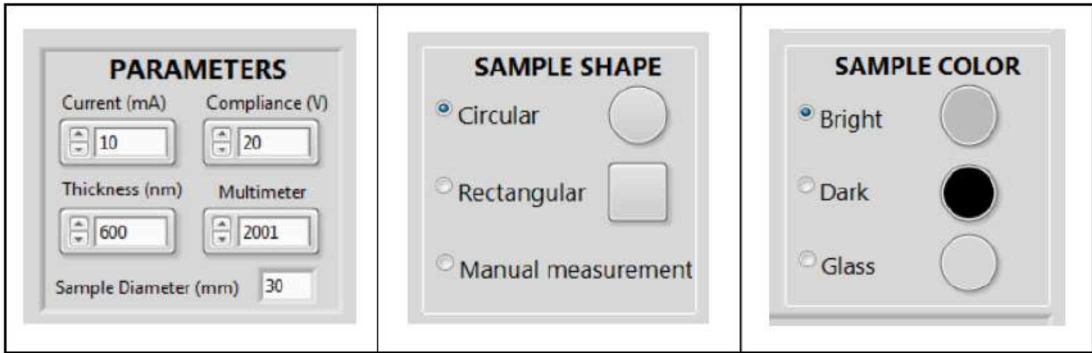

Figure 3.10: Configuration of the parameters for the measurement.The user set the parameters and indicates the sample's shape and color

The next part is the **CAMERA WINDOW** and the **FUNCTION BUTTONS** as can be seen in Figure 3.11. The CAMERA WINDOW shows a real-time image of the sample and the position of the four probes obtained from the digital camera. In this window, the visual tracking for the probes and more information according to the function is also shown; i.e. the symmetry lines, the area and the sample boundaries.

The FUNCTION BUTTONS are placed on the right side of the GUI. Each button represents a specific function of the software. Certain buttons are activated or deactivated for a particular measurement method. This section contains the Visual Tracking function and the MEASURE button to execute the resistivity measurement.

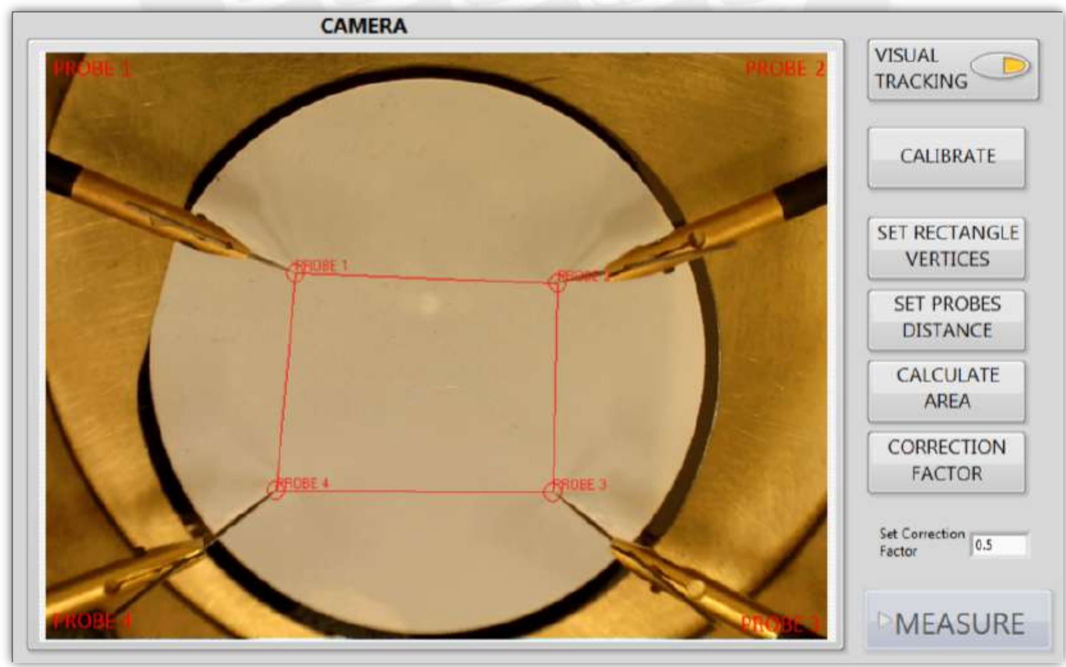

Figure 3.11: Display of the camera for visual tracking. Function Buttons are placed in the right side.

The **PROCEDURE BOX** section is shown in Figure 3.12. In this text box, the

Tesis publicada con autorización del autor
No olvide citar esta tesis

detailed steps the user must follow for each measurement method are indicated.

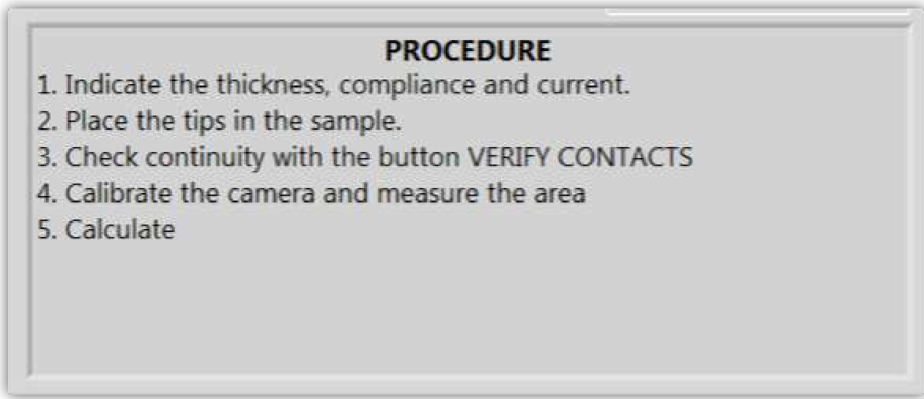

Figure 3.12: Procedure box. Show the steps the user must follow for each measurement method

The **RESULTS TABLE** is presented in the lower right side of the GUI and is shown in Figure 3.13. This table shows all the results data for each measurement. It includes the resistivity value and the most important parameters i.e. voltage, current, resistance and measurement method.

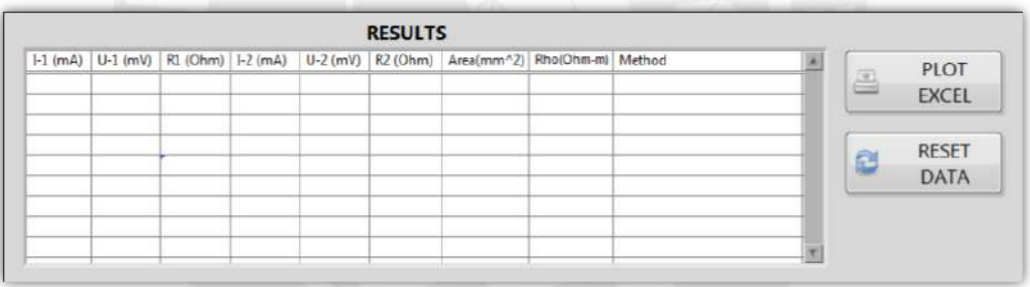

Figure 3.13: Results table. Show the results data for each measurement.

Each program function is represented by a button in the GUI. The Figure 3.14 shows all the functions of the program according to the corresponding method.

Tesis publicada con autorización del autor
No olvide citar esta tesis

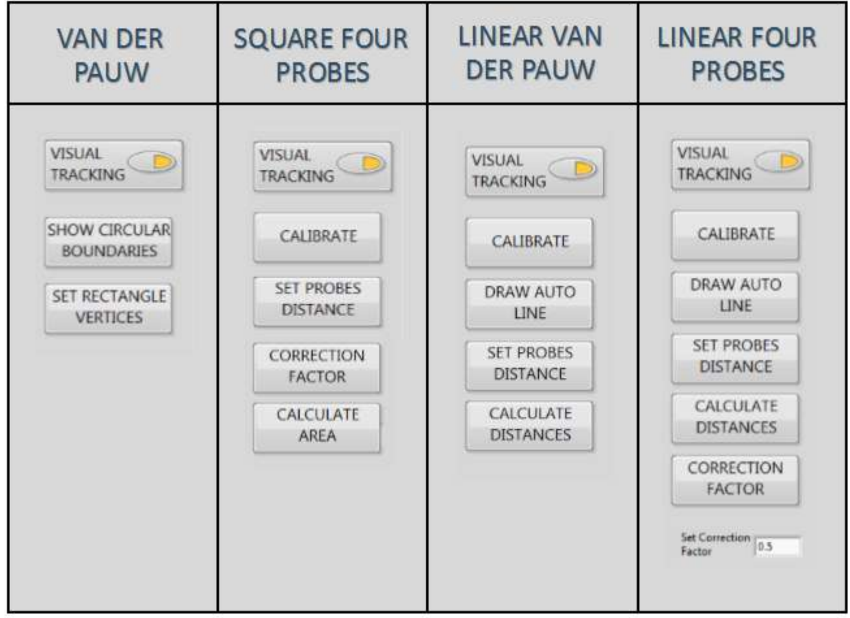

Figure 3.14: Buttons for each of the four different methods. The operation and design of each function will be explained in detail in the next sections of this chapter.

3.3 Camera system characteristics

The system uses a MicroCapturePro Camera provided by DNT, as can be seen in Figure 3.15. It has a resolution of 5 MP and can provide a 300x magnification. Additionally, it has a led illuminator that works with a 2.0 USB interface. The characteristics of the image obtained for the Visual tracking functions are:

- Image Resolution: 2048x1536
- Image type: 32-bit RGB

Figure 3.15: MicroCapturePro Camera.

Tesis publicada con autorización del autor
No olvide citar esta tesis

3.4 Real-time Probes Visual Tracking

A Visual Tracking system is implemented to determine the position of the probes during the measurement. A pattern matching technique was implemented using the VISION tool of LABVIEW. The Figure 3.16 shows the LabVIEW program designed for the visual tracking. The capital letters in the image represent a part of the program and are explained below the image.

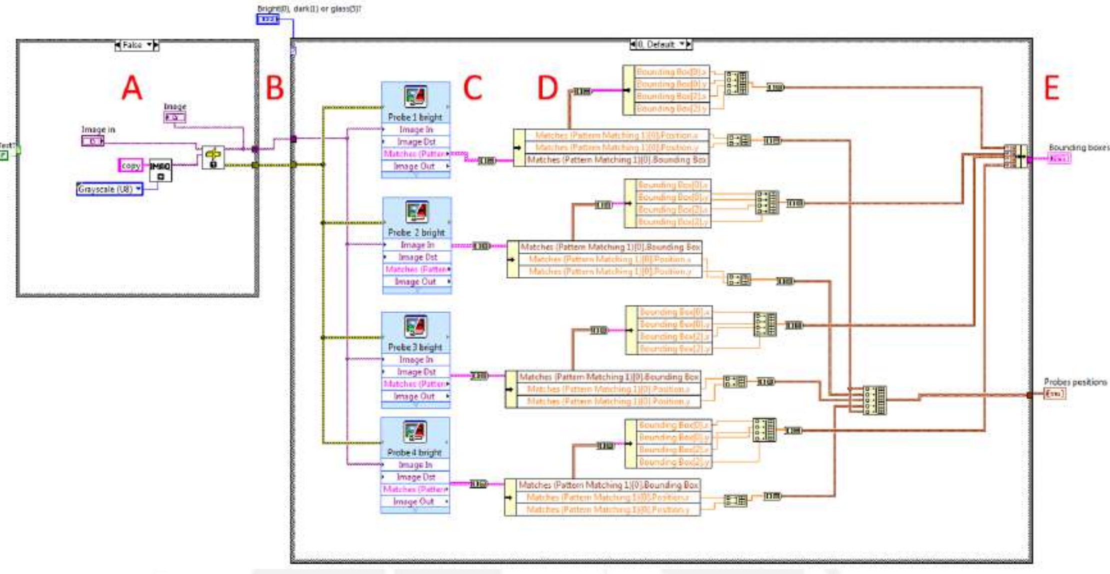

Figure 3.16: LabVIEW program for the Visual Tracking of the probes position.

- **A.** The image is obtained from the camera. The 32-bit RGB image is converted into a grayscale image using a Vision LabVIEW function.
- **B.** The user selects the color of the sample.
- **C.** The pattern matching is performed through the LabVIEW Vision Assistant. This part is detailed in the Figure 3.17. This function is applied to each probe and the probe's positions (in pixels) is obtained.
- **D.** The probe's positions are saved into arrays for the next applications.
- **E.** This program has two outputs: The probes positions array and the bounding boxes. They are the coordinates of the lines that indicates the probe's position on the screen.

Figure 3.18 shows the pattern images of the probes corresponding for each color of the sample (bright, dark and glass). Each image pattern has a size of 50x50 pixels. Figure 3.19 shows the parameters set for the matching pattern configuration in LabVIEW Vision Assistant. The selected method is the Pyramidal Matching technique because it provides good results for a shorter computational time.

Tesis publicada con autorización del autor
No olvide citar esta tesis

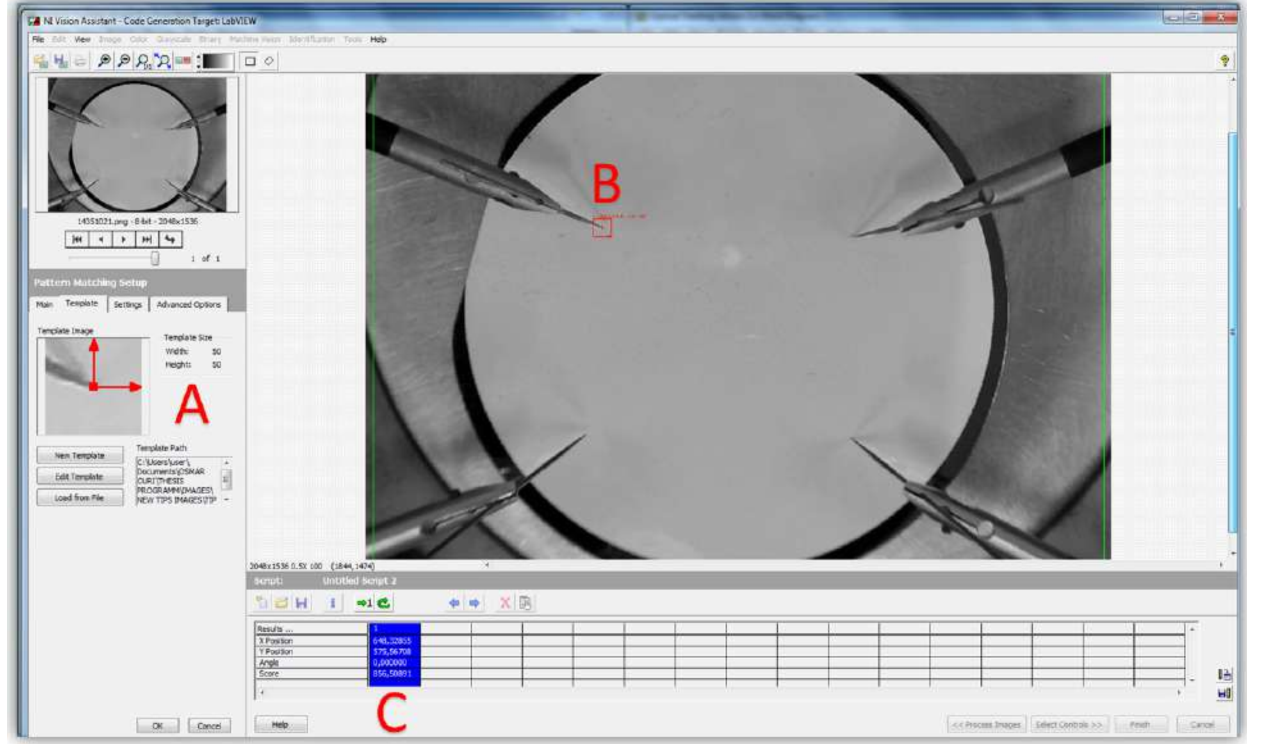

Figure 3.17: Visual tracking in the NI Vision Assistant for LabVIEW. This tool facilitates the application of the pattern matching algorithms.

A. The image pattern for each probe is set with the button *New template*. In this case, the pattern has a size of 50x50 pixels. The parameters for the pattern matching are set as can be seen in Figure 3.19.

B. The pattern (probe) is detected in the template image.

C. The matched pattern position (in pixels) is saved.

Tesis publicada con autorización del autor
No olvide citar esta tesis

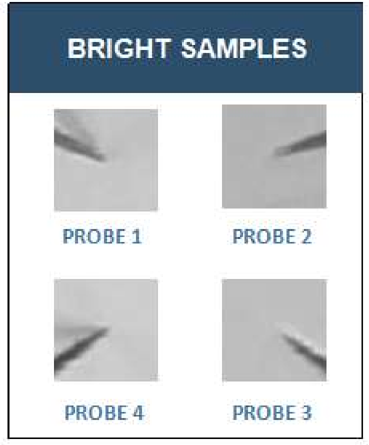

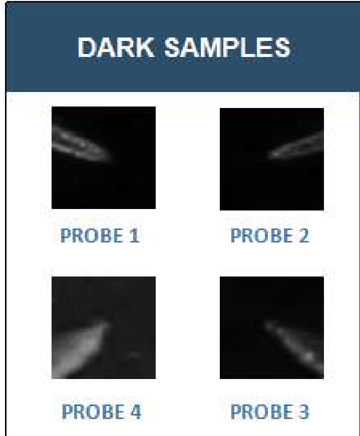

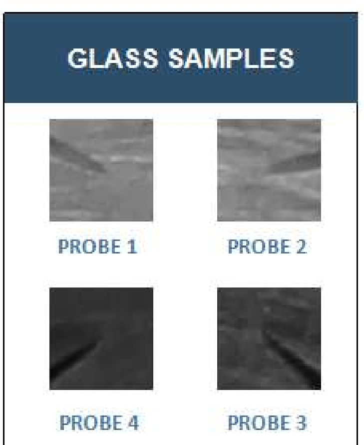

Figure 3.18: Patterns for the three different sample colors: Bright, Dark and Glass samples. Each Probe Pattern has a size of 50x50 pixels

As was explained in Chapter 2, the pattern matching algorithm is based on cross-correlation coefficient (score) calculation. The highest values of this score for a coordinate indicates the position of the desired pattern. The minimum score for the pattern matching algorithm is required in the LabVIEW configuration. The higher the minimum score is, the more time the system requires to find the position of the pattern. Therefore, this values must be optimized for each application. In this case, a score value of 800 is set because it is enough to detect the position of each probe in a short computational time.

Additionally, the system could be able to detect the probe even when the tip position is rotated. The detection of rotated pattern requires a higher computational time, for that reason the range of the angles must be not too large. In this case, the angle range for probe rotation is $\pm$ 20°.

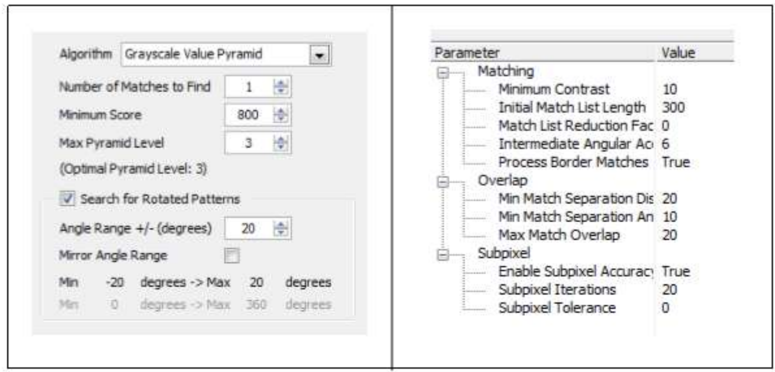

Figure 3.19: Configuration for the Matching Pattern in the LabVIEW Vision Assistant. The selected method is the Pyramidal Matching with a minimum cross-correlation coefficient (score) of 800 and an angle range for probe rotation of $\pm$ 20°

Tesis publicada con autorización del autor
No olvide citar esta tesis

3.5 Implementation of the resistivity measuring methods

3.5.1 Van der Pauw Method

In the VPM, the probes are placed at the sample's boundaries. In the GUI, the VPM is selected in the Select Method section as shown in Figure 3.20.

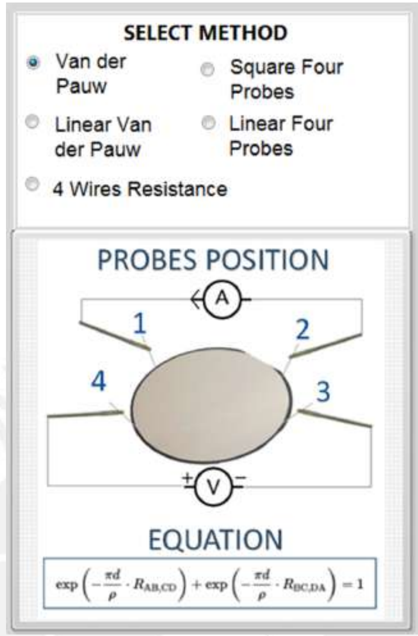

Figure 3.20: Selecting Van der Pauw Method in the GUI.

The next step consists of placing the probes at the boundaries of the sample as shown in Figure 3.20. The button SHOW CIRCULAR BOUNDARIES can be selected to visualize the area where the probes must be placed. After that, the current, compliance, thickness, multimeter and diameter of the sample are set in the respective selector boxes as shown in Figure 3.22. Then, the continuity between the probes is checked pressing the button VERIFY PROBES. When the 4 LEDs are lightened, the resistivity can be calculated pressing the button MEASURE.
The theory of the VPM is presented in detail in Chapter 2. The procedure to calculate the resistivity with the this method is the following:

1. Indicate the thickness, current and compliance for the Keithley instruments. The compliance is a safety limit value of voltage for the test.

2. Place the probes at the boundaries of the sample.

3. Check the electrical continuity with the button VERIFY PROBES and then, MEASURE.

Figure 3.24 shows the LabVIEW program designed for the VPM. The same program is also implemented for the LVP. Each step of the program's operation is indicated in the figure with capital letters, which are described in the following items.

A. The channels are closed in the switching equipment. As shown in Figure 3.24, the current is applied trough probes 1 and 2, and the voltage is measured between probes 3 and 4.

Tesis publicada con autorización del autor
No olvide citar esta tesis

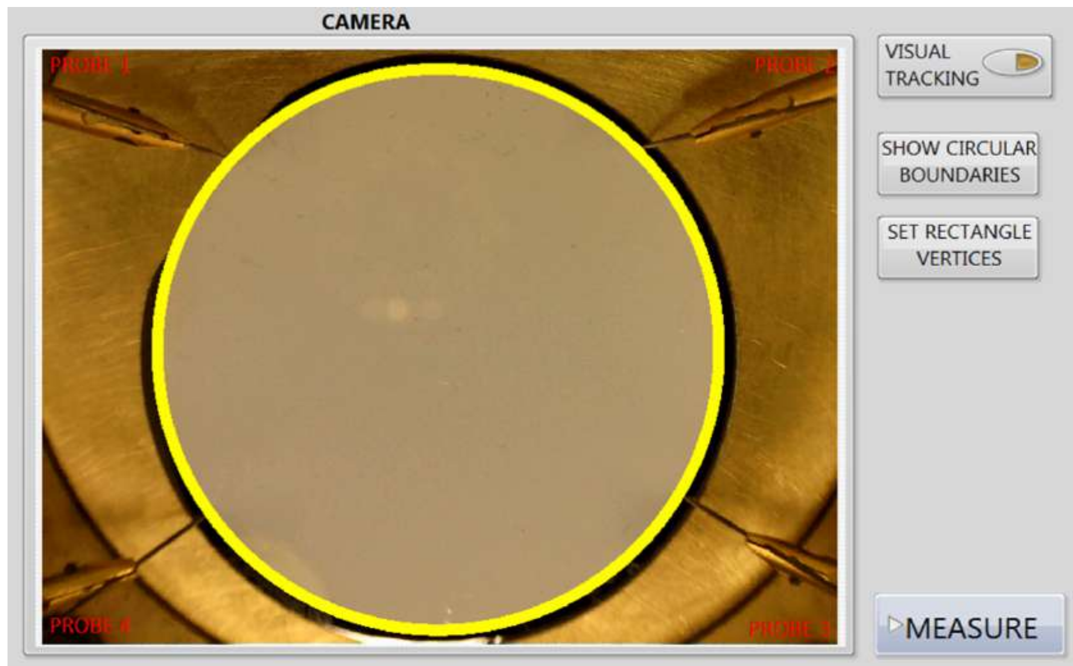

Figure 3.21: Configuration of the probes for Van der Pauw Method.

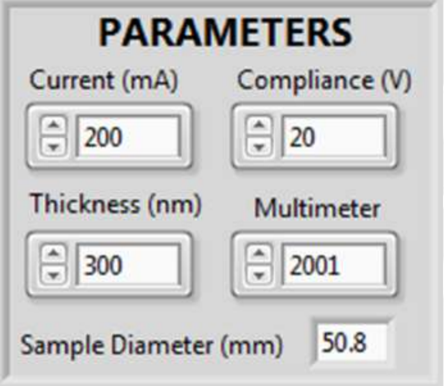

Figure 3.22: Parameters for Van der Pauw method measurements. Current, compliance, thickness, multimeter and diameter of the sample are set in the respective selector boxes.

B. The selected current is applied by the sourcemeter between probes 1 and 2.

C. The voltage and current are measured between pair of probes 1-2 and 3-4, respectively.

D. The sourcemeter is turned off and the channels in the switching equipment are opened.

E. The new configuration for the probes is set in the switching equipment: probes 2 and 3 for current, and 1 and 4 for voltage.

F. The selected current is applied by the sourcemeter between probes 2 and 3.

G. The voltage and current are measured between the pair of probes 1-4 and 2-3, respectively.

Tesis publicada con autorización del autor
No olvide citar esta tesis

H. The sourcemeter is turned off and the channels in the switch are opened.

I. The values are saved in an array.

The resistivity is calculated using the Van der Pauw equation presented in Equation 2.14. A LabVIEW program is designed to solve this equation through iterations, which is shown in Figure 3.23

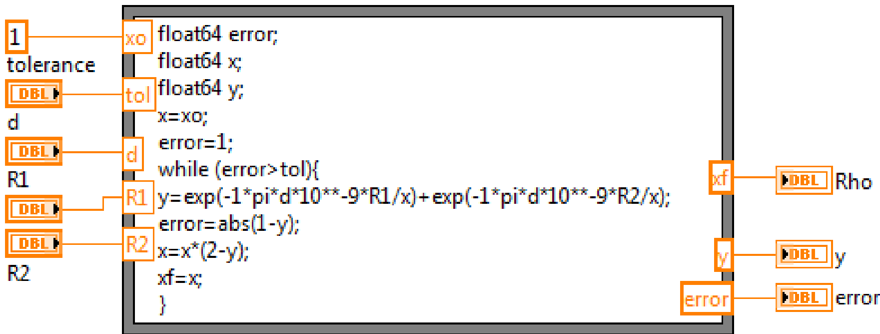

Figure 3.23: Program to solve the Van der Pauw equation by iterations.

Tesis publicada con autorización del autor
No olvide citar esta tesis

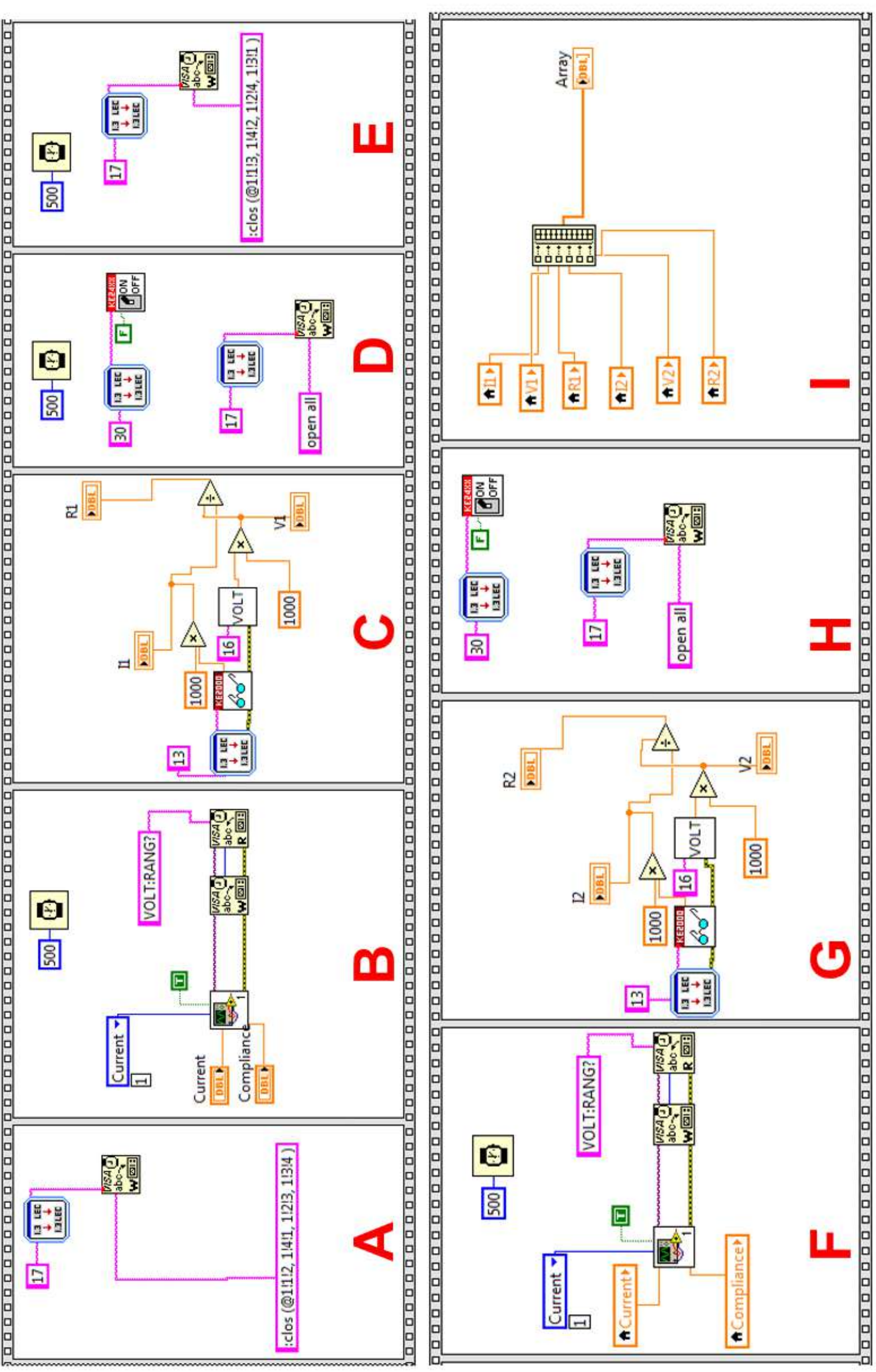

Figure 3.24: Van der Pauw Method - Lab VIEW program.

Tesis publicada con autorización del autor
No olvide citar esta tesis

3.5.2 Linear Van der Pauw Method

In the Linear Van der Pauw Method, the probes are placed on the sample along a symmetry line. Figure 3.25 shows the real-time image of the sample with the probes placed along a symmetry line. Furthermore, the corresponding buttons in the GUI for this method are presented.

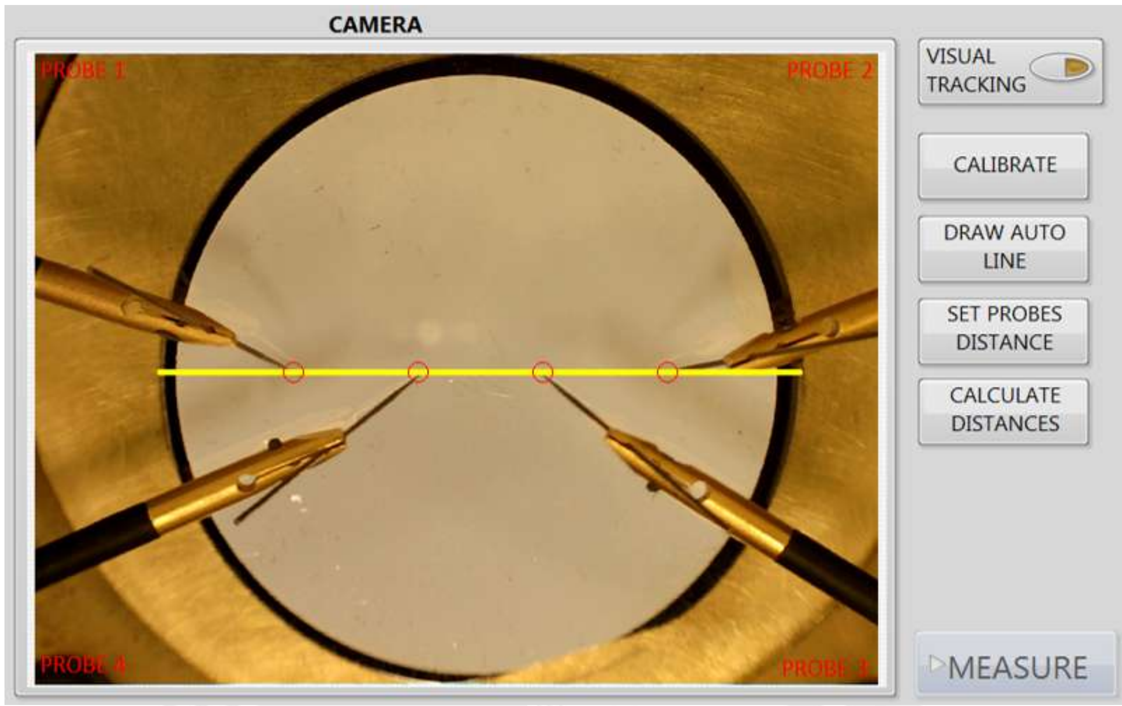

Figure 3.25: Probes configuration for Square Four Probes Method. The probes are placed along a symmetry line. The available buttons for this function are shown.

When the probes are placed, the current, compliance, multimeter, thickness and diameter of the sample are set in the PARAMETERS box following the same procedure executed in the previous methods.

Moreover, the continuity must be checked with the button VERIFY PROBES. In this method, the probes must be aligned along a symmetry line in the sample. For that reason, the button DRAW AUTO LINE is selected. The software detects the sample shape a draws a symmetry line on the sample. Finally, the button MEASURE is pressed to calculate the resistivity with this method.

3.5.3 Linear Four Probes Method

In the Linear Four Probes Method the probes are placed on the sample along a symmetry line. Besides, the probes must be placed equally spaced. The available functions for this method are shown in Figure 3.26. The user can select the desired distance for the probes spacing pressing the button SET PROBES DISTANCE. Then, four equally-spaced circles appear along the symmetry line. The user must place the probes into these circles. The VISUAL TRACKING function detects the positions of the probes and indicates the correct alignment of the probes. When the probes are correctly

Tesis publicada con autorización del autor
No olvide citar esta tesis

aligned, the user can MEASURE the resistivity with the respective button.

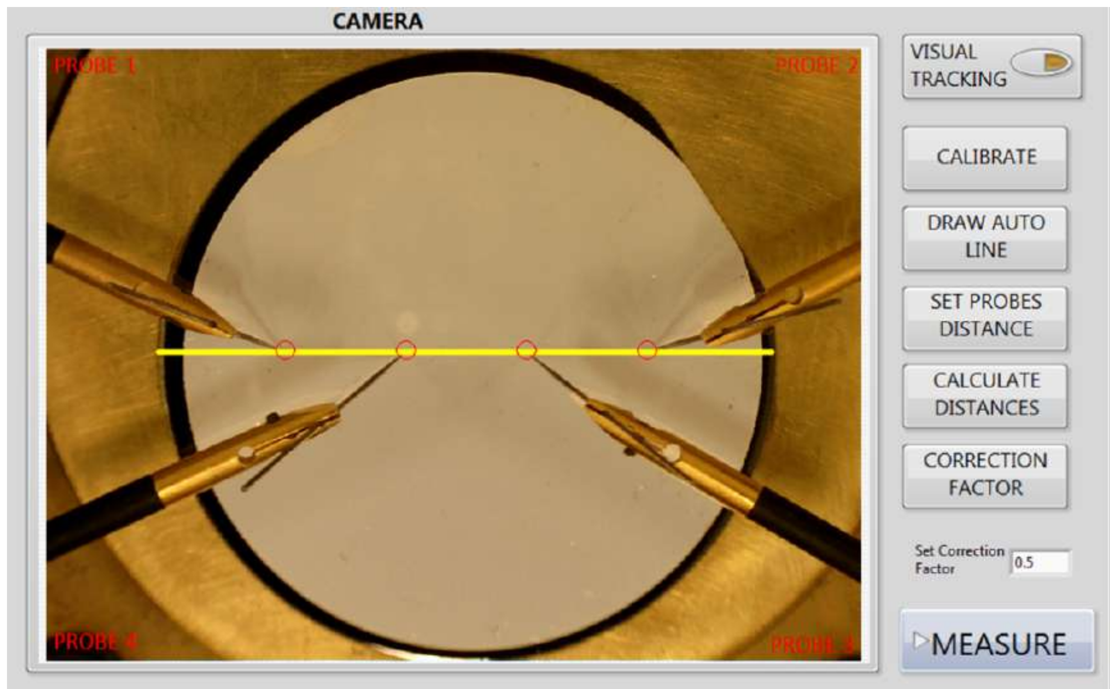

Figure 3.26: Probes configuration for Linear Four Probes. The probes are placed in a linear array configuration. The available buttons for this function are shown.

Then, the current, compliance, thickness and diameter of the sample are set in the PARAMETERS box. Moreover, the continuity between the probes must be checked with the button VERIFY PROBES. The correction factor is automatically calculated for this method.

Compared to the VPM, for this method, the probes must be placed forming a straight line on the sample and the equation only requires one measurement of voltage and current. In addition, the distances between the probes must be measured. Also, a correction factor must be considered for this method. Correction factors are detailed in Chapter 2.

When L4P is selected, two additional buttons appear in the GUI: DRAW SYMMETRY LINE and MEASURE DISTANCES. The first button allows to draw a symmetry line over the sample in the camera window. The probes must be placed in this line according to the configuration shown in the GUI. The second button measures the distances between the probes.

The procedure to calculate the resistivity using the L4P is the following:

1. Set the thickness, compliance and current.
2. Draw a symmetry line with the button DRAW SYMMETRY LINE.
3. Place the probes on the yellow symmetry line.
4. Check the electrical continuity with the button VERIFY CONTACTS.

Tesis publicada con autorización del autor
No olvide citar esta tesis

5. Measure the distances between each pair of probes (S1, S2 and S3).

6. Measure the resistivity with the button MEASURE.

The LabVIEW program implemented to calculate the resistivity with this method is shown in Figure 3.27.

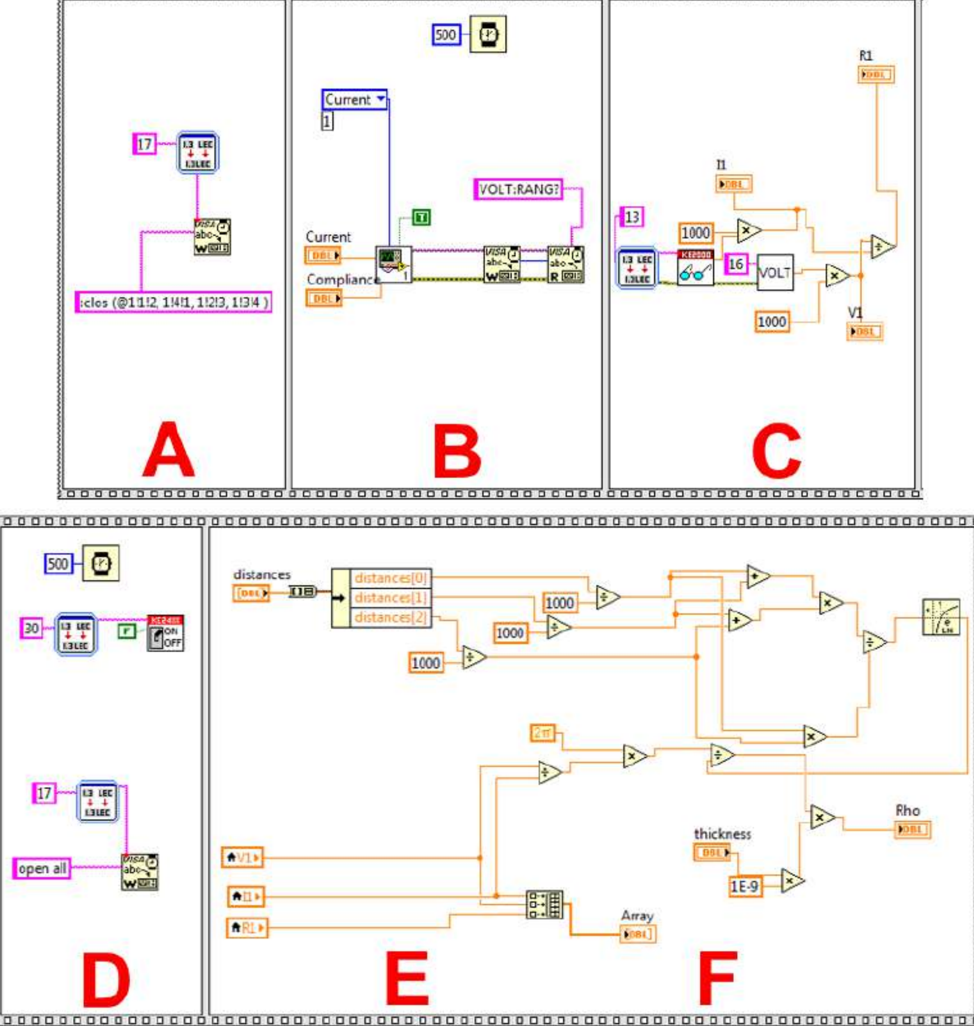

Figure 3.27: LabVIEW program to measure the resistivity using the Linear Four Probe Method.

A. The channels are closed in the switching equipment. The current is applied trough probes 1 and 2, and the voltage is measured between probes 3 and 4.

B. The selected current is applied by the sourcemeter between probes 1 and 2.

C. The voltage and current are measured between the pair of probes 1-2 and 3-4, respectively.

D. The sourcemeter is turned off and the channels in the switching equipment are opened.

Tesis publicada con autorización del autor
No olvide citar esta tesis

E. With the measured values, the resistivity is calculated with the equation shown in Equation 3.1.

$$\rho = (\frac{V}{I})(\frac{2\pi}{ln(\frac{(s_2+s_3)(s_1+s_2)}{s_1 s_3})})d \tag{3.1}$$

3.5.4 Square Four Probes Method

In the Square Four Probes Method, the probes are placed on the sample surface forming a square arrangement. Figure 3.28 shows the real time image of the sample with the position of the four probes in the *Camera Window* and the corresponding buttons for this method.

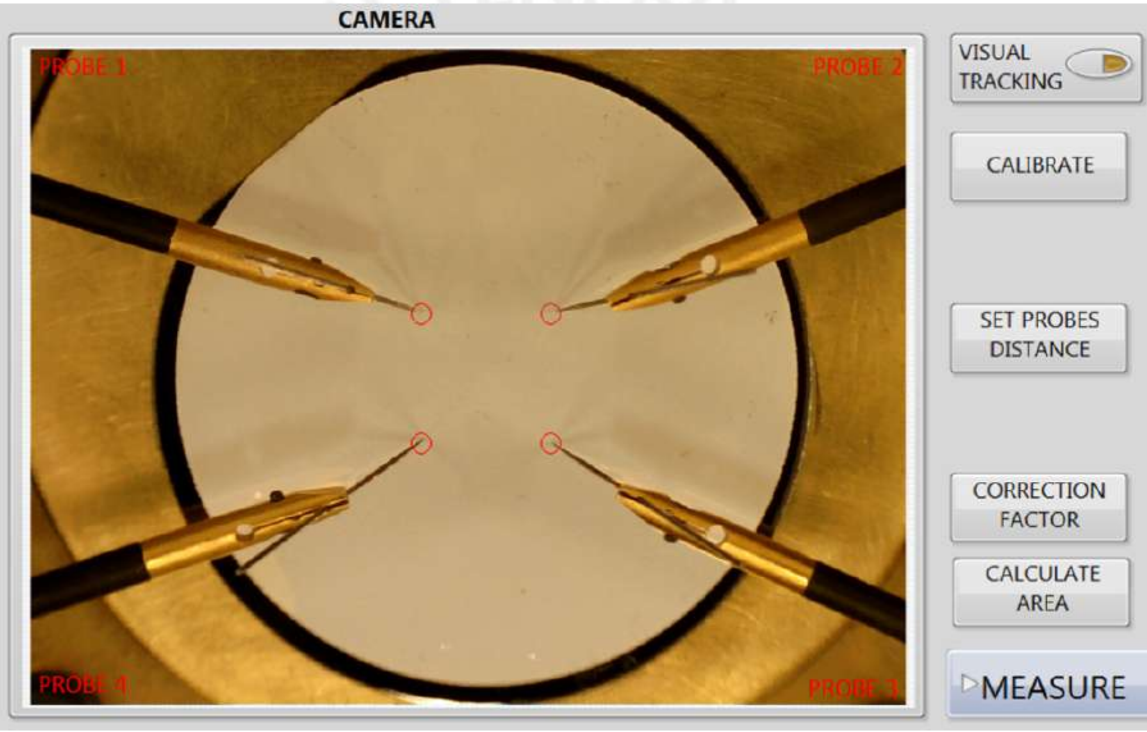

Figure 3.28: Configuration of the probes for Square Four Probes method. Probes are placed in a square array configuration. The available buttons for this function are shown.

The first step to apply this method consists of calibrating the visual system to calculate the distances between the probes. To calibrate the camera system, the button CALIBRATE in the GUI must be pressed.

Then, the user can set the distance for the probes spacing pressing the button SET PROBES DISTANCE. A window is displayed and the user sets the distance in millimeters. After that, a square array of 4 circles will appear on the sample surface. The user must place the tips onto these circles. Then, the button VERIFY PROBES can be pressed to check the electrical continuity between the probes and the sample. The 4

Tesis publicada con autorización del autor
No olvide citar esta tesis

LED's indicates the electrical continuity in each probe. After that, the thickness, compliance, input current, and sample diameter are set in the respective PARAMETERS box.

The CORRECTION FACTOR for this method is calculated automatically considering the values of the sample diameter and the probes spacing. It can be displayed pressing the button CORRECTION FACTOR. Additionally, the area formed by the probes can be calculated automatically pressing the function CALCULATE AREA in the GUI shown in Figure 3.28. At this point, the resistivity can be measured pressing the button MEASURE.

The principal difference of this method with the Linear Four Probes Method is that the probes must be placed forming a square array on the sample. A correction factor must be also considered for this method. When Square Four Probe method is selected, four additional buttons appear in the GUI: CALIBRATE, SET PROBES DISTANCES, CORRECTION FACTOR and CALCULATE AREA.

The procedure to calculate the resistivity with the Square Four Probes Method is the following:

1. Indicate the thickness, compliance, current and sample diameter.

2. Calibrate the camera system with the button CALIBRATE.

3. Press the button SET PROBES DISTANCE. The user sets the desired distance between the probes. The system will show the correct placement of the probes.

4. Place the probes in the sample on the red circles that appeared in the previous step.

5. Check the electrical continuity with the button VERIFY PROBES.

6. Measure the resistivity with the button MEASURE

The LabVIEW program to calculate the resistivity with this method is shown in Figure 3.29.
The description of each step of the program is the following:

A. The channels are closed in the switching equipment. The current is applied trough probes 1 and 2, and the voltage is measured between probes 3 and 4.

B. The selected current is applied by the sourcemeter between probes 1 and 2.

C. The voltage and current are measured between the pair of probes 1-2 and 3-4, respectively.

D. The sourcemeter is turned off and the channels in the switching equipment are opened.

E. With the measured values, the resistivity is calculated with the equation shown in the image.

Tesis publicada con autorización del autor
No olvide citar esta tesis

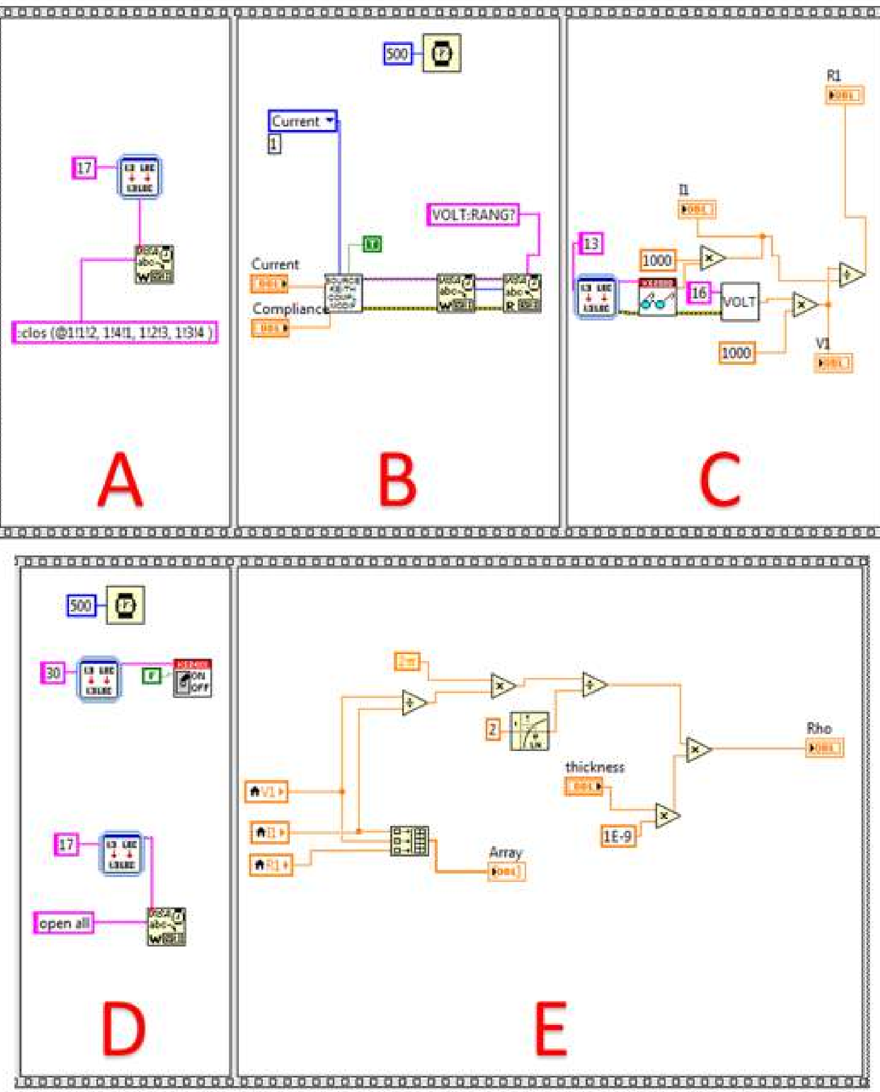

Figure 3.29: LabVIEW program to calculate the resistivity using the Square Four Probes Method.

3.6 Calibration of the visual system

In order to calculate the area and distances between the probes, it is necessary to calibrate the visual system. It consists of calculating a ratio between the number of image's pixels and the real distance according to Equation 3.2. This ratio depends on the distance of the camera from the sample and the image resolution. The procedure to calculate the calibration value can be shown in Figure 3.30. Furthermore, the description of each step is detailed below.

$$Calibration\ Value = \frac{Number\ of\ images's\ pixels}{Real\ distance} \tag{3.2}$$

1. The user presses the button CALIBRATE in the GUI. A display window shows the current calibration value. The user can use this actual value or acquire a new one pressing the button *New calibration*.

Tesis publicada con autorización del autor
No olvide citar esta tesis

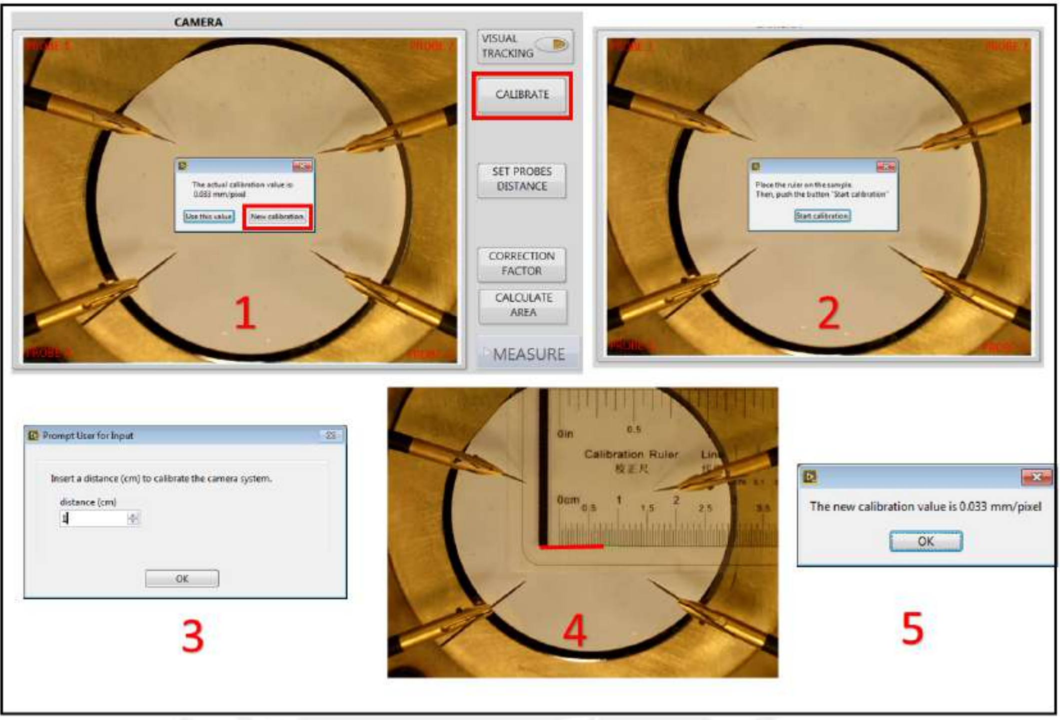

Figure 3.30: Procedure to calibrate the visual system.

2. A new message window is displayed. The user must place the ruler on the sample. Then, press the button *Start calibration*.
3. The user inserts an appropriate distance (in cm) to calibrate the camera system.
4. A line with the set distance is drawn on the ruler, then, the button OK is pressed.
5. The new calibration value is shown and the user can set this as a default calibration value.

Figure 3.31 shows the LabVIEW program implemented for the calibration function. The red letters indicate the steps followed by the program to accomplish the calibration. These steps are detailed below the figure.

Tesis publicada con autorización del autor
No olvide citar esta tesis

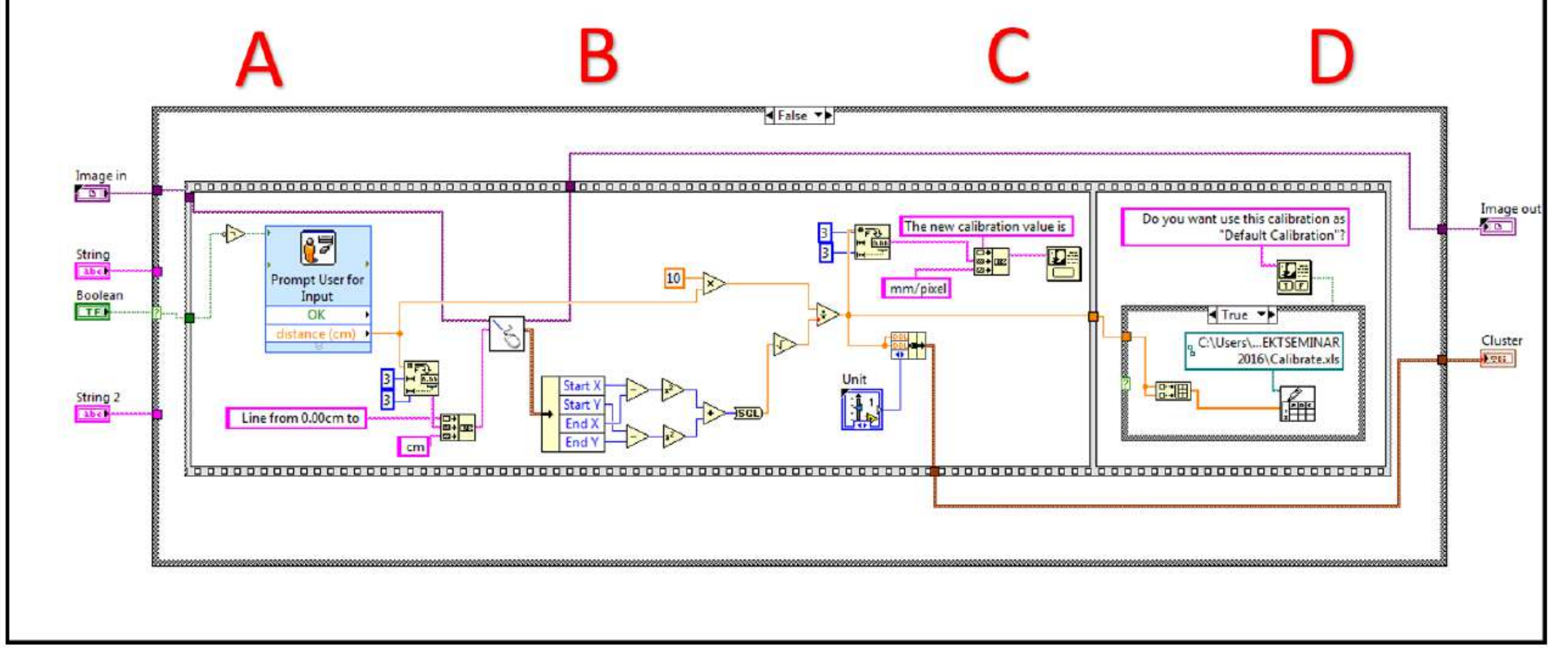

Figure 3.31: Lab VIEW Program for the CALIBRATE function. The camera is calibrated in order to accomplish digital measurements in the sample. The steps for the design are detailed below.

A. A dialog box is opened.the user decides whether a new calibration or a default calibration will be performed. For a new calibration, the user sets a calibration distance.

B. The user places a ruler in the sample area and selects a line in the camera window of the same distance specified in the previous step.

C. The length of the selected line, in pixels, is calculated. Then is divided by the real distance and a calibration ratio is obtained in mm/pixel.

D. The calibration value is shown in a window. The user decides if want to use this value as a default calibration value.

Tesis publicada con autorización del autor
No olvide citar esta tesis

3.7 Circular samples shape recognition

With this function, the software recognizes the sample's circular shape and draws a symmetry line on the sample in order to place the probes along it. It is necessary for the Linear Four Probes and Linear Van der Pauw methods. The circular recognition is performed using NI VISION LabVIEW module. Figure 3.32 shows the procedure of the program to execute the circular sample shape recognition. Moreover, the description of each step is detailed below.

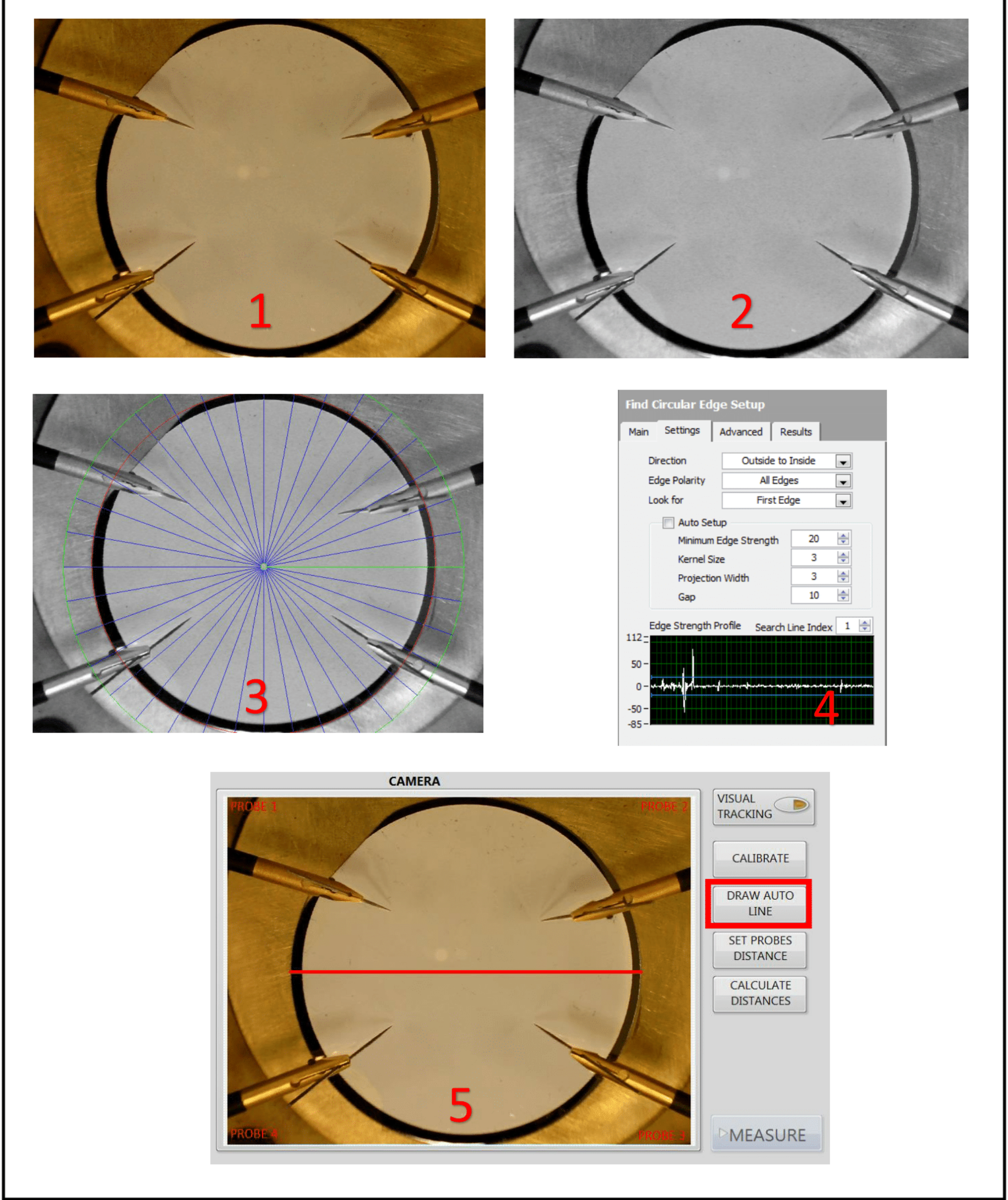

Figure 3.32: Procedure to detect the circular shape of the sample and draw the symmetry line on the sample.

1. A circular sample is placed in the camera area.

Tesis publicada con autorización del autor
No olvide citar esta tesis

2. The program converts the acquired image to a grayscale image.
3. The NI Vision module detects the circular shape in a defined area according to the parameters set by the user.
4. The user configure the parameters for the circular shape recognition.
5. The software detects the circular shape and provide the coordinates for the center of the circle. The user press the button DRAW AUTO LINE. The software detects the circular shape and a symmetry line appears on the sample.

Figure 3.33 shows the LabVIEW program implemented for the circular shape detection function. When the circular shape is detected, the program provides the coordinates for the symmetry line. The red letters indicate the steps followed by the program to accomplish its function. These steps are detailed below the figure.

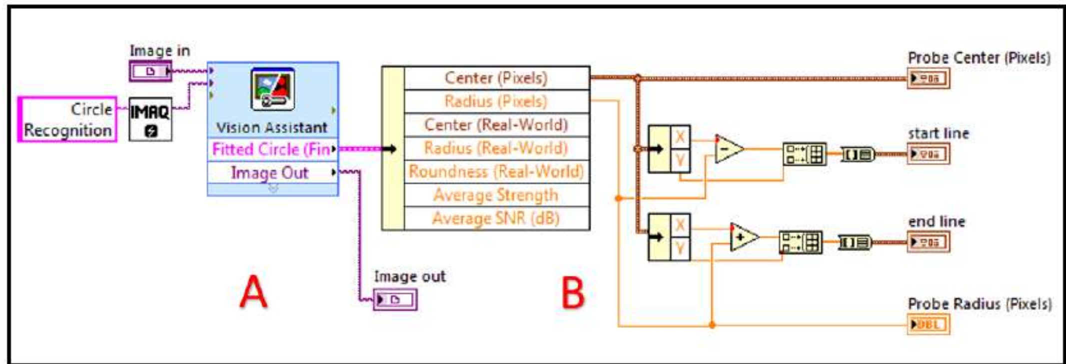

Figure 3.33: LabVIEW Program for Sample Recognition and Symmetry Line automatic drawing.

A. The *Vision Assistant* from the NI Vision Module is selected. The input for this library is the camera image and the outputs are the coordinates of the circular sample's center and its radius.

B. The coordinates of the circular sample are processed and the coordinates of the symmetry line are calculated.

Tesis publicada con autorización del autor
No olvide citar esta tesis

3.8 Set distance for probes spacing

The user sets a determined distance for the probes spacing. The program shows the correct position of the probes according to the set distance and the method. A square array of red circles will be shown for Square Four Probes Method and a linear array for Linear Four Probes and Linear Van der Pauw Methods. Figure 3.34 shows the GUI and the SET PROBES DISTANCE button.

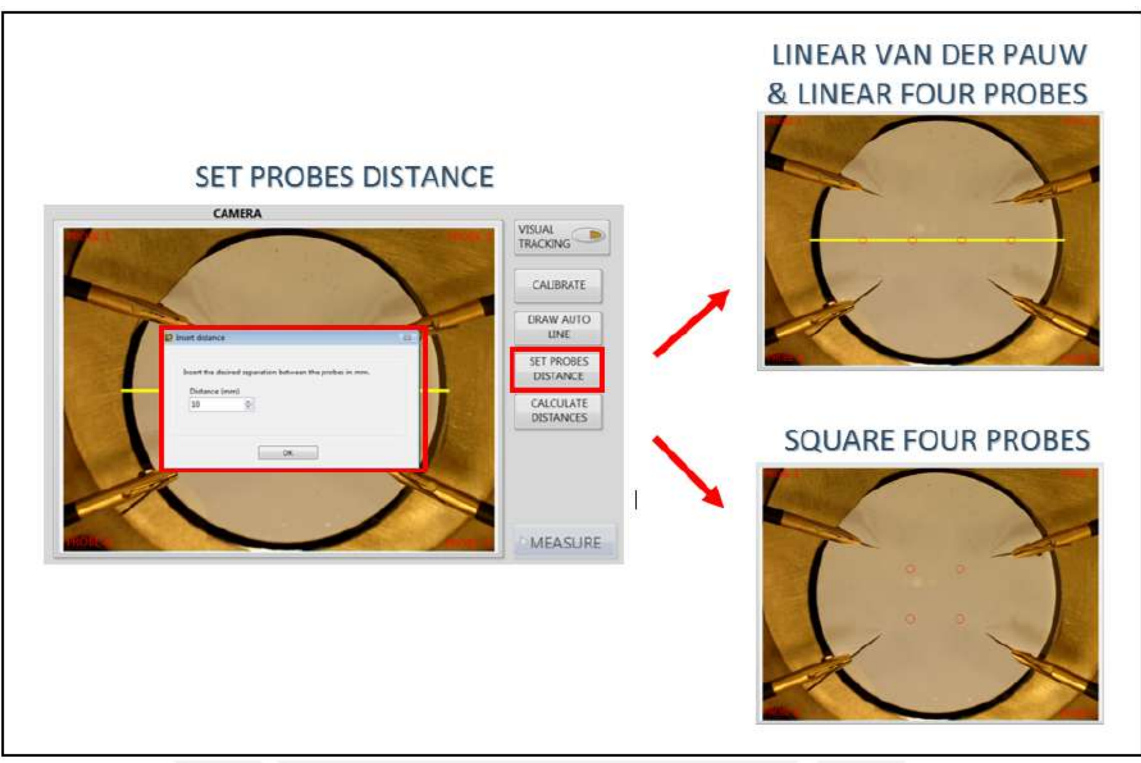

Figure 3.34: Procedure to set the distance for the probes spacing. The program shows the correct position for the probes according to the distance set by the user and the method.

Figure 3.35 shows the LabVIEW program implemented for SET PROBES DISTANCE function. The software shows arrays of circles that indicates the correct position for the probes. The red letters indicate the steps followed by the program to accomplish its function. These steps are detailed below.

Tesis publicada con autorización del autor
No olvide citar esta tesis

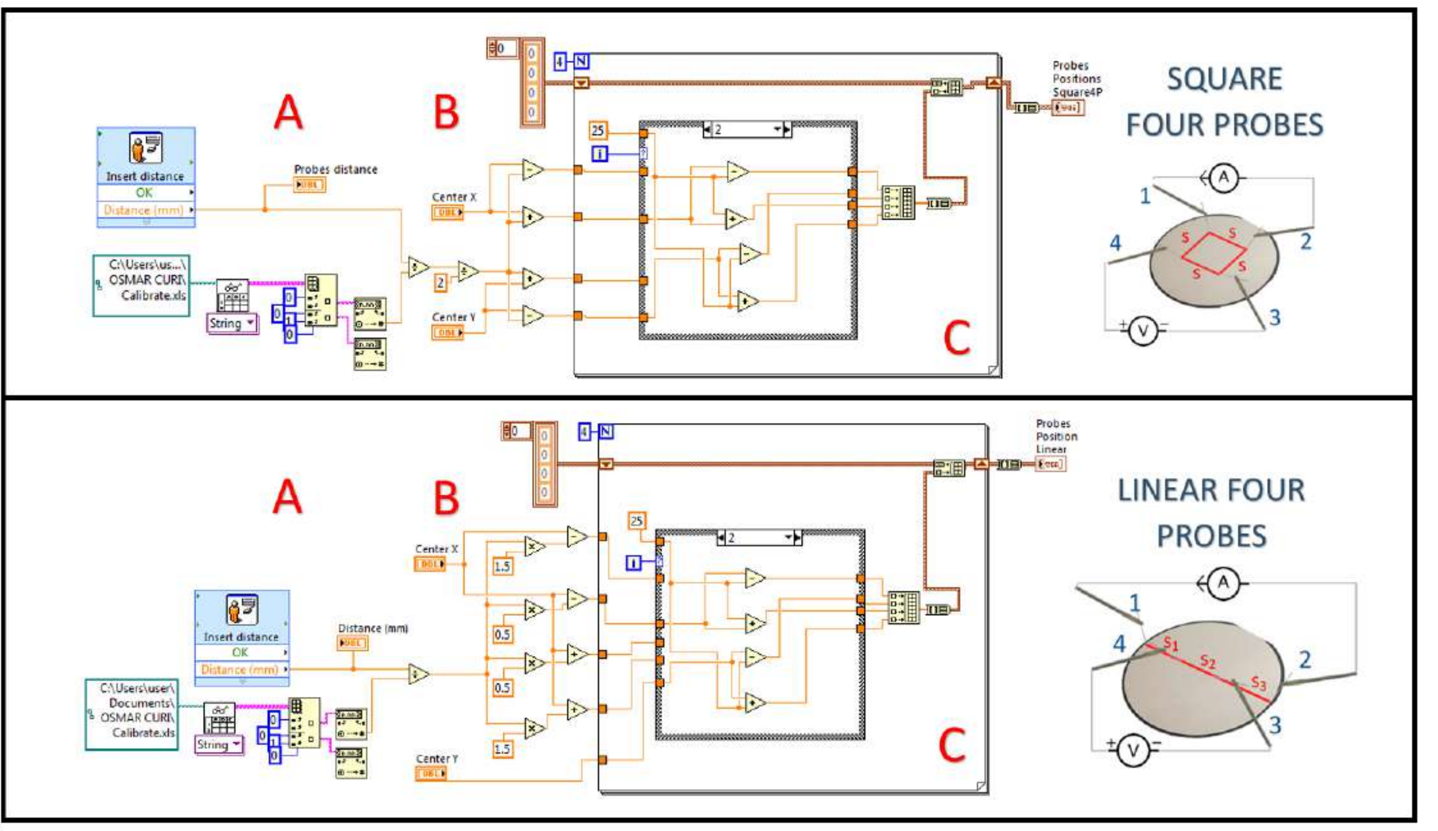

Figure 3.35: Lab VIEW Program for SET PROBES DISTANCE function.

A. A dialog box, as shown in Figure 3.34, is displayed . The user must set the desired distance for the probes spacing.

B. The positions for each probe is calculated.

C. The probes position are saved in an array. Then, red circles will be displayed to indicate the correct placement of the probes.

Tesis publicada con autorización del autor
No olvide citar esta tesis

3.9 Probes Alignment in the Symmetry Line

The misalignment of the probes induces errors in the resistivity measurements. A more precise tool for a correct alignment of the probes is necessary. Based on the implemented visual tracking system, a function for a correct probes alignment was implemented in order to reduce the errors caused by the misalignment.

The visual tracking detects the probe's position. Then, the Probes Alignment function detects if the probes are placed along the symmetry line. The symmetry line changes its color if a probed is being placed correctly along the symmetry line. Figure 3.36 shows the sequence of the probes alignment function. The sequence is detailed below.

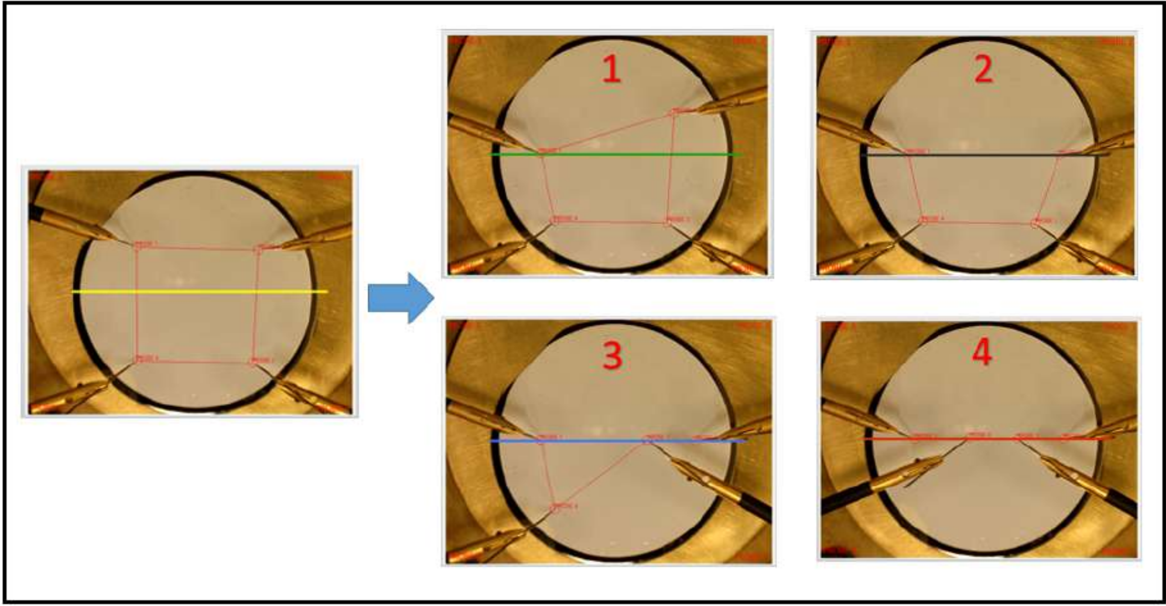

Figure 3.36: Probes alignment along the symmetry line. The line changes its color when the probes are correctly placed in the line.

1. The Visual Tracking system is executed. When the probe 1 is placed correctly, the symmetry line changes its color to green.
2. The probe number 2 is placed along the symmetry line and it changes its color to black
3. Probe number 3 is placed and the color of the line is blue.
4. Finally, the probe number 4 is aligned with the other probes and the color of the line is red. Therefore, the 4 probes are aligned.

Tesis publicada con autorización del autor
No olvide citar esta tesis

3.10 Automatic calculation of area and distances

For some methods, the measurement of the area formed by the probes and the distances between each pair of them is required. This measurement can be performed manually but normally it is not accurate enough and leads to measurement error. For that reason, two programs were implemented to calculate both the area formed by the probes and the distances between probes. Both programs are based on the visual tracking system to detect the probes positions.

Figure 3.37 shows the CALCULATE AREA function in the GUI. The system detects the probes position and calculates the area they form. This area (in mm^s) is shown in the camera window over the sample.

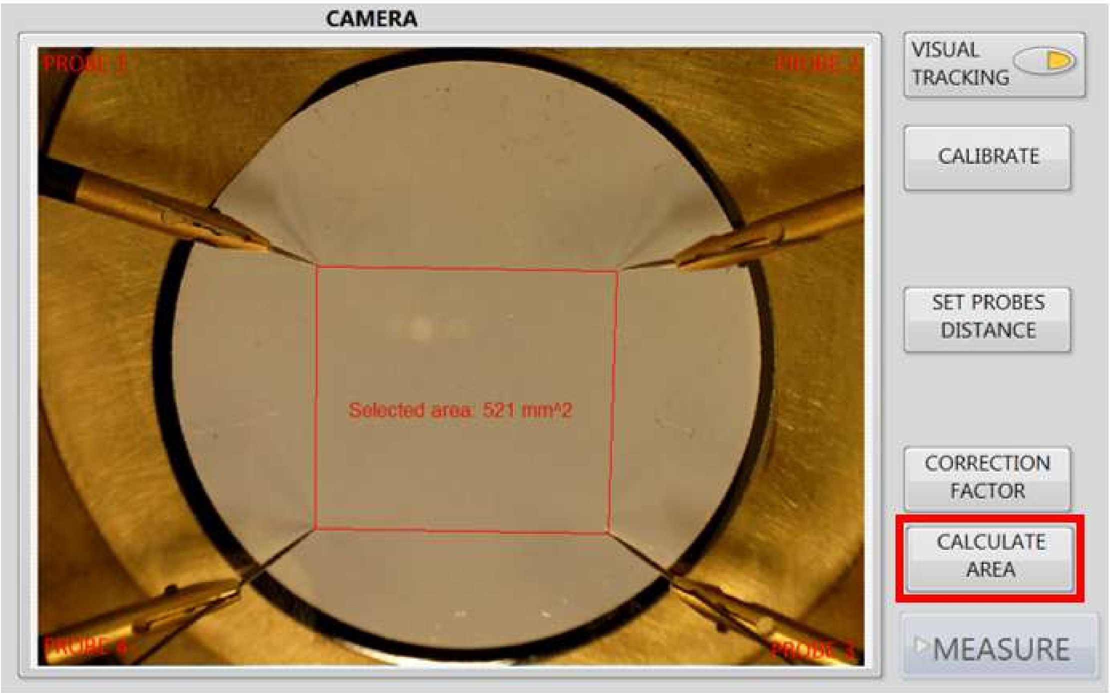

Figure 3.37: Calculate area formed by the probes. The program detects the probes position and calculates the area formed by the probes.

Figure 3.38 presents the LabVIEW program for the CALCULATE AREA function. The steps for the design of this program are presented below.

A. The calibration value defined with the CALIBRATION function is read from the file.

B. The probes positions are obtained from the VISUAL TRACKING function.

C. A VI from LabVIEW Vision Module is used to calculate the area formed by the probes positions.

The Figure 3.39 shows the CALCULATE DISTANCES function in the GUI. The system detects the position of the probes and calculates the distances between each pair of probes. The distances (in mm) are shown in the camera window over the sample.
The Figure 3.40 presents the LabVIEW program for the CALCULATE DISTANCES function. The steps for the design of this program are presented below.

Tesis publicada con autorización del autor
No olvide citar esta tesis

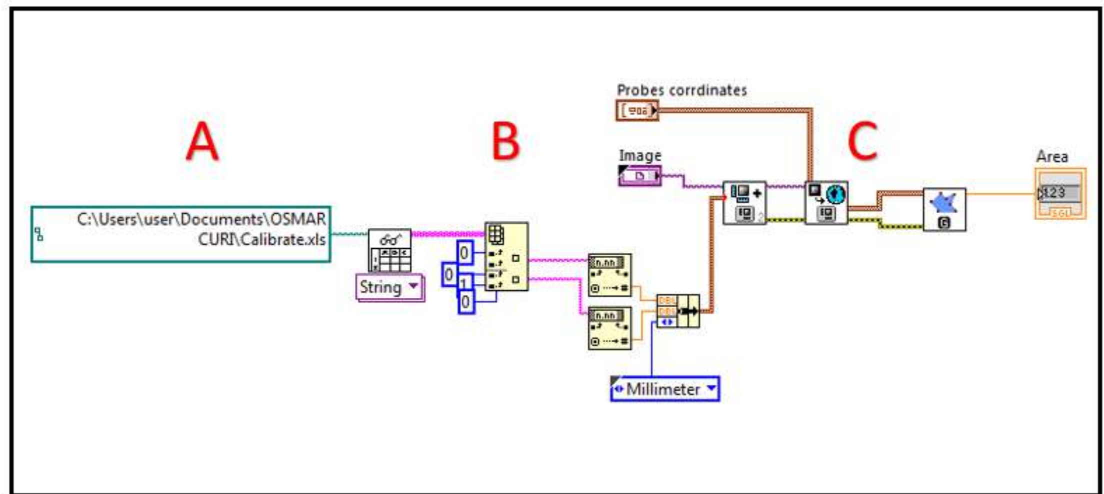

Figure 3.38: LabVIEW Program to Calculate the area formed by the probes. The program detects the probes position and calculates the area formed by the probes.

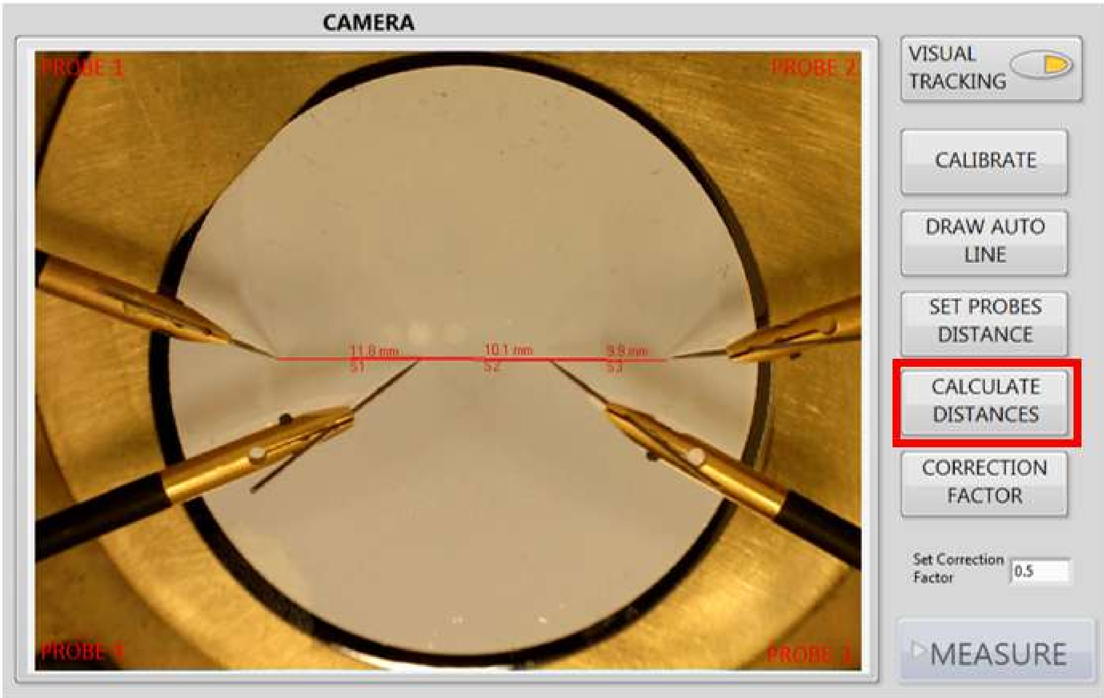

Figure 3.39: Calculate distances between the probes. The program detects the probes position and calculates the distances between each pair of probes.

A. The probes positions are obtained from the VISUAL TRACKING function.

B. The calibration value defined with the CALIBRATION function is read from the file. This value is necessary to convert the number of pixels in millimeters.

C. A VI from LabVIEW Vision Module is used to calculate the distance between each pair of probes. The results are saved in an array.

Tesis publicada con autorización del autor
No olvide citar esta tesis

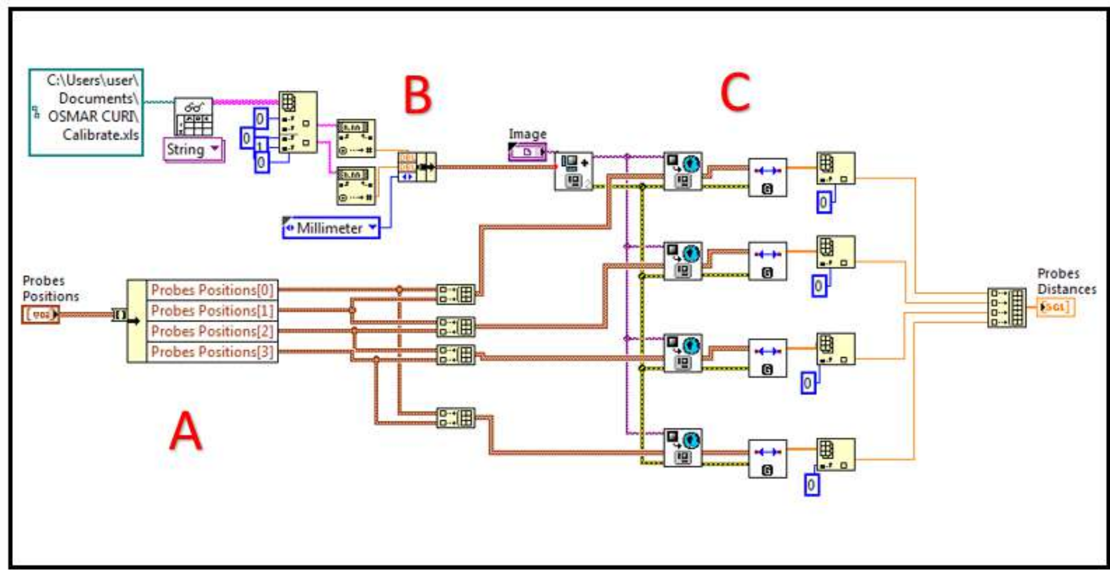

Figure 3.40: LabVIEW program to calculate the distances between the probes. The program detects the probes position and calculates the distances between each pair of probes.

3.11 Correction factors application

For the Four Probe Methods, both, linear and square, correction factors are required. The graphs are obtained from the work of Miccoli [10]. He presented correction factor curves for both, linear and square methods, in circular samples. The correction factor values depends on the sample diameter (D) and the probes spacing (s). The curves of correction factor for linear and square methods in circular samples were presented in Figure 2.6 in Chapter 2.

In order to facilitate the correction factor calculation for the user, the curves were approximated to a polynomial equation according to Miccoli [10]. The correction factor will be automatically calculated with the values of probes spacing, sample diameter and the correction factor's polynomial equation. The correction factor for the Linear Four Probes Method (CFL) is presented in Equation 3.3

$$CFL = \frac{ln2}{ln2 + ln\frac{(D/s)^2+3}{(D/s)^2-3}} \tag{3.3}$$

The correction factor for the Square Four Probes Method (CFS) is presented in Equation 3.4.

$$CFS = \frac{ln2}{ln2 + ln\frac{[(D/s)^2+2]^2}{(D/s)^4+4}} \tag{3.4}$$

Where x is the normalized diameter of the sample, D/s. The Figure 3.41 shows the implementation in LabVIEW of the correction factor for linear and square four probes methods.

Tesis publicada con autorización del autor
No olvide citar esta tesis

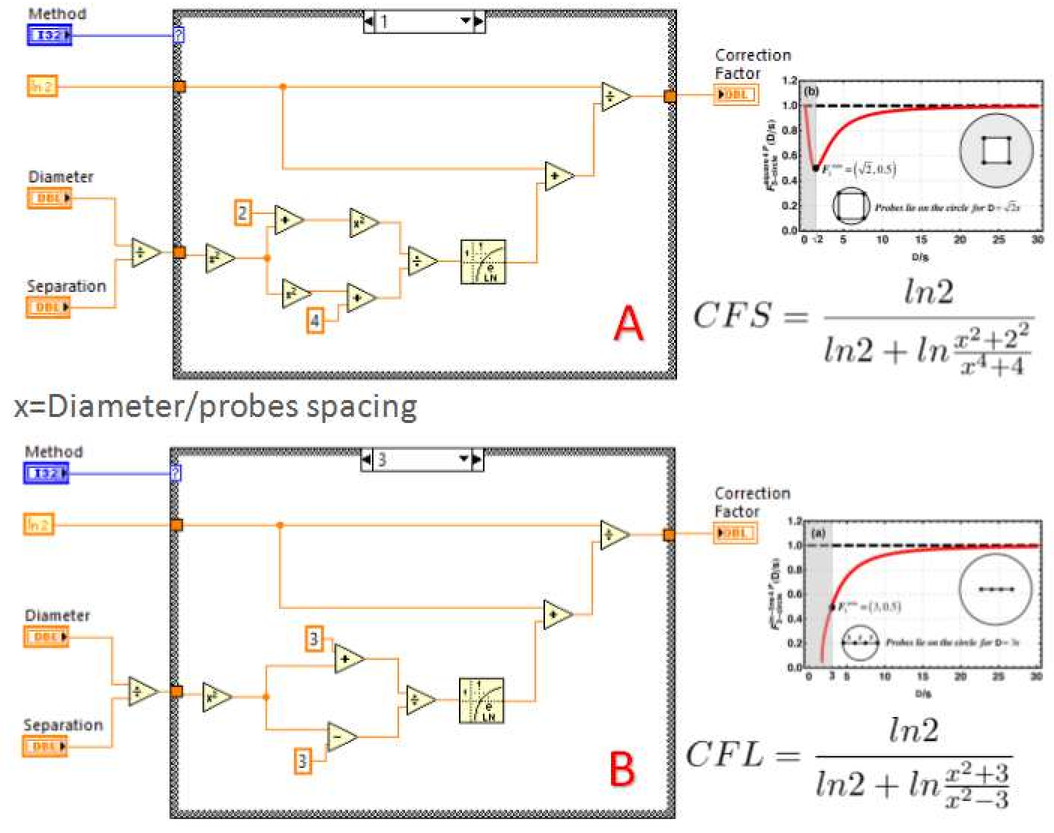

Figure 3.41: Implementation of Correction Factor in LabVIEW for (A) Square Four Probes Method and (B)Linear Four Probes Method. [10]

.

3.12 Preparation of thin films samples

The aims of this thesis do not include the preparation of thin films samples. Nevertheless, samples of tungsten and aluminum were prepared in the laboratory for a better understanding of the properties and characteristics of thin films.

A DC magnetron sputtering system was used to prepare tungsten and aluminum thin films, specifically, an LA 440S Von Ardenne Anlagentechnik GMBH equipment. Aluminum and tungsten were deposited onto a substrate of silicon which has a diameter of 2 inches. The thicknesses of the produced thin films are 100, 300 and 600 nm. In the case of the aluminum, the samples were prepared at two different temperatures: room temperature and 400° C. Figure 3.42 shows images of the tungsten samples preparation in the laboratory.

Sputtering techniques are used in industry and research for deposition of oxides, semiconductor and metallic thin films. In the sputtering process, a thin film of material, is deposited onto a substrate by evaporation of a target of the thin film material. A gaseous plasma is produced and then, the ions from this plasma are accelerated towards the target. Due to the impact of the Plasma, some atoms of the target acquire enough energy and detach from the target surface. This atoms are deposited onto the substrate and subsequently form the thin film [25].

Tesis publicada con autorización del autor
No olvide citar esta tesis

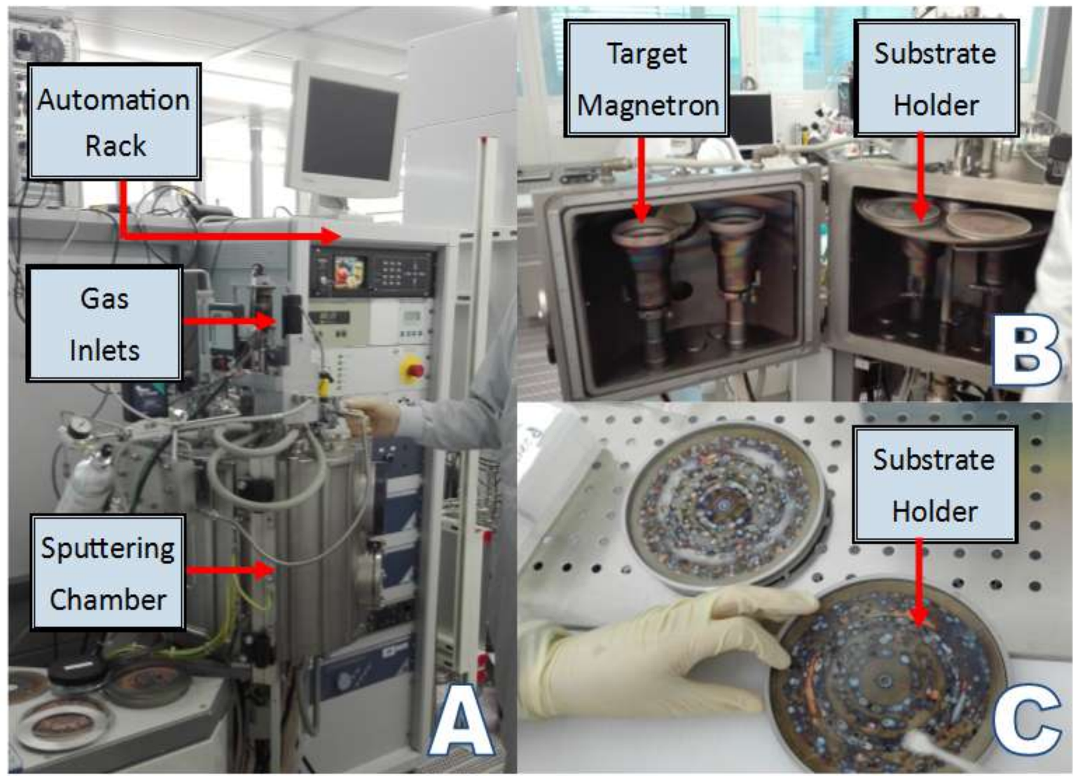

Figure 3.42: Sputtering Setup. Different parts of the sputtering system are shown in the figure. a. Magnetron sputtering system LA 440S Von Ardenne Anlagentechnik GMBH b.Sputtering chamber. c. Substrate holder preparation.

Tesis publicada con autorización del autor
No olvide citar esta tesis

Chapter 4

Results and discussion

In this Chapter, the performance of the implemented system was proved by measuring standard samples of aluminum and tungsten prepared on silicon substrates via sputtering. The samples have different thicknesses (100, 300 and 600 nm). The standard errors for each method are presented. The results are validated by comparison with experimental data from literature and thin films theoretical models (Fuchs-Sondheimer [38, 41], Mayadas-Shatzke [44] and combination of both models [45]). In addition, the influence of probes misalignment and probes spacing on resistivity measurement are analyzed.

4.1 Experimental results

Figure 4.1 shows the results of resistivity of the thin films tested to prove the performance of the measuring system. All the measurements were performed at room temperature. A detailed data and statistics can be seen in Table A.1.

As expected, this figure shows the dependence of the resistivity on the thin film thickness, specifically, the resistivity increases with the decrement of thin film thickness. The graph compares the results with the bulk resistivity of Al and W obtained from Table 4.1.

The resistivity values for Al-400 are, in average, 13% lower than Al results, which might indicates a reduction of resistivity for higher sputtering temperatures during the sample preparation. The comparison of the values obtained from the thickest samples (100 nm) with respect to the bulk resistivity, indicates and increment of 79% for Al and 269% for W samples. The possible causes of this difference will be discussed in the section corresponding to theoretical models.

Figure 4.2 shows the statistical standard error of the measurements for using each method. 20 different measurement were performed in each of the 9 samples using the four methods. All the methods have an error less than 1%, among them the VPM has the lowest error (0.3%) and the S4P the highest (0.9%). The lower error obtained using VPM are due to the fact that, unlike the other methods, this does not depend on the distribution of the probes nor the sample's shape. On the other hand, the S4P requires a 2-D arrangement, which produces errors caused by misalignment and probes configuration, besides, the samples shape has also an influence in the results. The linear methods (L4P and LVP) have similar errors (0.5%).

Tesis publicada con autorización del autor
No olvide citar esta tesis

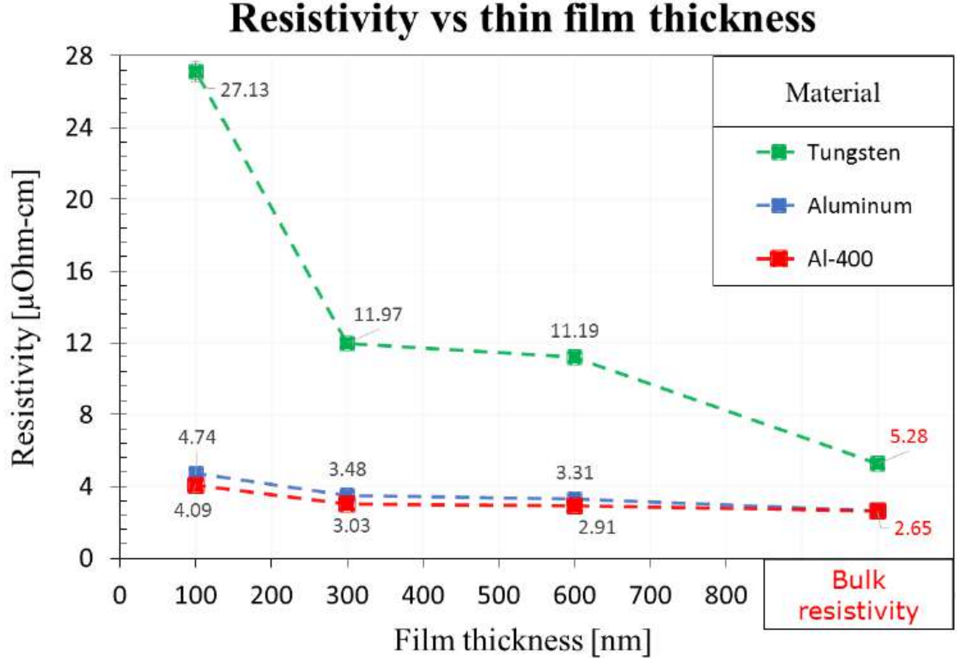

Figure 4.1: Resistivity vs thin film thickness for Al, Al-400 and W.

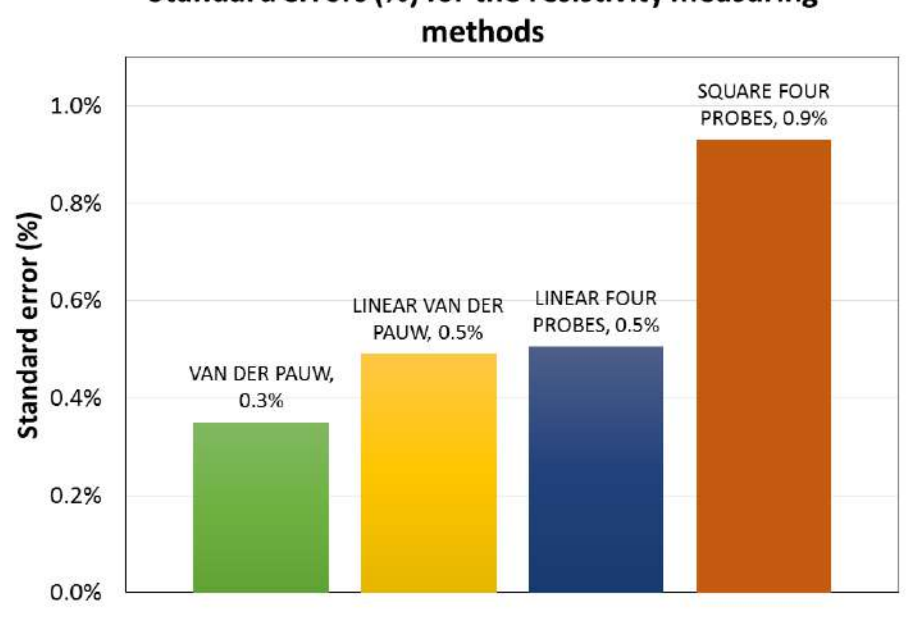

Figure 4.2: Standard errors obtained by using the four different methods

4.2 Results validation with experimental data

Resistivity in thin films depends not only in the material thickness, but also on many factors e.g. the surface scattering, the grain boundaries, the sample temperature, the fabrication process, etc. Figures 4.3 and 4.4 presents experimental resistivity data of thin

Tesis publicada con autorización del autor
No olvide citar esta tesis

films of Al (Ref. [30, 31]) and W (Ref. [32, 33]), respectively. The samples were prepared by different techniques and under different conditions. These results are compared to the experimental results obtained in this work. As can be seen, the technique and parameters used in the preparation of the sample affects the resistivity.

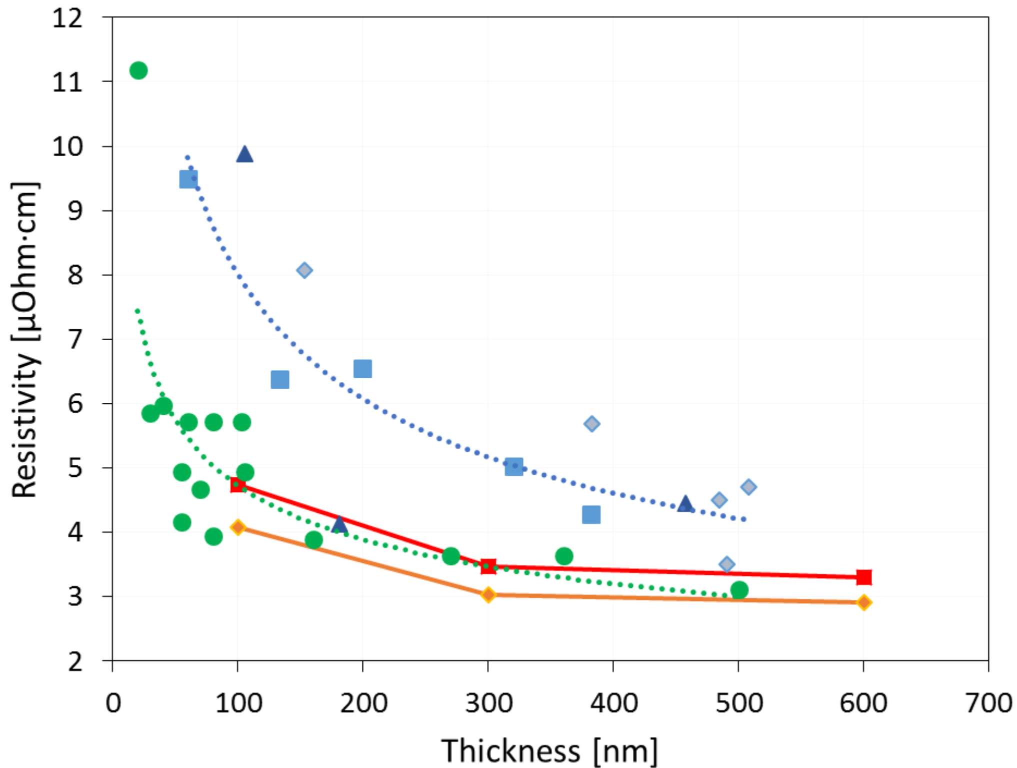

Figure 4.3: Experimental resistivity of Al samples prepared by different techniques [30, 31].

As can be seen in this graph the experimental results of Al are lower than those obtained by Mayadas [30], especially for the lowest thicknesses. The reason for this difference is that the mean free path obtained by Mayadas is some orders of magnitude smaller than

Tesis publicada con autorización del autor
No olvide citar esta tesis

the corresponding to the theoretical bulk value, which caused an increase of 60% in the results. The results obtained by Chaverri [31] fit better with the results of this thesis. In this case, the thin film was deposited in glass substrates at room temperature with a bulk-like behavior that starts at about 150 nm.

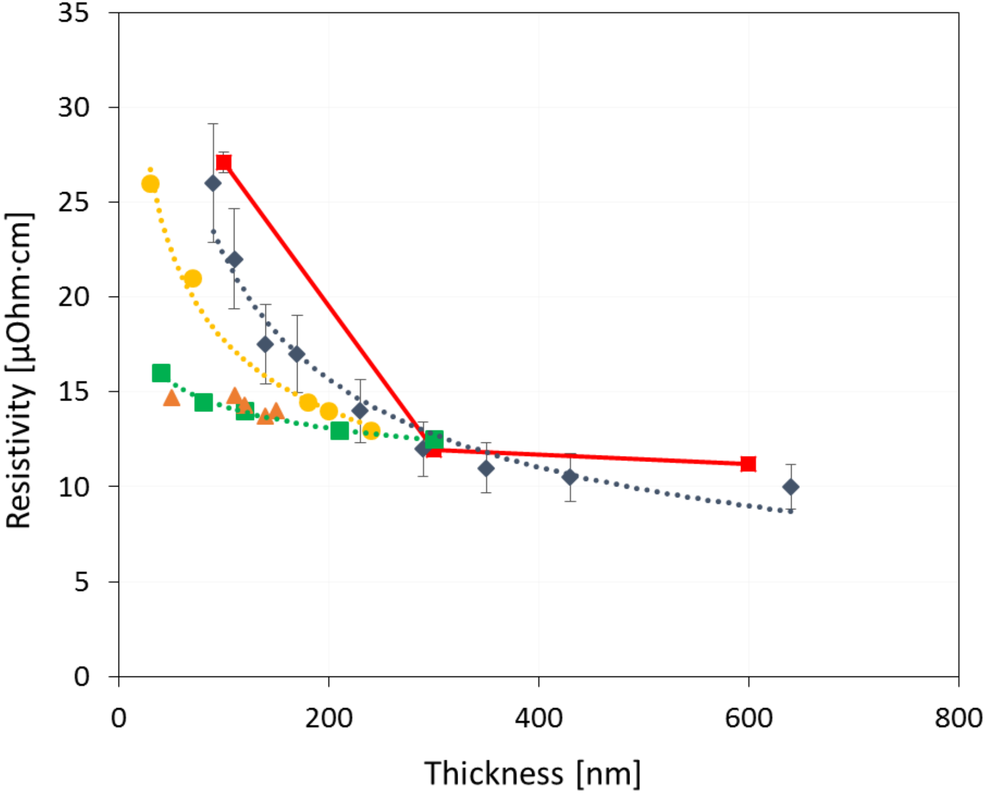

Figure 4.4: Experimental resistivity of W thin films prepared by different techniques [32, 33].

As can be seen in Figure 4.4 the obtained results for W are in accordance with other

Tesis publicada con autorización del autor
No olvide citar esta tesis

experimental works, specially with those obtained by Learn [32]. In that work the W thin films were deposited also on Si substrates but at a temperature of 400°C, which could explain the slightly lower values for resistivity. The same effect was noted between the results of Al and Al-400 in the previous section.

For an appropriate comparison with experimental results, all parameters must be at least similar, which is complicated and could be difficult if is tested a new material or combination of materials. For that reason, in the next section, the results will be compared with theoretical models that offer a correlation between the resistivity and thickness taking into account some inherent parameters and properties of the samples.

4.3 Theoretical models

The basic theory for metallic films was given by Fuchs [38], who proposed a model to describe the electron transport and estimate the resistivity in thin films. Since that many works have focused in proposing simplifications, modifications and improvements based in this model [1, 39, 40] .

4.3.1 Fuchs-Sondheimer (F-S) model

Sondheimer [41] based in Fuchs work proposed a theoretical model (F-S model) to determine the resistivity in thin films considering the bulk mean free path (λ), bulk resistivity $\rho_\circ$ and p, the proportion of electrons that are specularly reflected at the film surfaces (p=0, diffuse; p=1, specular scattering). These parameters can not be measured, but can be estimated comparing the theoretical model with experimental data [34].

The Fuchs-Sondheimer model, after some simplifications, can be represented as follow [42] [43]:

i For very thin films ($\lambda \gg t$),

$$\frac{\rho_\circ}{\rho} = \frac{3}{4}\frac{(1+p)}{(1-p)}k(\ln\frac{1}{k} + 0.4228) \tag{4.1}$$

ii For thick films ($\lambda \ll t$),

$$\frac{\rho}{\rho_\circ} = 1 + \frac{3}{8k}\frac{(1+p)}{(1-p)} \tag{4.2}$$

where $k = t/\lambda$.

4.3.2 Mayadas-Shatzke (M-S) model

Mayadas and Shatzkes [44] refined the F-S model considering the scattering of electrons caused by the grain boundaries. They established that the mean grain size play a predominant role in the increment of the resistivity in thin films. The M-S model is represented by Equation 4.3.

$$\frac{\rho_\circ}{\rho} = 3(\frac{1}{3} - \frac{1}{2}\alpha + \alpha^2 - \alpha^3\ln(1+\frac{1}{a})) \tag{4.3}$$

with

$$\alpha = \frac{\lambda}{D_{grain}}\frac{R}{1-R} \tag{4.4}$$

Where D_{grain} is the mean size of the grain and R is the grain-boundary reflection coefficient with values between 0 and 1.

Tesis publicada con autorización del autor
No olvide citar esta tesis

4.3.3 Combined model

A number of studies demonstrates that the increment of resistivity due the sample thickness is produced by two important mechanisms: surface and grain boundaries scattering [45]. Experimental results shows that F-S model explains the contribution of the surface scattering and M-S, of the grain boundaries, in the increment of the electrical resistivity. The experimental results can be validated considering both contributions with the following relation:

$$\rho_{exp} = \rho_{M-S} + \rho_{F-S} - \rho_{\circ} \tag{4.5}$$

4.3.4 Mola-Heras model

Mola and Heras [46] presented approximate equations to estimate the resistivity dependence on thickness based in the M-S model considering also the reflection parameter of the F-S model. These approximations can be applied in the range $0.2 \leq k \leq 5$ and is defined by Equation 4.6

$$\frac{\rho}{\rho_{\circ}} = 1 + \frac{3}{8k}\frac{(3r+1)}{(1-r)}(1-p) \tag{4.6}$$

with $k = t/\lambda$.

4.4 Results validation with the theoretical models

The theory proposes that the product of the electron mean free path λ and the resistivity ρ should be a constant independent, e.g. of density defects and temperature [34] [35]. Table 4.1 shows the values of bulk resistivity and mean free path for aluminum and tungsten obtained from Ref. [36] [37].

Table 4.1: Bulk resistivity and mean free path values for aluminum and tungsten [36] [37].

Material		bulk resistivity ρ ($\mu\Omega$-cm)	$\lambda \times \rho$ (10^{-16} Ω-m^2)	mean free path λ(nm)
Aluminum	Al	2.65	5.01	18.9
Tungsten	W	5.28	8.2	15.5

For the application of the M-S model, it is required the mean grain size value of the thin films. It can be determined by X-ray diffraction analysis (XRD). The grain size of the Al and Al-400 samples determined by XRD analysis can be seen in Figure 4.5.

Tesis publicada con autorización del autor
No olvide citar esta tesis

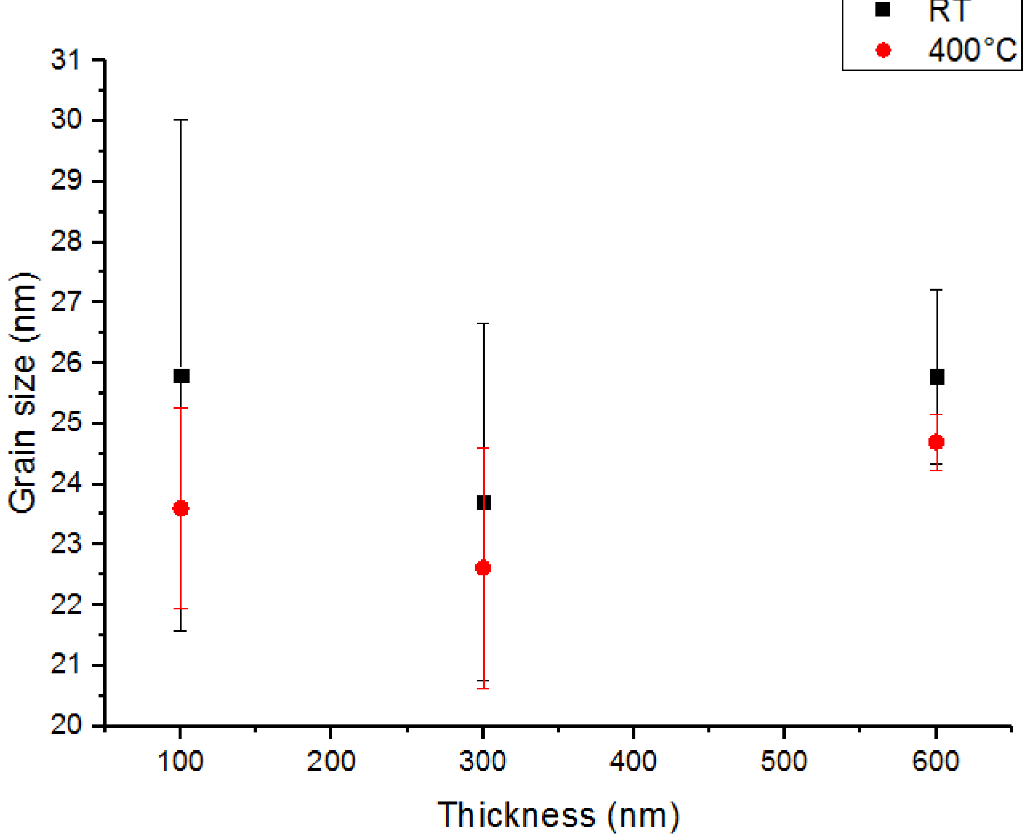

Figure 4.5: Grain size of Al and Al-400 samples measured by XRD analysis

In order to introduce the grain size dependence on the thickness into the models, the relation between mean grain size and thickness for Al and Al-400, based on the XRD analysys, are given by:

$$D_{grain} = 0.002t + 24.8 \tag{4.7}$$

for aluminum and

$$D_{grain} = 0.002t + 23 \tag{4.8}$$

for Al-400; where D_{grain} is the grain size and t, the thin film thickness.

To estimate the mean grain size of tungsten thin films, it was considered the following relation based on experimental data obtained by Learn [32]:

$$D_{grain} = 0.300t + 38.33 \tag{4.9}$$

For Tungsten.

According to [45] and [42] it is necessary to consider the F-S and M-S for the comparison with experimental data. The F-S model regards the mechanism of surface scattering in the increment of the resistivity, meanwhile, the M-S take into account the effects of grain boundaries. For that reason, both models were computed considering the described

Tesis publicada con autorización del autor
No olvide citar esta tesis

properties of the thin films and the values of p, that represents the fraction of elastically dispersive surfaces and R, the reflection coefficient, were estimated. Considering the values from Table 4.1 and the grain sizes of Figure 4.5 and Equations 4.7 and 4.9, the F-S, M-S and combined models are shown in Figures 4.6, 4.7 and 4.8 compared to the obtained experimental results of aluminum, Al-400 and tungsten, respectively.

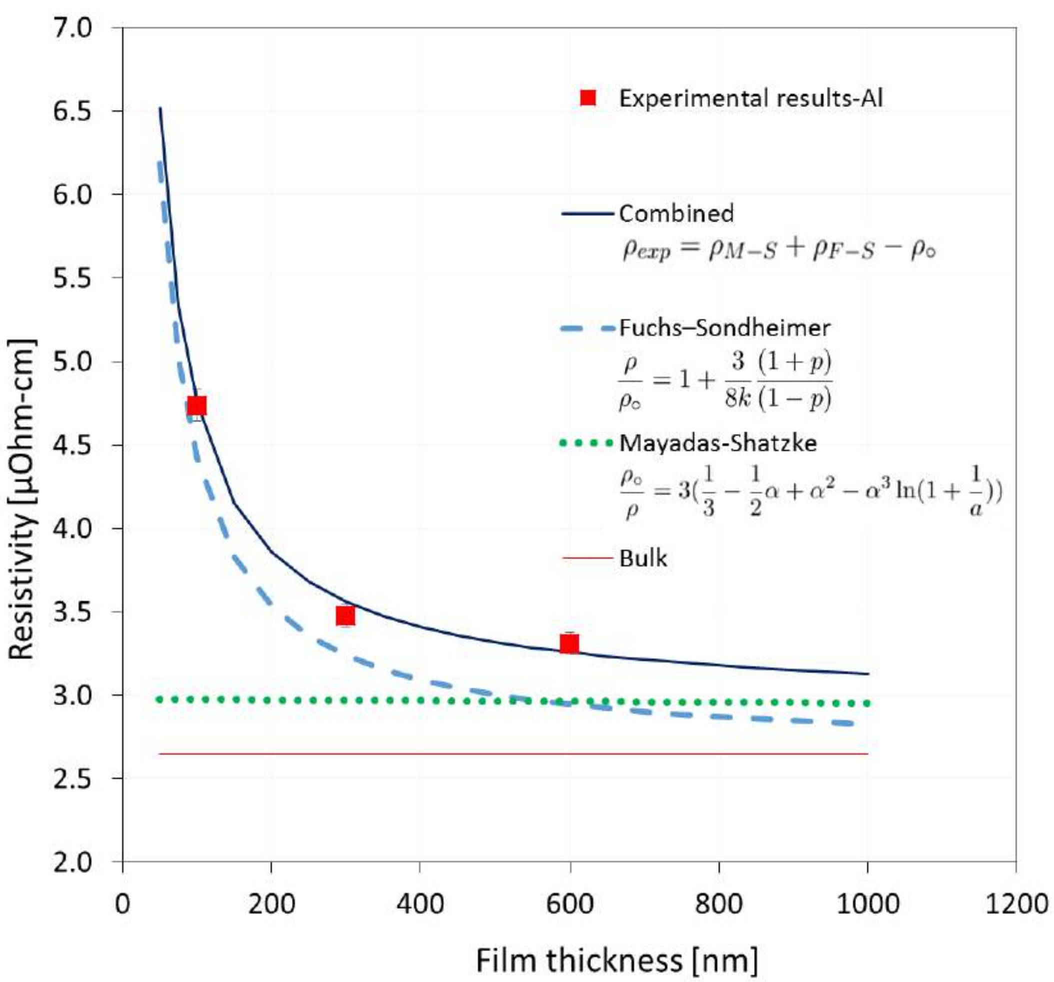

Figure 4.6: F-S, M-S and combined models compared to experimental results of aluminum. Parameters p=0.8 and R=0.1

Figure 4.6 shows the resistivity values of aluminum obtained in this work compared to the thin films theoretical models. Some recent works [42, 45] have demonstrated that experimental resistivity values can be explained from the contributions of both, surface scattering (considered by F-S model) and grain boundaries scattering (M-S model). The results are in accordance with this hypothesis. As can be seen, the combined model fits with the experimental results considering values of p=0.8 and R=0.1.

As illustrated in this figure, the contribution of the surface scattering (F-S) in resistivity is higher compared to the grain boundaries (M-S) influence. This behavior is produced because the grain size in these aluminum samples is almost invariant with thickness

Tesis publicada con autorización del autor
No olvide citar esta tesis

changes as can be seen in Figure 4.5. For that reason, the values of resistivity in the M-S model remain almost constant and the F-S model have more repercussion in the total resistivity values.

Figure 4.7 shows the comparison of Al-400 resistivity values compared to theoretical models. Similarly to the aluminum samples, the grain size of Al-400 samples does not change significantly with thickness variations. For that reason, the total resistivity increment is produced principally by surface scattering (F-S model) for the thinner films and the M-S model resistivity values remain almost constant.

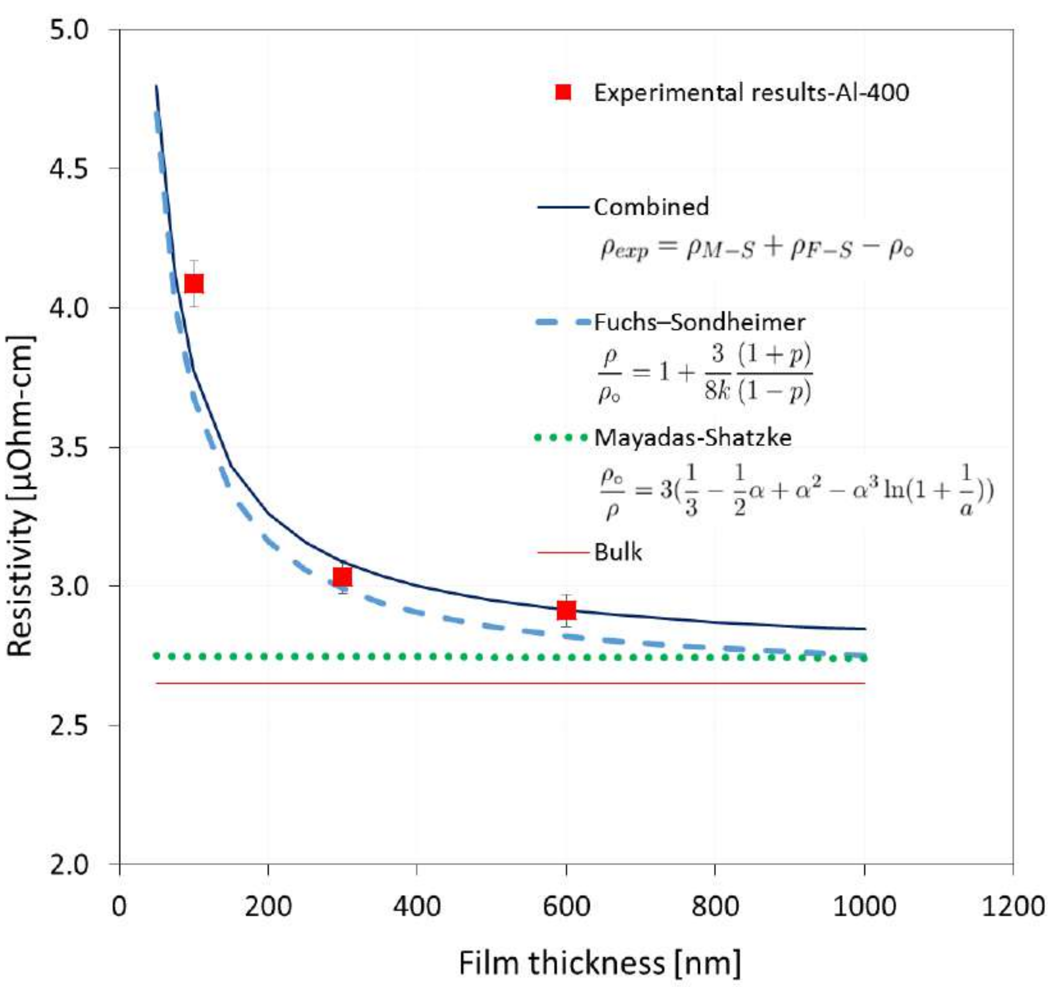

Figure 4.7: F-S, M-S and combined models compared to experimental results of Al-400. Parameters p=0.69 and R=0.03

The resistivity values obtained from tungsten films were also compared to theoretical model as illustrated in Figure 4.8. In contrast to the aluminum films, the main grain size for tungsten samples was considered dependent on the thickness film according to the results obtained by [32] which relation is presented in Equation 4.9.

Tesis publicada con autorización del autor
No olvide citar esta tesis

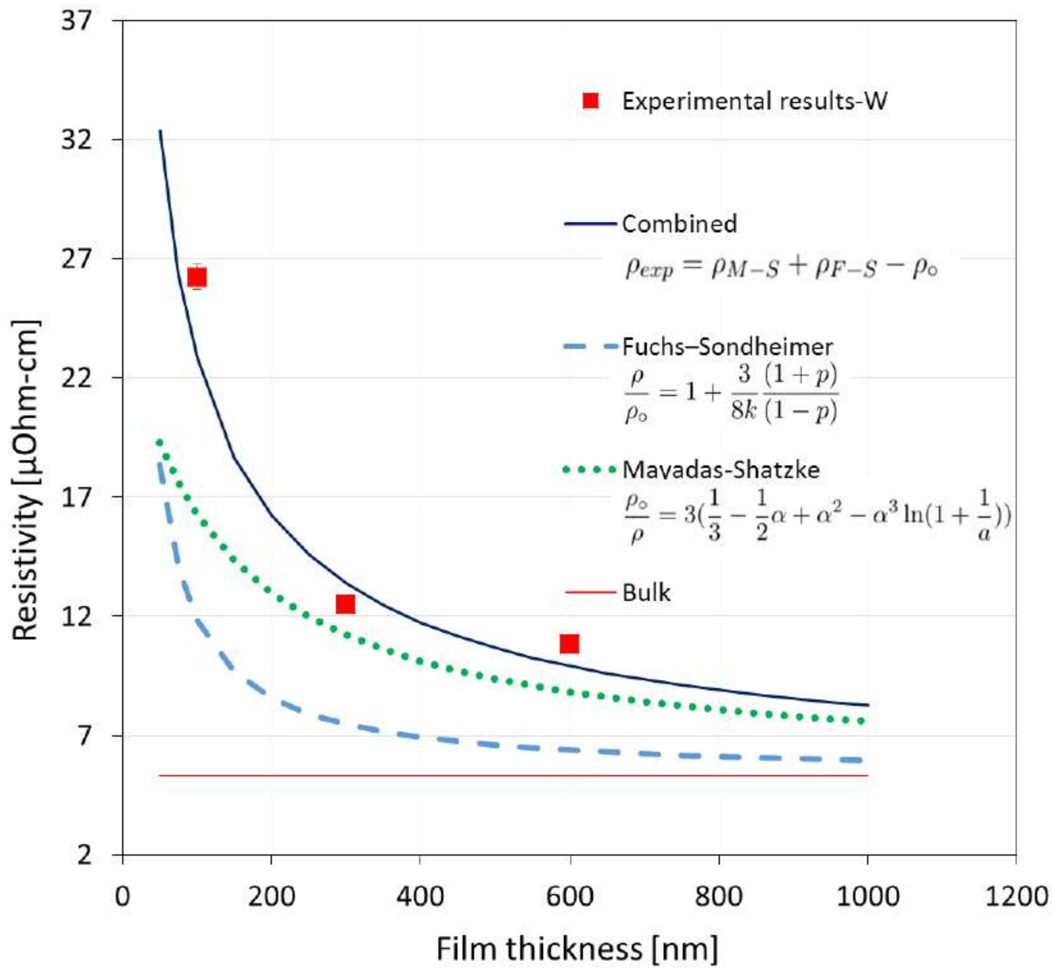

Figure 4.8: F-S, M-S and combined models compared to experimental results of tugnsten. Parameters p=0.9 and R=0.9

In opposition to the previous graphs, the resistivity in these tungsten samples is principally influenced by grain boundaries mechanism and the contribution of the surface scattering is minor. This behavior is in accordance with previous reports e.g. the results obtained by Durkan [45] that compared the experimental resistivity values of gold nanowires with the discussed theoretical models. The results obtained by Durkan are shown in Figure 4.9 and shows the contribution of both, F-S and M-S models to explain the experimental resistivity values, in the same way as the results achieved in this work.

Tesis publicada con autorización del autor
No olvide citar esta tesis

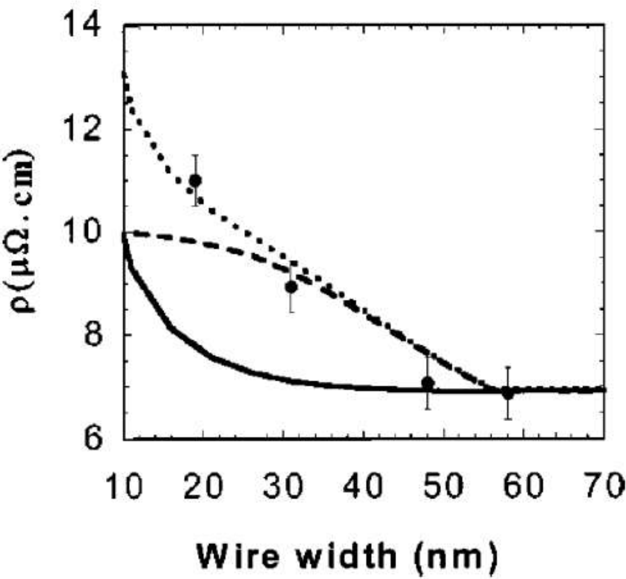

Figure 4.9: Contribution of both, F-S and M-S models to explain the experimental resistivity values of gold nanowires obtained by Durkan [45]

4.5 Effect of probes misalignment

The Linear Van der Pauw and Linear Four Probes methods require the correct alignment of the probes. One of the principals aims of the system is to avoid the errors caused by the misalignment during the measurement process. In this section, the errors caused by the probes misalignment using the linear methods will be quantified. The results show the relevance of the visual tracking system in order to reduce the errors caused by misalignment.

It was performed measurements for different probes configurations that include one or two misaligned probes. Figure 4.10 shows the four different probes positions measured in order to determine the error caused by misalignment. A sample of Al-400 having a thickness of 300 nm was tested using the LVP and the L4P. The probes were distributed linearly arranged with a probes spacing of 10 mm, where d_m is the distance of misalignment in each position. It was performed measurements for $d_m = 0.5$ and $d_m = 1.0$ mm. Table 4.2 shows the errors (in %) of the measurements for each position with respect to the values obtained when the probes were correctly aligned.

As can be seen in Table 4.2, the error caused by misalignment is higher when the distance of misalignment of the probe (d_m) increases. That indicates that the the reduction of d_m, achieved by the visual tracking system, improves the measuring system accuracy. Additionally, the results indicates that the errors caused by misalignment are higher when using the L4P (up to 13.4%) in comparison to using the LVP (up to 3.7%).

Tesis publicada con autorización del autor
No olvide citar esta tesis

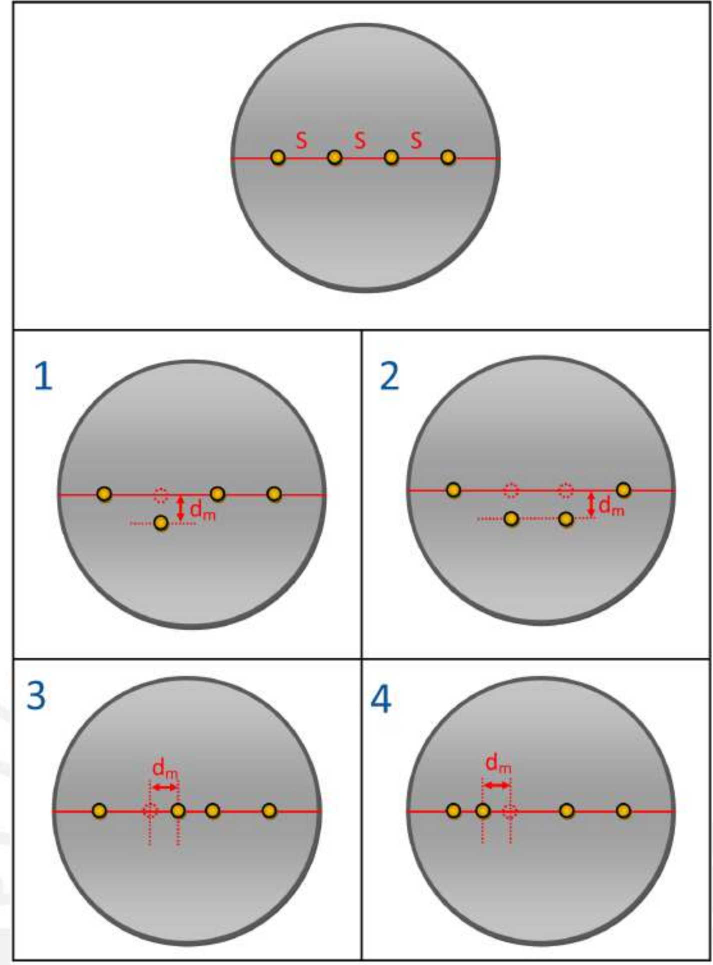

Figure 4.10: Position of the probes for the analysis of misalignment. It was tested an Al-400 film of 300 nm using L4P and LVP. d_m is the distance of misalignment in each case.

Table 4.2: Errors caused by the probes misalignment. It was tested an Aluminum sample of 300 nm using Linear Four Probes and Linear Van der Pauw methods. d_m is the distance of misalignment in each case.

PROBES POSITION	LINEAR FOUR PROBES		LINEAR VAN DER PAUW	
	d_m= 0.5 mm	d_m= 1 mm	d_m=0.5 mm	d_m= 1 mm
POSITION 1	1.8%	2.2%	1.4%	3.7%
POSITION 2	2.2%	2.6%	0.3%	1.7%
POSITION 3	5.4%	6.3%	1.0%	1.5%
POSITION 4	11.7%	13.4%	0.0%	1.0%

Tesis publicada con autorización del autor
No olvide citar esta tesis

4.6 Influence of the probes spacing

Compared to Van der Pauw, when using the other 3 methods, the obtained resistivity values might be influenced by the probes spacing. For that reason, in this section, the effect of the probes spacing will be analyzed. It was performed resistivity measurement for different probes spacing using the four methods. Al and W films having a thickness of 600 nm for probes spacing from 2 to 30 mm were measured. Figure 4.11 shows the results without the application of correction factor. Then the corresponding correction factors were applied and are shown in Figure 4.12

Figure 4.11: Resistivity vs Probes spacing without correction factor for Al and W films of 600 nm using LVP, L4P and S4P.

Results presented in Figure 4.11 demonstrates that the resistivity varies with the probes spacing for L4P and S4P. The higher values of resistivity are obtained when the probe spacing is higher. This influence must be eliminated using the correction factors.

Tesis publicada con autorización del autor
No olvide citar esta tesis

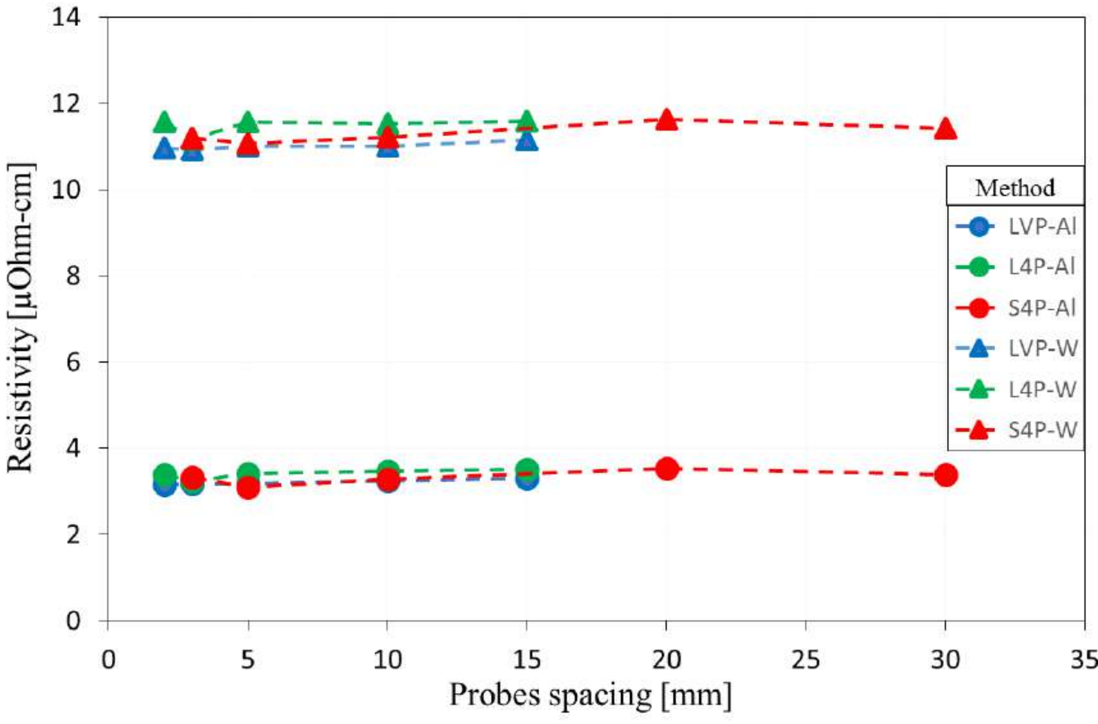

Figure 4.12: Resistivity vs Probes spacing applying correction factors for Al and W films of 600 nm using LVP, L4P and S4P.

The results shown in Figure 4.12 evidence that there is not an appreciable influence of probes spacing into the resistivity values after the application of correction factors. It was achieved by the correct implementation of the correction factors that reduces considerably the influence of probes spacing and sample shapes in the resistivity.

Tesis publicada con autorización del autor
No olvide citar esta tesis

Chapter 5

Conclusions

In order to overcome the constraints of measuring the resistivity in thin films, in the present thesis, a thin films resistivity measurement system was implemented. This system allows the application of four different methods for resistivity measurement: Van der Pauw, Square Four Probes, Linear Van der Pauw and Linear Four Probes. The measuring system comprises a LabVIEW program, GPIB Keithley instruments, a digital camera and a visual tracking system that allows a more precise automated measurement using the four methods.

In this work, a visual tracking function was implemented to track the probes position during the measurement. The system is based on image processing techniques and was developed using LabVIEW tools and a microscope digital camera. The visual tracking system incorporates several functions that improve the usability of the program. This system reduces the errors caused by the probes misalignment and the human factor. Additionally, the program provides a more user-friendly graphical user interface. Furthermore, it is the first step for the automation of the measuring system.

The performance of the developed system was proved by using standard samples of Al and W. Al and W thin films with different thickness (100, 300, and 600 nm) prepared on Si substrate via sputtering were measured for understanding the effect of thin films thickness on resistivity. The samples were measured using the four different methods obtaining and standard error less than 1%.

The results were validated by comparison with experimental data from literature and thin films theoretical models (Fuchs-Sondheimer, Mayadas-Shatzke and combination of both models). The results have a correlation with both, experimental data and theoretical models, therefore, the resistivity dependence on the thickness was confirmed. Also, it was shown that the grain-boundary and surface scattering effects produces the increment of electrical resistivity in thin films.

Moreover, the effect of the probes misalignment during the measurement was quantified for the linear methods (L4P and LVP). The errors caused by misalignment are greater for the Linear Four Probes (13.4%) than for the Linear Van der Pauw method (3.7%). The error caused by the misalignment seems to be considerable and it is significantly reduced with the implementation of the visual tracking system.

Furthermore, the effect of probes spacing was analyzed comparing the Linear and Square Four Probes, and Linear Van der Pauw methods. A dependence on the probes position was not verified. It validates the effectiveness of the implemented automated correction

Tesis publicada con autorización del autor
No olvide citar esta tesis

factor. The correction factor eliminates the influence of the geometry and the probes spacing in the resistivity values.

In future, this system can be applied for measuring the resistivity of semiconductor materials and samples of different shapes. Moreover, the influence of both, the thin film preparation technique and the substrate, in the resistivity will be studied. Furthermore, a system to control the positioning of the probes based on the visual tracking system could be implemented.

Tesis publicada con autorización del autor
No olvide citar esta tesis

Bibliography

[1] Fred Lacy. Developing a theoretical relationship between electrical resistivity, temperature, and film thickness for conductors. *Nanoscale research letters*, 6(1):1, 2011.

[2] S. H. N. Lim, D. R. McKenzie, and M. M. M. Bilek. Van der pauw method for measuring resistivity of a plane sample with distant boundaries. *Review of Scientific Instruments*, 80(7):075109, 2009.

[3] Sune Thorsteinsson, Fei Wang, Dirch H. Petersen, Torben Mikael Hansen, Daniel Kjær, Rong Lin, Jang-Yong Kim, Peter F Nielsen, and Ole Hansen. Accurate microfour-point probe sheet resistance measurements on small samples. *Review of Scientific Instruments*, 80(5):053902, 2009.

[4] Daniel Jasper. *SEM-based motion control for automated robotic nanohandling*. Verlag Dr. Hut, 2011.

[5] MC Rao and MS Shekhawat. A brief survey on basic properties of thin films for device application. In *International Journal of Modern Physics: Conference Series*, volume 22, pages 576–582. World Scientific, 2013.

[6] Chaoyang Shi, Devin K Luu, Qinmin Yang, Jun Liu, Jun Chen, Changhai Ru, Shaorong Xie, Jun Luo, Ji Ge, and Yu Sun. Recent advances in nanorobotic manipulation inside scanning electron microscopes. *Microsystems & Nanoengineering*, 2, 2016.

[7] Egbert Hesse. A four-point probe method with increased accuracy for the local determination of the thickness of thin, electrically conducting layers. *IEEE Transactions on Instrumentation and Measurement*, 1001(3):166–175, 1982.

[8] Leopoldo B. Valdes. Resistivity measurements on germanium for transistors. *Proceedings of the IRE*, 42(2):420–427, 1954.

[9] Akira Shimamoto, Keitaro Yamashita, Hirofumi Inoue, Sung-mo Yang, Masahiro Iwata, and Natsuko Ike. A nondestructive evaluation method: measuring the fixed strength of spot-welded joint points by surface electrical resistivity. *Journal of pressure vessel technology*, 135(2):021501, 2013.

[10] I. Miccoli, F. Edler, H. Pfnür, and C. Tegenkamp. The 100th anniversary of the four-point probe technique: the role of probe geometries in isotropic and anisotropic systems. *Journal of Physics: Condensed Matter*, 27(22):223201, 2015.

[11] John Albers and H. L. Berkowitz. An alternative approach to the calculation of four-probe resistances on nonuniform structures. *Journal of the Electrochemical Society*, 132(10):2453–2456, 1985.

Tesis publicada con autorización del autor
No olvide citar esta tesis

[12] A. A. Ramadan, R. D. Gould, and A. Ashour. On the van der pauw method of resistivity measurements. *Thin Solid Films*, 239(2):272–275, 1994.

[13] L. Van der Pauw. A method of measuring specific resistivity and hall effect of discs of arbitrary shape. *Philips Res. Rep.*, 13:1–9, 1958.

[14] T Kingler. *Image processing with LabView and IMAQ vision.* Prentice Hall PTR, 2003.

[15] Kye-Si Kwon and Steven Ready. *Practical Guide to Machine Vision Software: An Introduction with LabVIEW.* John Wiley & Sons, 2014.

[16] Christopher G Relf. *Image acquisition and processing with LabVIEW.* CRC press, 2003.

[17] Changhai Ru, Yong Zhang, Yu Sun, Yu Zhong, Xueliang Sun, David Hoyle, and Ian Cotton. Automated four-point probe measurement of nanowires inside a scanning electron microscope. *IEEE Transactions on Nanotechnology*, 10(4):674–681, 2011.

[18] Armen Petrosyan. Vision system for disabled people using pattern matching algorithm. In *Proceedings of the Seventh International Conference on Computer Science and Information Technologies*, pages 343–346, 2009.

[19] Torsten Sievers. Real-time object tracking inside an sem. In *Automated Nanohandling by Microrobots*, pages 103–128. Springer, 2008.

[20] Mohammad Gharavi-Alkhansari. A fast globally optimal algorithm for template matching using low-resolution pruning. *IEEE Transactions on Image Processing*, 10(4):526–533, 2001.

[21] Sergej Fatikow, Thomas Wich, Torsten Sievers, M Jähnisch, V Eichhorn, J Mircea, H Hülsen, and Ch Stolle. Automatic nanohandling station inside a scanning electron microscope. *Proceedings of the Institution of Mechanical Engineers, Part B: Journal of Engineering Manufacture*, 222(1):117–128, 2008.

[22] Kemal Berk Yesin and Bradley J Nelson. A cad model based tracking system for visually guided microassembly. *Robotica*, 23(04):409–418, 2005.

[23] Bradley E Kratochvil, Lixin Dong, and Bradley J Nelson. Real-time rigid-body visual tracking in a scanning electron microscope. *The International Journal of Robotics Research*, 28(4):498–511, 2009.

[24] National Instruments. Imaq vision concepts manual. 2003.

[25] Markku Tilli, Teruaki Motooka, Veli-Matti Airaksinen, Sami Franssila, Mervi Paulasto-Krockel, and Veikko Lindroos. *Handbook of silicon based MEMS materials and technologies.* William Andrew, 2015.

[26] Keithley. 2400 series source meter user's manual. *Seventh Printing, Cleveland, Ohio, USA*, 2002.

[27] Keithley. Model 2000 multimeter user's manual. *Eighth Printing, Cleveland, Ohio, USA*, 2003.

[28] Keithley. Model 2001 multimeter operator's manual. *Seventh Printing, Cleveland, Ohio, USA*, 1999.

Tesis publicada con autorización del autor
No olvide citar esta tesis

[29] Keithley. Model 7001 switch system quick reference guide. *Cleveland, Ohio, USA*, 1992.

[30] AF Mayadas. Intrinsic resistivity and electron mean free path in aluminum films. *Journal of Applied Physics*, 39(9):4241–4245, 1968.

[31] Diego Chaverri, Alejandro Saenz, and Victor Castano. Grain size and electrical resistivity measurements on aluminum polycrystalline thin films. *Materials Letters*, 12(5):344–348, 1991.

[32] Arthur J Learn and Derrick W Foster. Resistivity, grain size, and impurity effects in chemically vapor-deposited tungsten films. *Journal of applied physics*, 58(5):2001–2007, 1985.

[33] Y Pauleau, Ph Lami, A Tissier, R Pantel, and JC Oberlin. Tungsten films produced by selective deposition onto silicon wafers. *Thin solid films*, 143(3):259–267, 1986.

[34] GN Gould and LA Moraga. A method for fitting the fuchs-sondheimer theory to resistivity-thickness measurements for all film thicknesses. *Thin Solid Films*, 10(2):327–330, 1972.

[35] Daniel Josell, Sywert H Brongersma, and Zsolt Tőkei. Size-dependent resistivity in nanoscale interconnects. *Annual Review of Materials Research*, 39:231–254, 2009.

[36] Daniel Gall. Electron mean free path in elemental metals. *Journal of Applied Physics*, 119(8):085101, 2016.

[37] William M Haynes. *CRC handbook of chemistry and physics*. CRC press, 2014.

[38] K Fuchs. The conductivity of thin metallic films according to the electron theory of metals. In *Mathematical Proceedings of the Cambridge Philosophical Society*, volume 34, pages 100–108. Cambridge Univ Press, 1938.

[39] U Jacob, J Vancea, and H Hoffmann. A new method for determining the electronic mean free path in polycrystalline metals. *Journal of Physics: Condensed Matter*, 1(49):9867, 1989.

[40] D Schumacher. New evidence for the validity of the fuchs-sondheimer theory. *Thin Solid Films*, 152(3):499–510, 1987.

[41] E Hi Sondheimer. The mean free path of electrons in metals. *Advances in physics*, 1(1):1–42, 1952.

[42] Juan M Camacho and AI Oliva. Morphology and electrical resistivity of metallic nanostructures. *Microelectronics Journal*, 36(3):555–558, 2005.

[43] EH Sondheimer. The mean free path of electrons in metals. *Advances in Physics*, 50(6):499–537, 2001.

[44] AF Mayadas and M Shatzkes. Electrical-resistivity model for polycrystalline films: the case of arbitrary reflection at external surfaces. *Physical review B*, 1(4):1382, 1970.

[45] C Durkan and ME Welland. Size effects in the electrical resistivity of polycrystalline nanowires. *Physical review B*, 61(20):14215, 2000.

[46] EE Mola and JM Heras. Exact and approximate equations for the thickness dependence of resistivity and its temperature coefficient in thin polycrystalline metal films. *Thin Solid Films*, 18(1):137–144, 1973.

Tesis publicada con autorización del autor
No olvide citar esta tesis

Appendices

Tesis publicada con autorización del autor
No olvide citar esta tesis

Appendix A

Resistivity and standard errors for Al, Al-400 and W using the four methods

Tesis publicada con autorización del autor
No olvide citar esta tesis

Table A.1: Resistivity and standard errors for Al, Al-400 and W using the four methods

Resistivity(μOhm-cm) and standard error(%) for Al, Al-400 and W using the four methods																												
Mat.	Thick.	VAN DER PAUW			LINEAR VAN DER PAUW								LINEAR FOUR PROBES								SQUARE FOUR PROBES							
		Mean	Desv Stand	St. Error (%)	Probes spacing (mm)					Mean	Desv Stand	St. Error (%)	Probes spacing (mm)					Mean	Desv Stand	St. Error (%)	Probes spacing (mm)					Mean	Desv Stand	St. Error (%)
					2	3	5	10	15				2	3	5	10	15				3	5	10	20	30			
Al	600	3.29	0.06	0.4%	3.16	3.17	3.18	3.24	3.30	3.21	0.06	0.4%	3.39	3.24	3.40	3.46	3.51	3.40	0.10	0.7%	3.31	3.10	3.29	3.52	3.38	3.32	0.15	1.0%
	300	3.43	0.06	0.4%	3.34	3.33	3.38	3.40	3.47	3.38	0.06	0.4%	3.53	3.49	3.57	3.60	3.66	3.57	0.07	0.4%	3.56	3.29	3.52	3.69	3.57	3.53	0.15	0.9%
	100	4.93	0.12	0.5%	4.72	4.84	5.13	5.30	5.55	5.11	0.34	1.5%	4.31	4.40	4.67	4.55	4.56	4.50	0.14	0.7%	4.19	4.40	4.30	4.60	4.55	4.41	0.17	0.9%
Al-400	600	2.90	0.04	0.3%	2.92	2.86	2.81	2.83	2.86	2.85	0.04	0.3%	2.90	2.85	2.90	3.10	3.13	2.98	0.13	1.0%	2.90	2.70	2.83	3.13	3.01	2.91	0.16	1.3%
	300	2.96	0.07	0.5%	3.12	3.00	2.89	2.93	2.99	2.99	0.09	0.7%	3.17	3.07	3.12	3.11	3.25	3.14	0.07	0.5%	3.13	2.82	2.99	3.19	3.09	3.04	0.15	1.1%
	100	4.03	0.07	0.4%	3.93	3.90	3.91	3.97	4.07	3.96	0.07	0.4%	4.26	4.20	4.22	4.25	4.46	4.28	0.10	0.5%	3.95	3.82	4.12	4.32	4.18	4.08	0.20	1.1%
W	600	10.95	0.09	0.2%	10.96	10.92	11.01	11.00	11.15	11.01	0.09	0.2%	11.57	11.17	11.56	11.53	11.59	11.48	0.18	0.3%	11.19	11.06	11.22	11.62	11.43	11.31	0.22	0.4%
	300	11.66	0.13	0.3%	11.60	11.55	11.61	11.69	11.88	11.67	0.13	0.3%	12.51	12.39	12.35	12.27	12.67	12.44	0.15	0.3%	12.93	11.27	12.09	12.42	11.91	12.12	0.62	1.1%
	100	26.33	0.19	0.2%	27.22	26.92	27.83	27.80	27.37	27.43	0.39	0.3%	28.09	27.82	27.87	27.76	27.57	27.82	0.19	0.2%	27.96	26.28	26.78	27.29	26.41	26.94	0.69	0.6%
STANDARD ERROR				0.3%	STANDARD ERROR							0.5%	STANDARD ERROR							0.5%	STANDARD ERROR							0.9%

Tesis publicada con autorización del autor
No olvide citar esta tesis